

REAL-TIME MODEL-BASED ESTIMATION OF TRANSFER CASE CLUTCH
PARAMETERS AND TRACTION TORQUE

By

Wenpeng Wei

A DISSERTATION

Submitted to
Michigan State University
in partial fulfillment of the requirements
for the degree of

Mechanical Engineering – Doctor of Philosophy

2021

ABSTRACT

REAL-TIME MODEL-BASED ESTIMATION OF TRANSFER CASE CLUTCH PARAMETERS AND TRACTION TORQUE

By

Wenpeng Wei

This dissertation provides a clear path for model-based real-time estimation of transfer case clutch parameters and wheel traction torque with improved accuracy for a 4-Wheel-Drive (4WD) vehicle.

Transfer case clutch, distributing the traction torque between front and rear tires, is a key component for 4WD vehicle propulsion system. When the clutch is disengaged, driving torque from transmission is distributed to rear tires only through the solid connection between rear differential and transmission, resulting in 2-Wheel-Drive operating mode for improved fuel economy. When the clutch is engaged, traction torque is distributed to both front and rear tires through transfer case clutch, leading to 4WD operating mode for better traction performance. The amount of traction torque for front or rear tires is determined by the clutch status, given the total traction torque from transmission is known. However, the actual torque distribution ratio, determined by real-time clutch operating status, is typically unknown due to the unavailability of multiple clutch parameters and/or direct measurement of traction torque. Therefore, for accurate traction torque control, real-time estimation of transfer case clutch parameters (such as touchpoint displacement, friction coefficient, output torque, etc.) and wheel traction torque is imperative.

One significant step is to estimate the clutch touchpoint displacement based on the clutch actuation system since it is proportional to the clutch normal force (or clutch output torque). The touchpoint displacement is initially designed as a constant. However, there are also many factors that may render it to change. Therefore, this dissertation lumps all the factors that causes variation of touchpoint displacement to a variation displacement parameter and proposes to estimate this variation displacement in real-time with adaptive parameter estimation algorithm.

Although the aforementioned approach achieves estimation quite well, the estimation is separated from the desired clutch displacement control. Therefore, an integrated approach is proposed

to estimate the touchpoint displacement and track the desired clutch displacement simultaneously. This is realized by using the deadbeat adaptive backstepping control technique based on the clutch actuation system. This approach not only is more concise for implementation but also may reduce production cost.

Another significant step to estimate clutch surface friction coefficient is to estimate the clutch output torque. This can be achieved neck-by-neck with the estimation of traction torque on the tires. In this dissertation, the tire traction forces are estimated under different clutch operation conditions: open, slip and overtaken. A integrated model incorporating time-varying effective tire radius, vehicle speed estimation and clutch-slip speed compensation is proposed, which shows good accordance with the measured torque under different clutch conditions.

Although the aforementioned modeling approach for clutch output torque calculation shows promising results. It is obvious that this modeling approach is sensitive to measurement noise, especially the clutch output torque calculation is involved with the difference between vehicle speed and tire linear speed. Therefore, an Extended Kalman Filter based estimation algorithm is proposed to deal with measurement noise. This estimation algorithm is developed based on the integrated clutch output torque model suitable for both clutch slip and overtaken condition.

Finally, the clutch surface friction coefficient is estimated based on the estimated clutch touchpoint displacement and clutch output torque, note that this estimation approach will be clutch-parameter-dependent. In order to obtain an estimated clutch-parameter-independent friction coefficient, this dissertation further proposes an adaptive lookup table scheme, table nodes of which are updated by the well-known Recursive Least-Squares algorithm. The effectiveness of clutch-parameter-independent friction coefficient is confirmed by comparison and can be used for future clutch output torque control without knowing clutch parameters/operating statuses.

Copyright by
WENPENG WEI
2021

ACKNOWLEDGMENTS

Great things come from hard work and perseverance. No excuses.

— *Kobe Bryant*

Ever since the beginning of my Ph.D. program at the Michigan State University, I was so blessed that I can live and study in such a friendly and supportive community. All along the way, my deeply gratefulness shall be expressed to those who show their selfishness support, inspiring encouragement, and endless love whenever I needed toward the completion of my Ph.D. study.

First and foremost, my greatest gratitude shall be paid to my most respected advisor, Professor Guoming (George) Zhu, who consistently provides me with constructive and essential suggestions toward my Ph.D. research. With his solid expertise in control and automotive theory as well as extensive successful experience of real-world applications, not only my Ph.D. study progressed in a smooth fashion, but also the sponsored research work yielded great achievement. As a matter of fact, his guidance are far beyond research work. His unique wisdom toward life, his endless passion toward research interest, and his particular way of thinking have been, and will always be, a lighthouse that directs me toward the right direction. In addition, I 'd like to express my deepest gratitude to Prof. Zhu's wife, who gave me many practical advice when I was looking for a job. Also, her willingness to help and passion for life has enlighten me through my daily life.

Afterwards, I would like to express my gratefulness to the respected committee members, Professor Ranjan Mukherjee, Professor Zhaojian Li and Dr. Hussein Dourra, for their insightful comments and guidance with respect to my coursework and research work. Thanks to Professors Ranjan Mukherjee and Zhaojian Li for their excellent courses, which laid a solid foundation for my ongoing research and to Dr. Hussein Dourra for his plentiful experience and profound suggestions in the process of my research work.

I would also like to thank the ERC (engineering research court) community and my dear friends. The study atmosphere of ERC community is exceptional, which drives me continuously to surmount myself. Great appreciation shall be expressed to all the lab peers throughout these years. They are, Dr. Jie Yang, Dr. Ruitao Song, Dr. Yingxu Wang, Dr Yifan Men, Dr. Ruixue Li, Dr. Tianyi He,

Mr. Shen Qu, Mr. Anuj Pal, Mr. Jian Tang, Mr. Corey Gamache, Mr. Lingyun Hua, Mr. Yu He, Prof. Liang Liu, Prof. Xihong Zou, Dr. Donghao Hao, Mrs. Dawei Hu, and Mr. Haohao Wang. In addition, I would like to thank Mr. Zhuojun Yao, Dr. Pu Wang, and Mrs. Jing Huang for all the time we had enjoyed over the past few years and will be enjoying in the future.

Special appreciation and condolence shall be paid to Kobe Bryant, who has been motivating me over and over again throughout the tough time in the last decade. The inspiration from Mamba Mentality is invaluable lifelong fortune. In the real world, he faded away; but in my deep heart, legend never dies.

Last but not least, the gratitude from my deep soul shall be paid to my beloved family, without whom I would be nothing. Thanks to my beloved parents and two dearest sisters for their considerate attendance, unreservedly support and understanding. Thanks to my darling and lovely girl friend, Yulian Zhu, for making me to be a better and more responsible man. Your unselfish love means everything to me.

TABLE OF CONTENTS

LIST OF TABLES	x
LIST OF FIGURES	xi
CHAPTER 1 INTRODUCTION	1
1.1 Research Background	1
1.1.1 4-Wheel-Drive Vehicle Overview	1
1.1.2 4-Wheel-Drive Vehicle System Overview	2
1.2 Motivations	4
1.2.1 Necessity to Estimate Clutch Surface Friction Coefficient	4
1.2.2 Necessity to Estimate Clutch Touchpoint Displacement	5
1.2.3 Challenges to Estimate Clutch Torque	9
1.3 Contributions	10
1.3.1 Contributions of Touchpoint Estimation	10
1.3.2 Contributions of Clutch Traction Torque Estimation	11
1.3.3 Contributions of Clutch Friction Coefficient Estimation	12
1.4 Dissertation Outline	13
CHAPTER 2 MODEL-BASED ADAPTIVE TOUCHPOINT ESTIMATION WITH MOD- IFIED GENERAL KINETIC FRICTION MODEL	16
2.1 Overview	16
2.1.1 Chapter Organization	16
2.1.2 Review of Friction Modeling	17
2.2 Clutch Actuation System Modeling	18
2.3 Adaptive Estimation Algorithm Development	24
2.3.1 State-Space System Representation	24
2.3.2 Algorithm Development	25
2.3.3 Convergence Analysis	26
2.4 Preliminary Results and Discussion	28
2.5 Friction Model Development	30
2.5.1 Coulomb Friction Model	30
2.5.2 General Kinetic Friction Model	31
2.5.3 Modified General Kinetic Friction Model	34
2.6 Algorithm Evaluation and Validation	36
2.6.1 Two Acceleration Data Set Validation	37
2.6.2 Two Acceleration Data Validation with Trigger Condition	39
2.6.3 Multiple Acceleration Data Validation with Trigger Condition	43
2.6.4 Adaptiveness of the Adaptive Estimation Algorithm	44
2.7 Conclusions	45

CHAPTER 3	INTEGRATED TOUCHPOINT ESTIMATION AND POSITION TRACKING USING DEADBEAT ADAPTIVE BACKSTEPPING	46
3.1	Overview	46
3.1.1	Chapter Organization	46
3.1.2	Review of Backstepping Control	46
3.2	System Transformation for Backstepping Design	48
3.2.1	Parametric Semi-Strict Feedback Formulation	49
3.2.2	Discretized Parametric Semi-Strict Feedback Formulation	50
3.3	Deadbeat Adaptive Backstepping Algorithm Development	50
3.3.1	Non-Lyapunov-Function-Based Deadbeat Adaptive backstepping control design	50
3.3.2	Stability and Convergence Analysis	53
3.4	Results Performance Evaluation	58
3.4.1	Reference Signal: 2WD Case	59
3.4.2	Reference Signal: 4WD Case	62
3.5	Conclusions	63
CHAPTER 4	CLUTCH TORQUE MODELING AND VALIDATION UNDER VARIOUS CLUTCH OPERATION CONDITIONS	65
4.1	Overview	65
4.1.1	Chapter Organization	65
4.1.2	Review of Clutch Torque Estimation	66
4.2	Clutch Torque Model Flow Chart	68
4.3	Clutch Torque Modeling	69
4.3.1	Baseline Clutch Torque Model (CTM-1)	70
4.3.1.1	Tire dynamics	70
4.3.1.2	Vehicle Speed Model	71
4.3.1.3	Effective Tire Radius Model	73
4.3.2	Overtaken-Clutch Torque Model (CTM-2)	75
4.3.3	Slip-Clutch Torque Model (CTM-3)	76
4.4	Overtaken-Clutch Torque Model Validation	78
4.4.1	Overtaken-Clutch Torque Results with CTM-1	78
4.4.2	Overtaken-Clutch Torque Results with CTM-2	79
4.4.3	Rear Effective Tire Radius Analysis	84
4.5	Slip-Clutch Torque Model Validation	84
4.5.1	Slip-Clutch Torque Results with CTM-2	85
4.5.2	Slip-Clutch Torque Results with CTM-3	86
4.6	Conclusions	88
CHAPTER 5	CLUTCH TORQUE ESTIMATION USING AN EXTENDED KALMAN FILTER WITH UNKNOWN INPUT	90
5.1	Overview	90
5.1.1	Chapter Organization	90
5.1.2	Review of Unknown input Observer	91
5.2	4WD Vehicle Propulsion System Model	92

5.2.1	Tire dynamics	92
5.2.2	Vehicle Speed Model	93
5.2.3	Effective Tire Radius Model	95
5.3	System Transformation	95
5.4	Extended Kalman Filter based Unknown Input Observer	96
5.5	Experiment Validation	99
5.5.1	Model Initialization	100
5.5.2	Overtaken-clutch Torque Estimation Validation	101
5.5.3	Slip-clutch Torque Estimation Validation	106
5.6	Conclusion	108
CHAPTER 6	CLUTCH FRICTION COEFFICIENT ESTIMATION VIA ADAPTIVE RECURSIVE LEAST-SQUARE LOOKUP TABLE	109
6.1	Chapter Overview	109
6.1.1	Chapter Organization	109
6.1.2	Review of Adaptive Lookup Table	110
6.2	Clutch Surface Friction Coefficient Model	111
6.3	Real-time Recursive Least-Squares Adaptive Lookup Table	112
6.3.1	Recursive Least-Squares based Adaptive 1-D Lookup Table Algorithm	112
6.3.2	General 1-D Adaptive Table Structure	113
6.3.3	RLS Adaptive Table Algorithm	114
6.3.4	Complete Road Map of Friction Coefficient Estimation	116
6.4	Result Evaluation	116
6.5	Conclusion	120
CHAPTER 7	CONCLUSIONS AND FUTURE WORK	121
7.1	Conclusions	121
7.2	Recommendation for Future Work	122
APPENDIX	124
BIBLIOGRAPHY	127

LIST OF TABLES

Table 2.1: Estimation trigger conditions	40
Table 2.2: Touchpoint Estimation Results Comparison	44
Table 3.1: DC Motor Parameters	58
Table 4.1: Parameters of targeted vehicle	79
Table 4.2: Estimation error summary	88
Table 5.1: Overtaken-estimation error summary	105
Table 6.1: Pseudo code of Thomas Algorithm	115

LIST OF FIGURES

Figure 1.1: 4WD vehicle market share	1
Figure 1.2: 4WD vehicle propulsion system	2
Figure 1.3: Energy and load flow of 4WD vehicle	4
Figure 1.4: Typical relationship between clutch normal force and actual displacement	6
Figure 1.5: Clutch touchpoint variation diagram	7
Figure 1.6: Clutch torque profile change vs. touchpoint displacement variation x_0	8
Figure 1.7: Current scheme for actual displacement control	11
Figure 1.8: Dissertation overview	13
Figure 2.1: Chapter organization overview	16
Figure 2.2: Transfer case clutch actuation system	18
Figure 2.3: Cam and following-cam mechanism	20
Figure 2.4: Cam profile	20
Figure 2.5: Free body diagram of the ball	23
Figure 2.6: Adaptive estimation diagram	25
Figure 2.7: Touchpoint x_0 estimation results without friction. (a) applied input voltage of the clutch actuation system, (b) measured cam position, (c) estimated touchpoint x_0	29
Figure 2.8: Graphical illustration of Coulomb friction model	31
Figure 2.9: Performance evaluation of Coulomb Friction. (a) measured ball velocity. (b) Coulomb Friction	32
Figure 2.10: Graphical illustration of GKF model	32
Figure 2.11: Friction force using GKF model	33

Figure 2.12: Graphical illustration of MGKF model	34
Figure 2.13: Friction Force using MGKF model	35
Figure 2.14: Performance evaluation of MGKF model. (a) clutch Δ rpm; (b) ball velocity; (c) estimated x_0 with MGFK model	35
Figure 2.15: Touchpoint x_0 estimation results without friction. (a) input voltage (b) output ball position	37
Figure 2.16: Two acceleration data validation, the plots are corresponding to (a) vehicle speed (b) clutch actuation input voltage (c) ball position	38
Figure 2.17: Two acceleration data validation, the plots are corresponding to (a) clutch Δ rpm (b) ball velocity (c) estimated touchpoint displacement x_{ct}	39
Figure 2.18: Two acceleration data validation, results for the first acceleration, the plots are corresponding to (a) clutch Δ rpm (b) ball velocity (c) estimated touchpoint displacement x_{ct}	40
Figure 2.19: Two acceleration data validation with trigger condition, the plots are corre- sponding to (a) vehicle speed (b) trigger condition (c) estimated touchpoint displacement x_{ct}	41
Figure 2.20: Two acceleration data 1 validation with trigger condition, the plots are corre- sponding to (a) vehicle speed (b) trigger condition (c) estimated touchpoint displacement x_{ct}	42
Figure 2.21: Two acceleration data 2 validation with trigger condition, the plots are corre- sponding to (a) vehicle speed (b) trigger condition (c) estimated touchpoint displacement x_{ct}	42
Figure 2.22: Multiple acceleration data validation with trigger condition	43
Figure 2.23: Demonstration of Adaptiveness of Adaptive Estimation Algorithm	44
Figure 3.1: Chapter organization overview	46
Figure 3.2: Transfer case clutch actuation system	48
Figure 3.3: Comparison of canonical and deadbeat designs	58
Figure 3.4: Tracking for deadbeat design	59
Figure 3.5: Tracking for canonical design	59

Figure 3.6: States for deadbeat design	60
Figure 3.7: States for canonical design	61
Figure 3.8: Unknown term estimation	61
Figure 3.9: Control effort	62
Figure 3.10: Reference tracking	62
Figure 3.11: Closed-loop States estimation	63
Figure 3.12: Control effort for 4WD case	63
Figure 4.1: Chapter organization overview	65
Figure 4.2: 4WD vehicle system overview	68
Figure 4.3: Clutch torque estimation flow chart	69
Figure 4.4: Longitudinal force vs slip ratio	71
Figure 4.5: Vehicle Free Body Diagram	72
Figure 4.6: Tire radius diagram	74
Figure 4.7: Clutch torque results with CTM-1 under clutch overtaken condition: (a) Vehicle speed estimation; (b) Clutch slip Δr_{pm} ; (c) Brake pedal status; (d) Clutch torque result.	80
Figure 4.8: Clutch torque results with CTM-2 under clutch overtaken condition: (a) Vehicle longitudinal acceleration; (b) Front effective tire radius comparison; (c) Vehicle speed estimation; (d) Clutch torque result.	81
Figure 4.9: Error analysis under clutch overtaken condition: (a) Absolute error; (b) Relative percentage error.	82
Figure 4.10: Other data sets torque validation: (a) Data 2 validation; (b) Data 3 Validation.	83
Figure 4.11: Influence of rear effective tire radius compensation with CTM-2 under clutch overtaken condition on clutch torque estimation: (a) Rear effective tire radius with different compensation coefficients; (b) Clutch torque with different compensation coefficients.	85

Figure 4.12: Clutch torque results with CTM-2 under clutch slip condition: (a) Vehicle speed estimation; (b) Clutch slip speed Δrpm ; (c) Torque result.	86
Figure 4.13: Clutch torque results with CTM-3 under clutch slip condition: (a) Vehicle speed estimation; (b) Torque result.	87
Figure 4.14: Error analysis under clutch slip condition: (a) Absolute error; (b) Relative percentage error.	87
Figure 5.1: Chapter organization overview	90
Figure 5.2: 4WD vehicle propulsion system architecture	93
Figure 5.3: Longitudinal force vs slip ratio	94
Figure 5.4: Estimation Algorithm Diagram	96
Figure 5.5: EKF-UIO Estimation Flow Diagram	100
Figure 5.6: Known input u_2 for data set 1	101
Figure 5.7: Estimated system states \hat{x} for data set 1	102
Figure 5.8: Front tire slip ratio and estimated system unknown input \hat{u}_1 for data set 1	103
Figure 5.9: Estimated system unknown input \hat{u}_1 for data set 2	104
Figure 5.10: Estimated system unknown input \hat{u}_1 for data set 3	104
Figure 5.11: Known input and clutch Δrpm	106
Figure 5.12: Estimated states under clutch slip condition	107
Figure 5.13: Estimated unknown input under slip condition	108
Figure 6.1: Real-time μ_c estimation flow	109
Figure 6.2: Clutch disk section view	111
Figure 6.3: Illustrative diagram of 1-D lookup table	112
Figure 6.4: Structure of $R(t)$	115
Figure 6.5: Real-time μ_c estimation road map	116

Figure 6.6: Clutch Torque and Associated Signals	117
Figure 6.7: Adaptive table nodes convergence vs. time	118
Figure 6.8: Adaptive table nodes convergence vs. Δrpm	118
Figure 6.9: 3D convergence view	119
Figure 6.10: μ_c obtained from adaptive lookup table	119
Figure 6.11: Torque estimation obtained from adaptive lookup table	120

CHAPTER 1

INTRODUCTION

1.1 Research Background

1.1.1 4-Wheel-Drive Vehicle Overview

Traditional internal combustion engine-powered vehicles, especially 4-Wheel-Drive (4WD) vehicles [1], [2], [3] still play an important role in automotive industry (see Figure 1.1) due to its excellent ability to switch between 2-Wheel-Drive (2WD) for improved fuel economy [4], [5] and 4WD for optimal traction performance [6], [7]. This switch is usually accomplished by controlling the vital component, transfer case clutch [8], [9], of the vehicle propulsion system.

However, it is necessary to have accurate transfer case clutch output torque through either measurement or estimation for closed loop control. As a matter of fact, the clutch output torque is related to several clutch parameters such as clutch friction coefficient, touchpoint displacement, and so on. In practice, these parameters are time-varying and/or parameter dependent. Due to the fact that direct measurements are impossible due to high sensor cost and low sensor reliability, it is imperative to develop estimation algorithms to obtain these parameters for accurate clutch output torque control.



Figure 1.1: 4WD vehicle market share

1.1.2 4-Wheel-Drive Vehicle System Overview

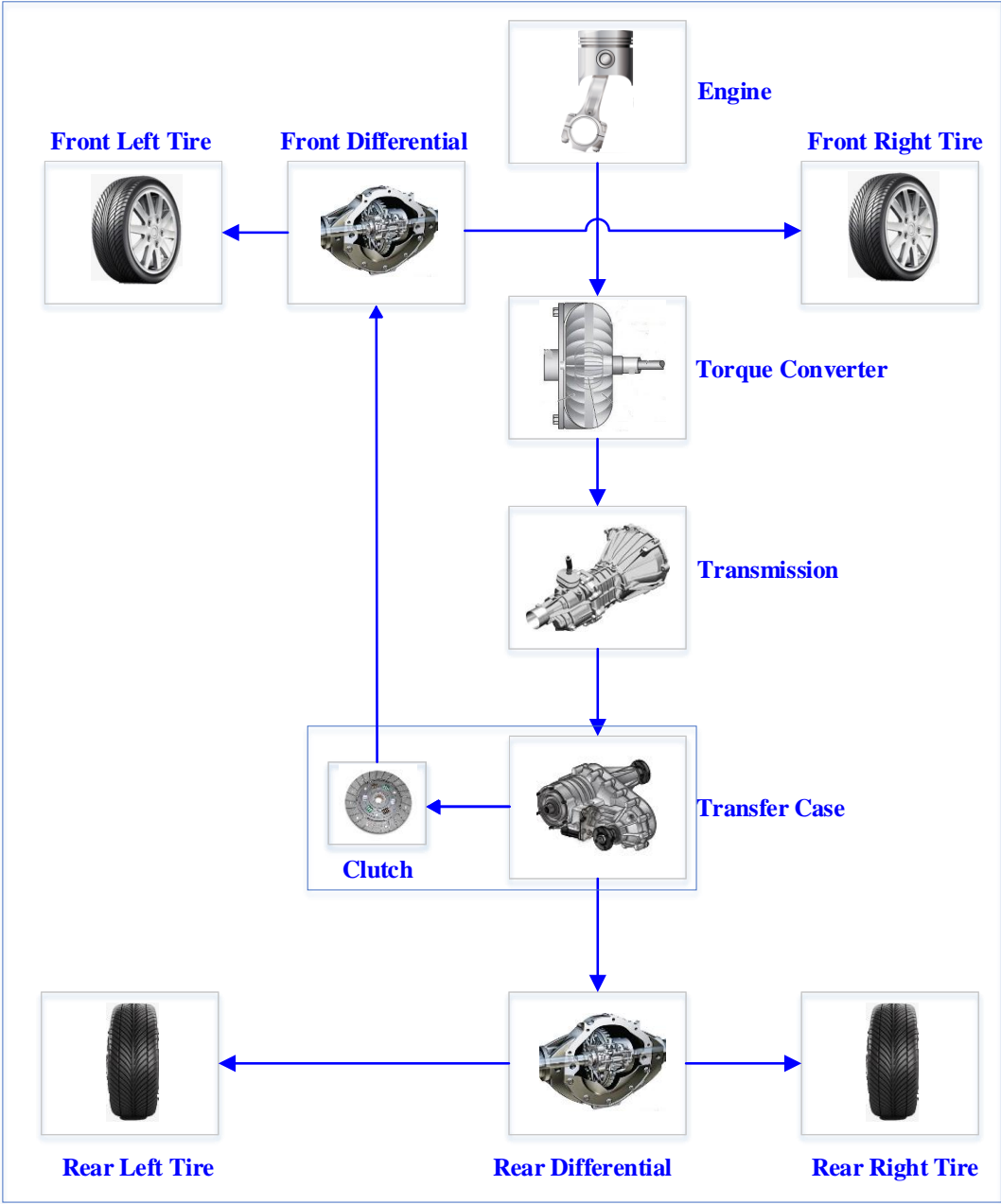


Figure 1.2: 4WD vehicle propulsion system

Figure 1.2 shows a typical 4WD vehicle propulsion system architecture, which includes the main components such as engine, torque converter, transmission, transfer case, clutch, differentials, front and rear tires, and vehicle body [10], [11]. The driving power of the entire vehicle originates

from the internal combustion engine that generates mechanical energy by combustion of air-fuel mixture [12], [13]. The torque converter [14], in replace of a mechanical clutch in a manual transmission system, multiples output torque from engine and generates driving for the vehicle propulsion system, and thus is the first bridge between power source and the propulsion system. The transmission [15] then sends amplified (or reduced) torque from the torque converter to the transfer case according to the selected gear determined by the vehicle electric control unit, and at the same time adjusts the rotational speed to a desired and safe level.

And then comes to the transfer case, a vital component of the 4WD vehicle. On one hand, it controls the switch between 2WD and 4WD modes by engaging and disengaging the transfer case clutch. Particularly, if the transfer case clutch is disengaged, the torque will be transmitted to rear wheels only and the vehicle will be in the two-wheel-drive (2WD) mode; while if the clutch is engaged, the torque will be distributed to all wheels based on the desired torque distribution ratio [16], thus in this case the vehicle is in the four-wheel-drive (4WD) mode. That is, the transfer case clutch manages the torque distribution between front and rear tires when the vehicle is in the 4WD mode. Normally, the reference torque distribution ratio is generated by the vehicle control module according to the driver's command. Since the engine torque can be estimated at any given instance, a corresponding reference clutch torque (or front torque) is generated. Due to the fact that the clutch torque is proportional to the clutch displacement [15], [17], it is intuitively that the actual clutch torque can be controlled by controlling the actual clutch displacement. As a results, the torque distribution ratio between front and rear tires can be controlled.

The front and rear differentials, which connects the tires with transfer case, split the torque and at the same time changes the torque direction perpendicularly to drive the vehicle.

Therefore, the energy and load flow of a 4WD vehicle can be summarized in Figure 1.3. As discussed before, the powertrain torque comes from the engine combustion process, it transmits through the propulsion components and eventually to the vehicle body, and the resulting torque moves the vehicle. Meanwhile, once the vehicle moves, the vehicle load and vehicle speed flow backward to the engine in terms of torque load.

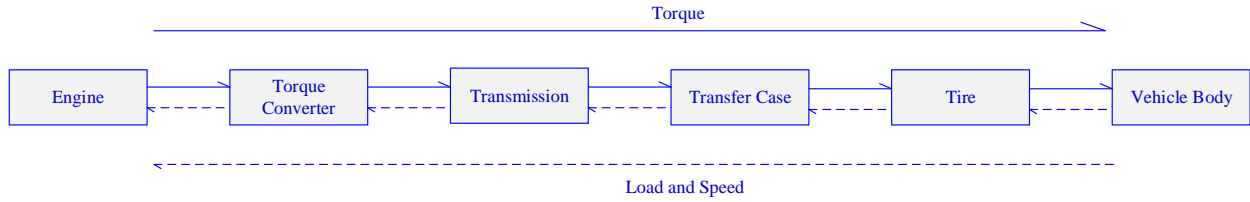


Figure 1.3: Energy and load flow of 4WD vehicle

1.2 Motivations

1.2.1 Necessity to Estimate Clutch Surface Friction Coefficient

In this research work, one of the goals is to estimate the clutch surface friction coefficient [18], [19] so that accurate clutch torque control, or equivalently torque distribution ratio between front and rear tires, can be achieved. In fact, a well-known approach to calculate the clutch torque [17] at clutch level is to relate the clutch torque with the clutch geometry parameters when the clutch is engaged and it can be described mathematically below.

$$T_c = n_c \mu_c F_N r_{eff} \quad (1.1)$$

where T_c is the clutch torque; μ_c is the friction coefficient; n_c is the number of clutch engaging surfaces and r_{eff} is the effective clutch radius, both of which would be constant for a given clutch assembly; and F_N is the clutch normal force proportional to the effective clutch displacement to be discussed later.

In general, the clutch surface friction coefficient is assumed to be a known constant for the given clutch material and surface condition, in this case, the clutch torque can be controlled by controlling the clutch normal force, or equivalently clutch displacement. However, the constant assumption of clutch surface friction coefficient may not be practical, since the friction coefficient may be affected by various factors. For example, it may be affected by clutch wear, since with the clutch operating along its life span, each engagement of clutch driving and driven disks would introduce certain wear, leading to change of effective clutch engagement displacement. This effect would possibly result in an increase of the touchpoint displacement and change of friction coefficient (especially

for a new, green clutch). Also, while the clutch is engaging, the speed difference between the clutch driving and driven disks may also have an impact on the friction coefficient according to empirical experience. Furthermore, engagement of clutch will inevitably increase the clutch temperature when the clutch is slipping, and the thermal effect of clutch pack [20], [21], [22] is very likely to change the clutch surface friction coefficient. In summary, a constant friction coefficient may be reasonable for a fixed operational condition, while for practical applications, the actual friction coefficient may deviate from its initial constant. This motivates to estimate the clutch surface friction coefficient in real-time, considering various factors.

As a matter of fact, an approach to estimate the friction coefficient is to rearrange the well-known equation (1.1) to the following:

$$\mu_c = \frac{T_c}{n_c F_{Nr_{eff}}} \quad (1.2)$$

However, with the friction coefficient becomes unknown, the clutch torque will no longer be available according to the well-known equation (1.1). Therefore, an estimation algorithm for clutch torque beyond clutch level becomes imperative, the challenges of estimating the clutch torque will be discussed in Section 1.2.3. Another yet important aspect to reach the estimation of the friction coefficient is to obtain the clutch normal force, and this will be discussed next in Section 1.2.2.

1.2.2 Necessity to Estimate Clutch Touchpoint Displacement

As mentioned in the last Section, the clutch normal force is proportional to the effective clutch displacement. Strictly, since the effective clutch displacement consists of actual clutch displacement and clutch touchpoint displacement, the clutch normal force will be a piecewise continuous function of the actual clutch displacement according to empirical data shown in Figure 1.4 according to reference [15], which shows a typical relationship between the clutch normal force and clutch displacement. The piecewise function can be expressed as

$$F_N = \begin{cases} 0, & x_a \leq x_{c0} \\ k_c(x_a - x_{c0}), & x_a > x_{c0} \end{cases} \quad (1.3)$$

where k_c is the clutch stiffness (or the multiplication factor); x_a is the actual clutch displacement; and x_{c0} is the designed nominal clutch touchpoint displacement. When the actual clutch displacement x_a is less than nominal touchpoint displacement, there is no force generated; while when the actual clutch displacement is greater than the nominal touchpoint displacement, the clutch normal force is proportional to the effective clutch displacement ($x_a - x_{c0}$).

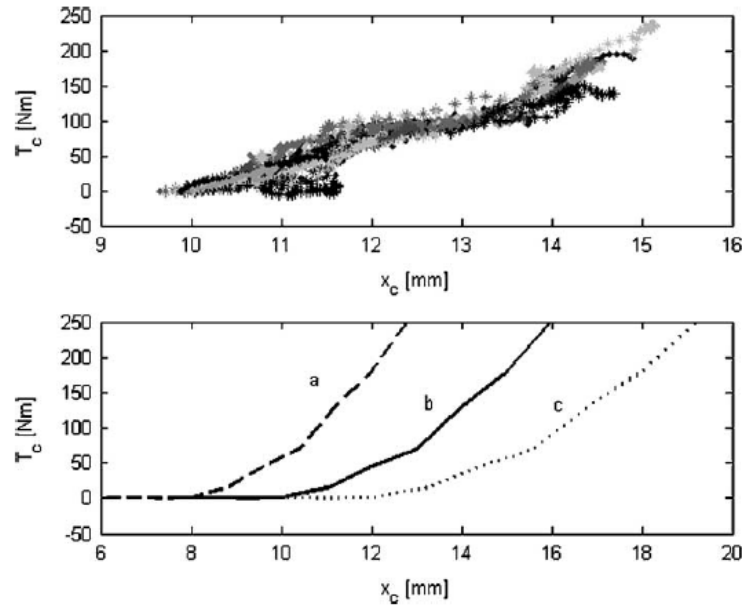


Figure 1.4: Typical relationship between clutch normal force and actual displacement

Currently, the actual clutch displacement is controlled using a PID (proportional-integral-derivative) control scheme to track the desired clutch position, therefore, once the reference position is given, the actual clutch displacement is usually available. However, the trick lies in the clutch touchpoint displacement. For a given clutch, the touchpoint is first designed as a constant, x_{c0} , introduced in equation (1.3). A more intuitive relationship can be observed from the upper portion of Figure 1.5, which shows the ideal case or initial design of the touchpoint displacement.

However, in reality, this touchpoint displacement varies due to plenty of reasons. First of all, a most obvious factor is the clutch wear. Due to the increased number of clutch engagement, clutch wear will decrease the clutch pack thickness, which directly increases the touchpoint displacement. Note that this process is slow since the clutch wear rate is relatively slow. Secondly, the clutch

actuation system components part-to-part variation (or component parameter uncertainties) may affect the final controlled actual clutch displacement, and this will indirectly affect the touchpoint position. Furthermore, factors such as clutch temperature variation will also affect the touchpoint displacement due to thermal expansion. In summary, similar to the clutch surface friction coefficient, a constant assumption of clutch touchpoint displacement is not realistic either.

Therefore, as shown in Figure 1.5, for practical applications, a varying touchpoint displacement is considered to compensate for the factors discussed above. The total touchpoint displacement x_{ct} would now become the sum of nominal touchpoint displacement and the touchpoint variation displacement ($x_{c0} + x_0$).

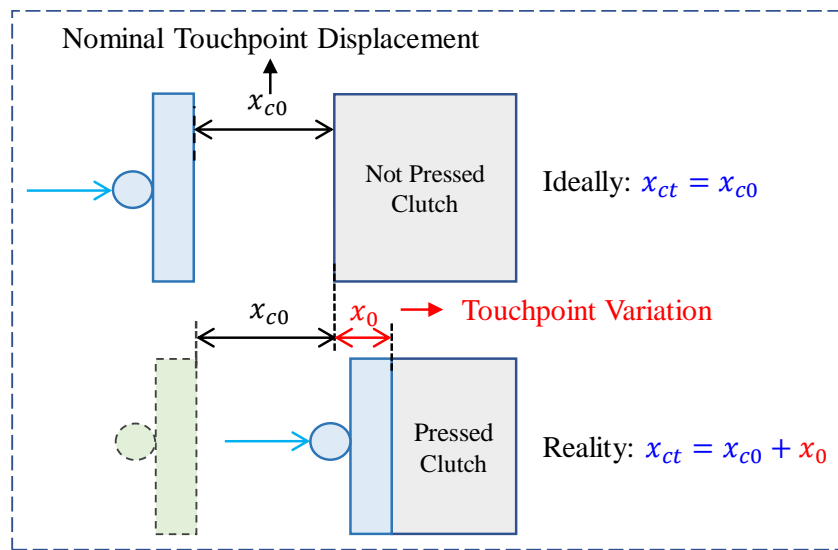


Figure 1.5: Clutch touchpoint variation diagram

Figure 1.6 shows the influence of touchpoint variation displacement on the clutch torque. For the ideal design, the clutch torque is initiated when the clutch actuator displacement reaches x_{c0} , and then it increases almost linearly as a function of effective clutch displacement ($x_c - x_{c0}$). However, with the influence of the touchpoint variation x_0 as discussed above, the initial point of clutch torque generation will be delayed by the displacement of x_0 . Therefore, in this case, the clutch torque is initiated when the clutch actuator displacement reaches to the level of $x_{c0} + x_0$, and with further increase of the actuator displacement, the torque is linearly proportional to the effective

actuator displacement ($x_c - x_{c0} - x_0$). In this way, it is obvious that without compensating the touchpoint variation displacement x_0 , the actual clutch torque will deviate from the desired clutch torque. Therefore, a real-time estimation and compensation of touchpoint variation displacement x_0 (or total touchpoint displacement ($x_{ct} = x_{c0} + x_0$)) is imperative for accurate clutch torque control.

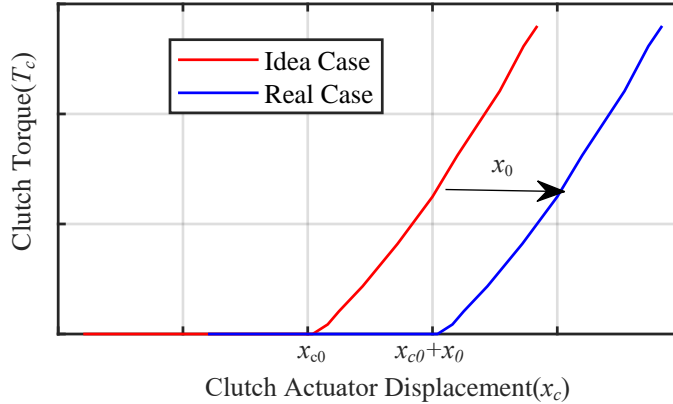


Figure 1.6: Clutch torque profile change vs. touchpoint displacement variation x_0

The challenge lies in the fact that once the clutch is mounted to the transfer case, there is no measurement available to measure the touchpoint variation. An existing scheme used to estimate the touchpoint displacement is called direct detection method. Note that when the clutch actuation displacement passes the touchpoint, there will be a sudden change in clutch output torque, which is further transmitted to the vehicle axle, causing changes in wheel speed. The direct detection method detects the output torque changes from wheel speed variations and uses it to detect clutch touchpoint displacement. However, this change could be relatively small, making it challenge to detect. Also, the wheel speed change could be caused by other factors such as potholes on the road, leading to unreliable estimation. Therefore, a new touchpoint estimation algorithm in real-time is necessary.

Once the touchpoint displacement is estimated, combining with the controlled actual clutch displacement, the clutch normal force will be available, which forms a foundation for estimation of clutch surface friction coefficient.

1.2.3 Challenges to Estimate Clutch Torque

As described in Section 1.2.1, since the clutch surface friction coefficient is changing overtime due to many factors, it becomes unknown in real-time, which renders the clutch torque to be also unknown in the clutch level by equation (1.1). Therefore, it is necessary to estimate the clutch torque from a different perspective.

Recall the propulsion system architecture shown in Figure 1.1.2, under the condition of clutch engagement, the generated clutch torque will be transmitted through the front differential and finally drive the front tires. Therefore, an obvious solution for obtaining the clutch torque is to establish the tire dynamics [23] so that the driving torque can be solved. The well-known tire dynamics formula is:

$$T_f i_{fd} = J_f \dot{w}_f + F_f r_f \quad (1.4)$$

where J_f is the total front tire inertia; w_f is the front tire rotational speed; i_{fd} is the front differential ratio; F_f is the front tires longitudinal force relating with the vehicle speed and effective tire radius; and r_f is the effective tire radius.

However, there are several challenges while estimating the clutch torque from the tire dynamics. The first challenge lies in the effective tire radius. In many references, the effective tire radius is assumed to be constant [24]. This assumption may be valid in the case when vehicle is coasting down or static. While when the vehicle is braking or accelerating, due to the pitch motion of the vehicle, the fact is that the center of gravity of the vehicle may change, leading to the redistribution of front and rear tire normal forces. Once the normal forces changes, the effective tire radius changes. Of course the constant effective tire radius assumption does not consider this effect. Furthermore, the tire pressure may also contribute to the change of effective tire radius. In fact, the tire can always be viewed as a mass-spring-damper system, and the tire pressure is closely related to the equivalent spring stiffness. Different tire pressures results in different stiffness, therefore, leading to a varying effective tire radius.

The second challenge goes to the vehicle speed. Although vehicle longitudinal acceleration can be measured using an accelerometer with reasonable accuracy, the vehicle longitudinal speed

obtained from direct integration of longitudinal acceleration is usually inaccurate due to accelerometer drift. On the other hand, the target vehicle used in this research does not equip with the vehicle speed measurement devices such as GPS (global position system), making it difficult to estimate the torque. In view of this, a new vehicle speed estimation method needs to be developed.

The third challenge lies in the clutch status. Unlike 2WD vehicles, whose driving mode is fixed, and there is no switch between driving modes. This research uses a 4WD vehicle, and its transfer case clutch is in charge of the mode switch between 2WD and 4WD mode. Note that the clutch have different operation status: disengaged (open) and engaged (including slip and overtaken). For a disengaged clutch, there is no torque transmitted. However, for an engaged clutch, the clutch may be slipping or overtaken. When the clutch is overtaken, the propulsion system connection between wheels and transmission is solid; while when the clutch is slipping, the connection between front wheels and transmission through the transfer case clutch is not solid, and the clutch slip affects the front tire speed, which changes the vehicle dynamics, and as result, different estimation model is required.

1.3 Contributions

With the motivations broken down in Section 1.2, the contributions of this dissertation solves the problems presented in Section 1.2, respectively. It can be discussed mainly in the following three aspects: touchpoint estimation, clutch/traction torque estimation, and clutch surface friction coefficient estimation.

1.3.1 Contributions of Touchpoint Estimation

The touchpoint displacement is related to the actual clutch displacement closely when calculating the clutch normal force. As a matter of fact, the current method controls the actual clutch displacement and estimates the touchpoint displacement separately. Figure 1.7 shows a diagram of current method, where the actual clutch displacement is controlled by three PID control loops, while the touchpoint estimation is fulfilled by the aforementioned direct detection method.

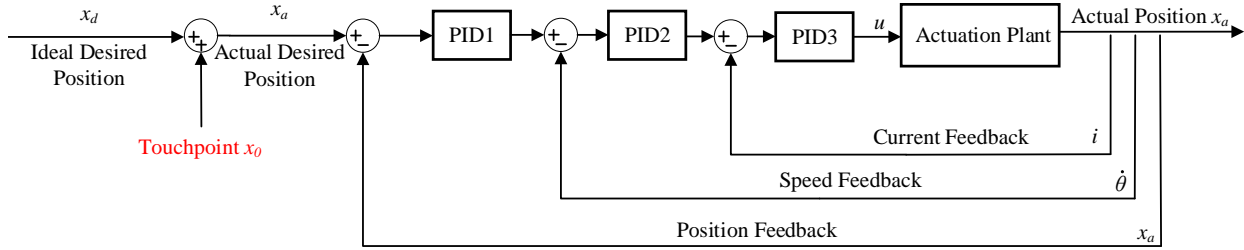


Figure 1.7: Current scheme for actual displacement control

My contributions of touchpoint displacement estimation are two-fold:

1. Preserving the current separated approach with three PID control loops, an adaptive estimation algorithm [13] of touchpoint displacement is proposed and validated experimentally with improved accuracy and robustness comparing with the existing direct detection method.
2. An integrated method based on the deadbeat adaptive backstepping design [25] that achieves simultaneously tracking the desired position and estimating the touchpoint displacement is proposed. On one hand, this method controls the clutch displacement and estimates its touchpoint displacement using only one control scheme; and on the other hand, this method reveals potential cost reduction.

1.3.2 Contributions of Clutch Traction Torque Estimation

For the clutch torque estimation, this dissertation first proposes the clutch output torque modeling in response to those challenges discussed before for model-based estimation.

1. Instead of using the constant effective tire radius assumption, this dissertation proposes to relate the effective tire radius to the vehicle acceleration to compensate for the pitch motion of vehicle and tire pressure to deal with the variation of tire stiffness. This method turns out to have a relative accurate effective tire radius with simple mathematical model for real-time applications.

2. Instead of considering complex vehicle dynamics, this dissertation proposes to use a simple bicycle vehicle body dynamics along with the longitudinal tire forces to estimate the vehicle speed based on the time-varying effective tire radius.
3. Considering the first two modifications, the clutch torque under clutch overtaken condition can be estimated accurately, however, this model does not apply to the situation when the clutch slips. Therefore, a slip speed compensation is proposed to the front tires to deal with the slip effect. And the modified model is able to estimate the clutch torque accurately under slip condition.

Furthermore, since modeling approach may suffer to measurement and processing noises, which will have adverse impact on clutch output torque estimation, this dissertation also proposes an Extended Kalman Filter based estimation algorithm. Note that this estimation utilizes the model developed from the clutch output torque modeling approach, which is further transformed to a system with unknown input. The Extended Kalman Filter with unknown input is then applied for the estimation with improved accuracy and reliability.

1.3.3 Contributions of Clutch Friction Coefficient Estimation

Lastly, with the clutch touchpoint and output torque estimated, equation (1.2) can be utilized to obtain the clutch surface friction coefficient.

1. This resulted friction coefficient will be time-varying, which is more practical comparing with the traditional constant assumption. Note that this friction coefficient is clutch-parameter-dependent, meaning that it is necessary to be updated based on clutch touchpoint and output torque.
2. To avoid this inconvenience, a clutch-parameter-independent approach based on adaptive lookup table is proposed. This table parameterize the friction coefficient as a function of clutch slip speed Δrpm (a function of tire rotational speeds). The table is adaptively updated use a real-time implementable Recursive Least-Squares Algorithm.

1.4 Dissertation Outline

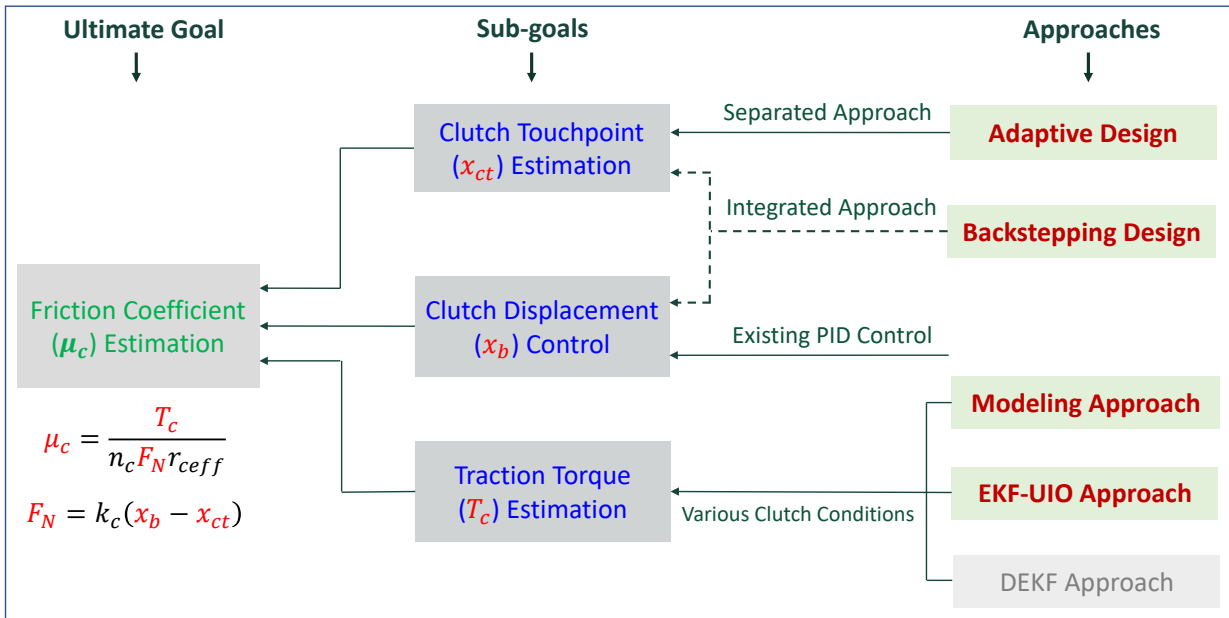


Figure 1.8: Dissertation overview

Figure 1.8 depicts an overview of this dissertation, an estimation model for clutch surface friction coefficient is proposed, which includes mainly three parts: touchpoint distance estimation, desired clutch displacement control and tires traction force estimation. The touchpoint distance can be estimated using the adaptive estimation algorithm which is independent of the desired clutch displacement control using the existing PID control scheme, or an integrated control scheme achieving the touchpoint estimation and desired clutch displacement tracking simultaneously with the deadbeat adaptive backstepping technique can be used. Lastly, the traction force estimation is performed under different clutch operation conditions. More specifically, the dissertation is organized as follows:

Chapter 2 retains the separated PID scheme and proposes the adaptive estimation algorithm for touchpoint displacement estimation. Specifically, the clutch actuation system is first modeled based on the physical clutch actuation system; and based on the model, the adaptive estimation algorithm using the normalized gradient method is developed; However, the preliminary simulation study does not conceive a promising estimation results, which motivates to the investigation of the

friction between the clutch ball and ball ramp while the actuation system is active; The simple Coulomb Friction model and the widely used General Kinetic Friction model are first investigated, which turns out to be deficient to depict the friction force in the actual system. And then, the modification was made to the General Kinetic Friction model to have the Modified General Kinetic Friction model, which eventually proves to be accurate, and is therefore adopted in the following simulations. Then comes to the validation of proposed algorithm with various experiment data and the comparison of touchpoint estimation with the direct detection method, which shows the improved accuracy and robustness over the existing method.

Chapter 3 discards the separated scheme and uses an integrated scheme to achieve the reference position tracking and touchpoint displacement estimation simultaneously. To be more specific, the two goals are accomplished by utilizing the deadbeat adaptive backstepping technique. The system transformation is first performed to reach the discretized parametric semi-strict feedback form in preparation for the design; Then, the design procedures are carried out so that the estimation algorithm and the control law are designed. The stability of closed-loop system are guaranteed by the dead-beat design, and the convergence analysis shows that this design provides the fastest response possible. Finally, the estimation results under different vehicle operational modes show the validity of the proposed algorithm.

In Chapter 4, the traction torque estimations under various clutch conditions are performed. First, a nominal clutch torque estimation model is developed. In this model, the effective tire radius is only related to the tire pressure, but not to the vehicle acceleration, and the vehicle speed estimation is also presented. However, this model fails to accurately estimate the clutch torque. Therefore, the vehicle acceleration compensation to the effective tire radius is proposed to deal with the torque estimation under clutch overtaken condition, and this proves to be accurate. However, when it comes to estimating the torque under clutch slip condition, the first two models are failed, which motivates to the slip speed compensation to the front tires, leading to the promising clutch torque estimation.

In Chapter 5, the Extended Kalman Filter with unknown input algorithm is proposed to estimate

the traction torque dealing with measurement and processing noises. First, based on the clutch torque model proposed in Chapter 4, an integrated clutch output torque estimation model is summarized; Then, the model is transformed into a third order nonlinear system model with unknown input; The Extended Kalman Filter with unknown input is applied for the torque estimation, which results improved estimation accuracy in terms of Absolute Mean Square Error and Relative Mean Square Error.

In Chapter 6, based on the estimated clutch touchpoint and output torque, a clutch-parameter-dependent time-varying friction coefficient is calculated. Furthermore, a clutch-parameter-independent friction coefficient is proposed for obtaining clutch output torque for closed-loop control in the future. This is done by adaptively updating the lookup table using the Recursive Least-Square algorithm. The friction coefficient from the lookup table is close to the clutch-parameter-dependent friction coefficient, and more importantly, the resulted clutch output torque also matches with the estimated clutch output torque.

Chapter 7 draws the conclusion based on the work presented in Chapters 2, 3, 4, 5 and 6, and proposes future work.

CHAPTER 2

MODEL-BASED ADAPTIVE TOUCHPOINT ESTIMATION WITH MODIFIED GENERAL KINETIC FRICTION MODEL

2.1 Overview

2.1.1 Chapter Organization

Figure 2.1 shows the overview of this chapter. Particularly, the work in this dissertation starts with the physical clutch actuation system. A clutch actuation system model based on physical system can be established, which is shown as the modeling process in the figure. In the clutch actuation system, the touchpoint variation displacement is an unknown parameter, and since the control voltage and the cam position of the physical system can be measured, an adaptive estimation algorithm is proposed to estimate it, which is shown in the algorithm development process. While estimating, the friction in the actual system is found to be an essential acting force, which leads to the development of friction model. Among the discussed friction models, the modified friction model turns out to be accurate and is finally adopted. The last part of this chapter shows the validation of the algorithm and the comparison results between the proposed algorithm and current direct detection method [26].

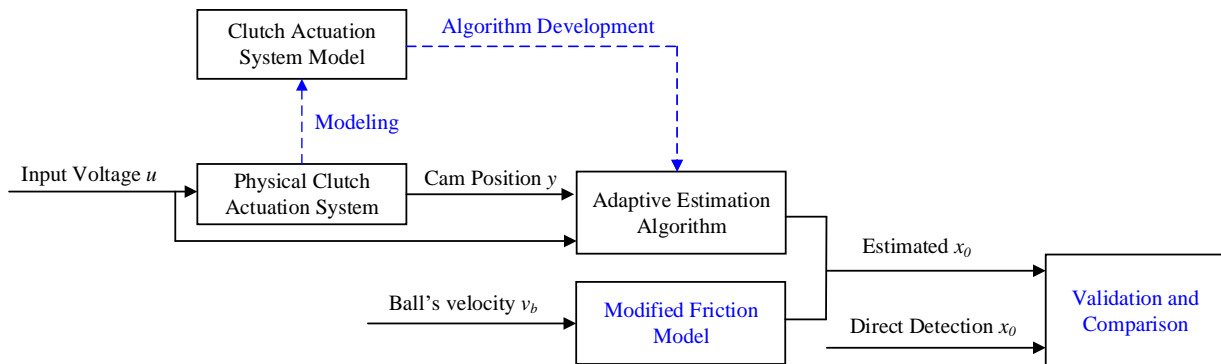


Figure 2.1: Chapter organization overview

2.1.2 Review of Friction Modeling

While modeling a physical system, one fundamental aspect is to take into consideration of the friction effect [27, 28] and a lot of research has been conducted in this area. The simplest friction model is the classical Coulomb friction [29] model, where the friction is modeled as a constant force in the direction opposite to the motion speed. Another simple model, the Viscous friction, is first proposed in fluid dynamics [30], stating that the friction force is positively proportional to the motion speed. A widely used friction model is the combination of Coulomb and Viscous frictions to reduce modeling error. Reference [31] designed sliding-mode controllers for self-balancing yaw motion of a two-wheel inverted pendulum utilizing both Coulomb and Viscous frictions compensations and validated it experimentally. Reference [32] performed experimental studies for measuring Coulomb and Viscous frictions using high-precision velocity sensors. However, the combined Coulomb and Viscous model fails to account for other friction behaviors. One such effect is called Stiction friction [33] defined as the initial force (or torque) to overcome to move an object from its stationary position, and this force is usually greater than the Coulomb friction. Another effect is the Stribeck effect [34], where the friction force decreases as the velocity increases from zero. A thorough combination of all the four friction effects has been referred as the General Kinetic Friction (GKF) or Stribeck friction model, where the detailed mathematical model can be found in Section IV. In [35], an observer was designed to estimate the effect of the Stribeck friction and compensate it. Reference [36] modeled the friction using the Stribeck friction formulation for a hydraulic valve actuator. However, the main problem of the aforementioned model is the discontinuity when the motion velocity crosses zero. Although replacing the infinite slope line at zero-velocity with a finite but steep slope line is often adopted to overcome the discontinuity, it does not capture the static friction characteristics. Actually, due to the existence of measurement noise, the measured velocity will not be exactly zero, which makes the aforementioned friction model can hardly capture the static friction. Therefore, this dissertation proposes a Modified General Kinetic Friction (MGKF) model, where when the absolute speed is smaller than or equal to a calibrated value, the friction is assumed to be static and equal to the external force, and when the absolute

speed is greater than the calibrated value, the friction is kinetic and follows the GKF model. It is noted that there will be no discontinuity in this model.

2.2 Clutch Actuation System Modeling

The transfer case clutch actuation system model is established based on the physical clutch actuation system. However, due to the confidential requirement of the project sponsor, the picture of physical clutch actuation system is not provided here.

Figure 2.2 shows the main components of transfer case clutch actuation system. It consists of the actuation and mechanical subsystems. The actuation subsystem contains only the DC actuator motor; while the mechanical subsystem consists of the reduction gear pair, cam mechanism, lever arm, plate and ball ramp. The mechanical subsystem receives and transmits the torque generated by the DC motor to move the balls installed in the ball ramp within the plate, and meanwhile generates the reaction load torque to the DC motor when the clutch is engaged.

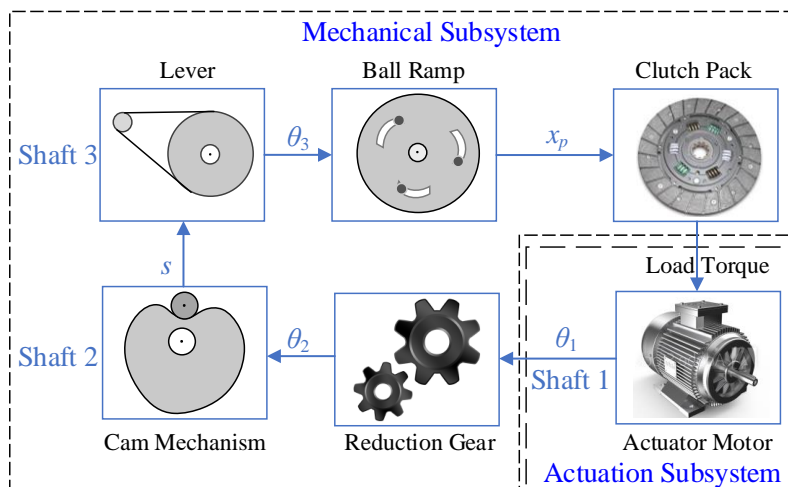


Figure 2.2: Transfer case clutch actuation system

The clutch actuator is just a DC motor. Note that the proposed adaptive touchpoint estimation scheme in the next section will be based on a linear clutch actuation model. Therefore, ignoring the nonlinearity of the DC motor, the Kirchhoff's and Newton's Second Law are used to model the

motor electric circuit and the rotational dynamics as following.

$$u = Ri + L \frac{di}{dt} + K_e \dot{\theta}_1 \quad (2.1)$$

$$J_m \ddot{\theta}_1 = K_m i - b_1 \dot{\theta}_1 - T_{l1} \quad (2.2)$$

where u is the motor input voltage; R is the resistance; i is the motor circuit current; L is the inductance; t is time trace; K_e is the electromotive force constant; $\dot{\theta}_1$ is the angular velocity of shaft 1; J_m is the electric motor shaft inertia; K_m is the motor torque constant; b_1 is the damping coefficient of shaft 1; T_{l1} is the load torque applied to shaft 1.

For the mechanical subsystem, a reduction gear is first used to increase the torque generated by the motor to drive shaft 2. Assume there is no gear lash, the reduction gear can be modeled below.

$$\theta_2 = \theta_1 / i_r \quad (2.3)$$

$$T_{l2} = T_{l1} i_r \eta_r \quad (2.4)$$

where i_r is the reduction gear ratio; θ_2 is the angular position of shaft 2; T_{l2} is the load torque on shaft 2; and η_r is the mechanical efficiency from shaft 1 to 2.

Shafts 2 and 3 are connected through the cam pair, i.e., Cam and Following-Cam mechanism (see Figure 2.3). In fact, the cam can rotate with shaft 2 in both clockwise and counterclockwise directions, corresponding to 4-L (Low) and 4-H (High) range of the transfer case, respectively. Position F is the initial position of the following cam. Typically, 4-L range corresponding to higher output torque, which would be used when the vehicle is climbing an uphill or some of the tires are stuck, while the 4-H range is more used in normal driving. As a matter of fact, in most of the time, the transfer case works within the 4-H range, whose positions are denoted in Figure 2.3 from position F to L when the shaft 2 is rotating counterclockwise. The relationship between the stroke (or displacement) of the following cam and the rotation angle of the cam shaft (shaft 2) is usually a nonlinear function (see Figure 2.4) that can be modeled by

$$s = g(\theta_2) \quad (2.5)$$

where s is the stroke of the following cam and θ_2 is the angular position of shaft 2 (cam rotation angle).

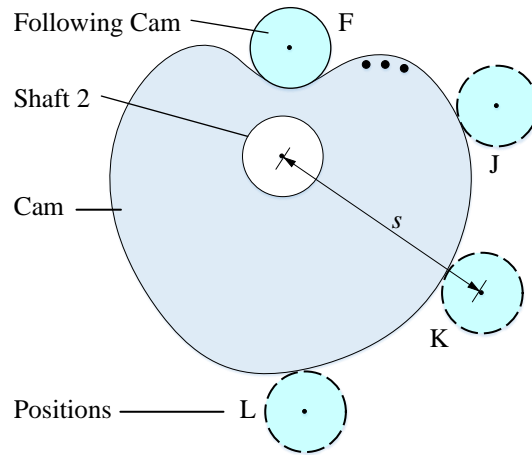


Figure 2.3: Cam and following-cam mechanism

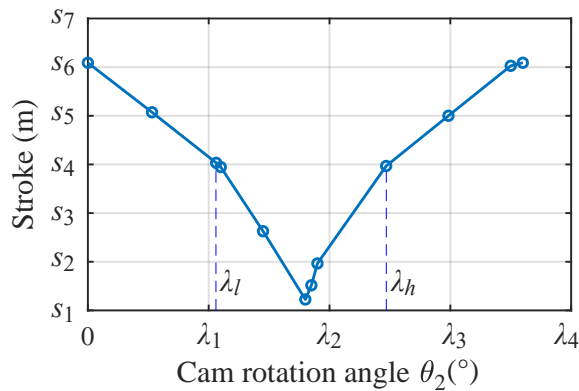


Figure 2.4: Cam profile

Empirically, to engage the clutch, the cam angle needs to satisfy $\theta_2 \geq \lambda_h$ for 4-H range and $\theta_2 \leq \lambda_l$ for 4-L range, indicating that the Cam-Following-Cam stroke relationship is almost linear (see Figure 2.4). And for the adaptive estimation algorithm to work, the system needs to be linear. Therefore, when the clutch is engaged, equation (2.5) can be approximated by an affine function

$$s = k_{cam}\theta_2 + b_{cam} \quad (2.6)$$

where k_{cam} is the slope and b_{cam} is the intercept, and for different ranges(4-L or 4-H), these two coefficients are different.

The following cam rotates the plate on shaft 3 through the lever arm, which connects with the plate mounted on shaft 3. With the rotation of the plate, the ball ramp mechanism moves the balls in axial direction along shaft 3. Note that the relationship between the following cam stroke and shaft 3 rotational angle, as well as the relationship between the rotation angle of shaft 3 and ball displacement are typically an affine linear function. Therefore, the linear relationship can be shortened from following cam stroke to ball displacement and can be modeled as follow.

$$x_b = k_{br}s + b_{br} \quad (2.7)$$

where x_b is the actuation motor-controlled ball displacement; k_{br} and b_{br} are combined coefficients between following cam stroke and ball displacement.

The effective clutch displacement introducing clutch normal force consists of the ball displacement by equation (2.7) and the total clutch touchpoint displacement. As a matter of fact, the total clutch touchpoint displacement includes the nominal touchpoint displacement x_{c0} and touchpoint variation displacement x_0 . The nominal touchpoint displacement x_{c0} is simply designed as a constant. However, the tricky lies in the touchpoint variation displacement since the touchpoint variation of clutch pack varies due to various factors such as clutch wear, clutch temperature variation, etc. For instance, considering the clutch wear, for a new clutch, there is no wear; while with the clutch engagement and slipping, clutch wear occurs gradually, reducing the clutch pack thickness and increasing clutch touchpoint displacement. Thus, it is important to consider a compensation displacement x_0 as the touchpoint variation distance. Therefore, the touchpoint is summed into a total clutch touchpoint displacement and is expressed as

$$x_{ct} = x_{c0} + x_0 \quad (2.8)$$

where x_{ct} is the total clutch touchpoint displacement; x_{c0} is nominal clutch touchpoint displacement; and x_0 is the touchpoint variation displacement. Note that the variation touchpoint displacement is typically unknown and need to be estimated.

The actual effective clutch displacement that can generate clutch normal force is therefore

modified to

$$x_e = x_b - x_{ct} \quad (2.9)$$

where x_e is the effective ball displacement.

In addition to the displacement relationship, the torque relationship between shafts 2 and 3 is modeled below

$$T_{l3} = T_{l2} i_s \eta_s \quad (2.10)$$

where T_{l3} is the load torque on shaft 3; i_s is the equivalent ratio from shafts 2 to 3; and η_s is the mechanical efficiency between both shafts.

As a matter of fact, the load torque on shaft 3 comes from the contact force between the balls and clutch pack. Figure 2.5 shows the rolling ball movement process. When the ball is disengaged with the clutch pack (corresponds to the upper ball position in the left of Figure 2.5), there is no load force generated in this case. As the ball moves and reaches to the touchpoint that begins contacting the clutch pack, normal force starts being generated between the clutch contact surfaces (corresponds to the middle position in the left plot of Figure 2.5). When the ball squeezes the clutch pack with certain displacement (see the lower position in Figure 2.5), certain amount of normal force will be generated. As a result, the clutch normal force can be modeled as a piece-wise linear function of the clutch displacement below.

$$F_N = \begin{cases} 0 & x_b \leq x_{ct} \\ k_c(x_b - x_{ct}) & x_b > x_{ct} \end{cases} \quad (2.11)$$

where F_N is the clutch normal force; k_c is the clutch stiffness.

According to Figure 2.5, for the balls, only the force tangential to the ball ramp orbit can generate load torque on shaft 3, and the tangential force is depicted as F_b , and can be calculated as:

$$3F_b = F_N \tan \beta \quad (2.12)$$

where F_b is the force tangential to the ball's orbit radius; and β is the angle between ball profile and plate plane.

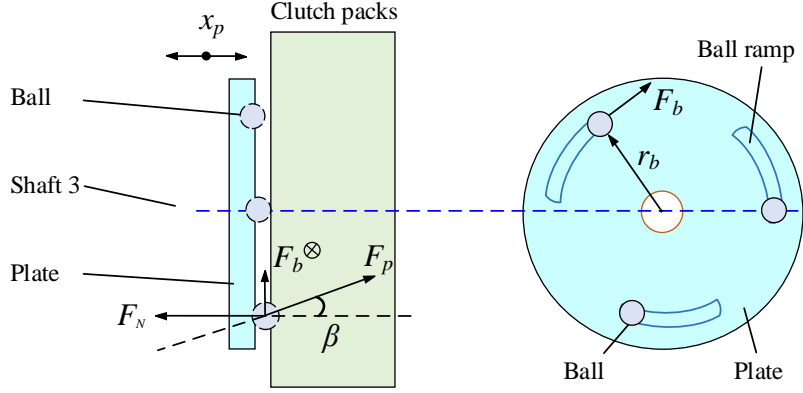


Figure 2.5: Free body diagram of the ball

Typically, there are a few balls distributed evenly in the plate. In our case, three balls are mounted, therefore, the load torque on shaft 3 is obtained by

$$T_{l3}\eta_p = 3F_b r_b \quad (2.13)$$

where r_b is the ball orbit radius; and η_p is the mechanical efficiency from shaft 3 to the clutch.

Combining equations from (2.11) - (2.13), the load torque on shaft 3, when $x_b > x_{ct}$, is

$$T_{l3}\eta_p = k_c(x_b - x_{ct}) \tan \beta r_b \quad (2.14)$$

The load torque on shaft 1 is, therefore, can be obtained from the following

$$\begin{aligned} T_{l1} &= \frac{T_{l2}}{i_r \eta_r} \\ &= \frac{T_{l3}}{i_r \eta_r i_s \eta_s} \\ &= \frac{F_b r_b}{i_r i_s \eta_r \eta_s \eta_p} \\ &= \frac{k_c(x_p - x_{c0}) \tan \beta r_b}{i_r i_s \eta_r \eta_s \eta_p} \\ &= \frac{k_c(k_{br} k_{cam} \theta_1 / i_r + k_{br} b_{cam} + b_{br} - x_{ct}) \tan \beta r_b}{i_r i_s \eta_r \eta_s \eta_p} \end{aligned} \quad (2.15)$$

Therefore, the load torque on shaft 1 can be trimmed to a function of the motor rotation angle θ_1 of the following form:

$$T_{l1} = K\theta_1 + d \quad (2.16)$$

where

$$K = \frac{k_c r_b \tan \beta k_{cam} k_{br}}{i_s i_r^2 \eta_r \eta_s \eta_p}$$

$$d = \frac{k_c r_b \tan \beta}{i_s i_r \eta_r \eta_s \eta_p} (k_{br} b_{cam} + b_{br} - x_{ct})$$

Note that since x_0 in x_{ct} is unknown, resulting d (or the load torque T_{l1}) is also unknown. In addition, although clutch touchpoint x_0 varies over time, the variation rate is very small. As a result, for real-time estimation, x_0 can be viewed as a constant, resulting in a constant d .

2.3 Adaptive Estimation Algorithm Development

2.3.1 State-Space System Representation

Equations from (2.1) to (2.16) describe the complete clutch actuation system dynamics and can be summarized below.

$$u = Ri + L \frac{di}{dt} + K_e \dot{\theta}_1 \quad (2.17)$$

$$J_m \ddot{\theta}_1 = K_t i - b_1 \dot{\theta}_1 - K \theta_1 - d \quad (2.18)$$

In general, the system contains the input as the control voltage, the unknown system parameter x_0 , and output motor position or cam position. However, choosing system states as $x = [x_1, x_2, x_3]^T = [\theta_1, \dot{\theta}_1, \frac{K_t}{J_m} i]^T$, corresponding to motor position, motor rotational speed and motor current, respectively, output as motor position $y = x_1$, known input as u , and exogenous unknown input as d yields the state-space system representation

$$\dot{x} = Ax + B_u u + B_d d \quad (2.19)$$

$$y = Cx$$

where $A = \begin{bmatrix} 0 & 1 & 0 \\ -\frac{K}{J_m} & -\frac{b}{J_m} & 1 \\ 0 & -\frac{K_e K_t}{J_m L} & -\frac{R}{L} \end{bmatrix}$, $B_u = \begin{bmatrix} 0 \\ 0 \\ \frac{K_e}{J_m L} \end{bmatrix}$, $B_d = \begin{bmatrix} 0 \\ -\frac{1}{J_m} \\ 0 \end{bmatrix}$, $C = \begin{bmatrix} 1 & 0 & 0 \end{bmatrix}$. This

transforms the system from one input to two inputs and gets ready for adaptive estimation algorithm development.

Based upon the applied known motor control voltage u and the measured output cam position y , the goal is to adaptively estimate the unknown input d so that the clutch touchpoint displacement x_0 can be estimated. The estimation scheme is shown in Figure 2.6.

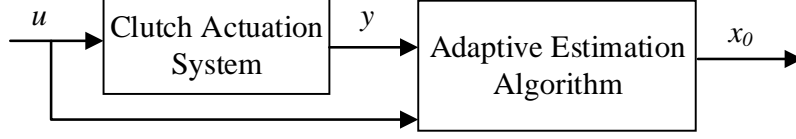


Figure 2.6: Adaptive estimation diagram

2.3.2 Algorithm Development

The system transfer function representation, with the hybrid notation, in continuous-time domain is

$$y(t) = G_u(s)u(t) + G_d(s)d(t) \quad (2.20)$$

where $G_u(s) = C(sI - A)^{-1}B_u$ is the transfer function from input $u(t)$ to output $y(t)$, and $G_d(s) = C(sI - A)^{-1}B_d$ is the transfer function from input $d(t)$ to output $y(t)$.

Discretizing the transfer functions $G_u(s)$ and $G_d(s)$ and time signals in equation (2.20) yields the following hybrid system in discrete-time domain:

$$y(k) = G_u(z)u(k) + G_d(z)d(k) \quad (2.21)$$

where $G_u(z) = C_d(sI - A_d)^{-1}B_{ud}$ is the discretized transfer function $G_u(s)$, and $G_d(z) = C_d(sI - A_d)^{-1}B_{dd}$ is the discretized transfer function $G_d(s)$, and the discretized system matrices are obtained through the exact discretization formula [37]: $A_d = e^{AT}$, $B_d = A^{-1}(e^{AT} - I)B$, $C_d = C$, where T is the sampling period for the discretization process.

Rearrange the hybrid system equation to the parametric form of

$$y'(k) = \theta^* \phi(k) \quad (2.22)$$

where $y'(k) = y(k) - G_u(z)u(k)$ is the output and $\phi(k) = G_d(z) \cdot 1$ is the regression signal. Since the system matrices are known, and the input voltage u and output cam position y can be measured,

leading to the signals $y'(k)$ and $\phi(k)$ to be available; and $\theta^* = d$ contains the touchpoint variation displacement is the unknown term to be estimated.

Let θ be an estimate of θ^* , the parametric estimation error can be expressed as

$$\epsilon(k) = \tilde{\theta}(k)\phi(k) \quad (2.23)$$

where $\tilde{\theta} = \theta(k) - \theta^*$ is the unknown term estimation error. A discrete-time normalized gradient adaptive estimation algorithm that guarantees the estimation convergence is designed as

$$\theta(k+1) = \begin{cases} \theta(k) - \frac{\Gamma\phi(k)\epsilon(k)}{m^2(k)} & \underline{\theta} < \theta(k) < \bar{\theta} \\ \theta(k) & \text{otherwise} \end{cases} \quad (2.24)$$

where $m^2(k) = \tau + \phi^T(k)\phi(k)$ is designed to guarantee the boundedness of the estimation algorithm, and $\tau > 0$ is a designing parameter that determines the estimation convergence rate. Γ is another design parameter satisfying $0 < \Gamma < 2I$ to guarantee the convergence of the output error, where I is an identity matrix with appropriate dimension; $\underline{\theta}$ and $\bar{\theta}$ are calibrated lower and upper bound for θ , respectively.

2.3.3 Convergence Analysis

1. Output Estimation Error Convergence Analysis:

The output estimation error convergence is analyzed by introducing a discrete-time Lyapunov function [25] for the update law $\theta(k+1)$:

$$V(k) = \tilde{\theta}^T(k)\Gamma^{-1}\tilde{\theta}(k) \quad (2.25)$$

Define the difference Lyapunov function between two adjacent time steps as $\Delta V(k) = V(k+1) - V(k)$, and the difference can be expanded as follows

$$\begin{aligned}
\Delta V(k) &= V(k+1) - V(k) \\
&= \tilde{\theta}^T(k+1)\Gamma^{-1}\tilde{\theta}(k+1) - \tilde{\theta}^T(k)\Gamma^{-1}\tilde{\theta}(k) \\
&= \left(\tilde{\theta}(k) - \frac{\Gamma\phi(k)\epsilon(k)}{m^2(k)}\right)^T \Gamma^{-1} \left(\tilde{\theta}(k) - \frac{\Gamma\phi(k)\epsilon(k)}{m^2(k)}\right) - \tilde{\theta}^T(k)\Gamma^{-1}\tilde{\theta}(k) \\
&= -2\frac{\tilde{\theta}^T(k)\phi(k)\epsilon(k)}{m^2(k)} + \frac{\phi^T(k)\Gamma\phi(k)}{m^2(k)} \frac{\epsilon^2(k)}{m^2(k)} \\
&= \left(-2 + \frac{\phi^T(k)\Gamma\phi(k)}{m^2(k)}\right) \frac{\epsilon^2(k)}{m^2(k)}
\end{aligned} \tag{2.26}$$

By definition, $m^2(k) > 0$, and the choice of Γ satisfying $0 < \lambda_{\max}(\Gamma) < 2I$ guarantees $\Delta V(k)$ is non-increasing and $V(k) \geq 0$. These two conditions ensure that $V(k)$ is bounded and $\Delta V(k)$ converges to 0 as k goes to infinity. Therefore, the output error $\epsilon(k)$ converges to 0.

2. Parameter Estimation Error Convergence Analysis:

The parameter convergence in the normalized gradient method is guaranteed by the PE (persistently exciting) [38] condition of the regression signal $\phi(k)$.

Definition of Persistence Exciting: A bounded vector signal $x(t) \in R^q, q \geq 1$ is

- exciting over the time interval $[\sigma, \sigma + \delta]$, $\delta \geq 0, \sigma \geq t_0$, if there is $\alpha \geq 0$ such that
$$\int_{\sigma}^{\sigma+\delta} x(t)x^T(t)dt \geq \alpha I$$
- persistence exciting if there is $\delta \geq 0, \alpha \geq 0$ such that $\int_{\sigma}^{\sigma+\delta} x(t)x^T(t)dt \geq \alpha I$, for any $\sigma \geq t_0$

To reach the PE condition of $\phi(k)$, the following Lemmas from [38] is needed.

Lemma 1: Consider a system $\phi(t) = G(s)u(t)$, where $u(t) \in R$, $\phi(t) \in R^n$ and the $n \times 1$ transfer function $G(s)$ is proper and stable. Assuming that $H(jw_i)$ are linearly independent for all $w_i, (i = 1, \dots, n)$, $\phi(t)$ is PE if and only if $u(t)$ is rich of order n . (Signal richness of order k : a signal $u(t)$ is of rich of order k if it has, at least, k frequency components)

Lemma 2: If the signal $\phi(k) \in L^\infty$ and $\phi(k)$ is PE, then the signal $\psi(k) = \frac{\phi(k)}{m(k)}$ is PE, and furthermore, the parameter estimation error converges to zero, i.e., $\lim_{k \rightarrow \infty} \|\tilde{\theta}(k)\|_2 = 0$, exponentially.

Lemma 1 can be easily extended to the discrete-time system. From equation (2.22), it is obvious that $\phi(k)$ is a scalar ($n = 1$), and the input for ϕ is stationary, which means that it is rich of order 1.

Therefore, by Lemma 1, $\phi(k)$ can be concluded to be PE. Since $\phi(k)$ is also a finite energy signal, which means that $\phi(k) \in L^\infty$. Therefore, by the Lemma 2, the convergence of $\tilde{\theta}(k)$ to 0 can be easily concluded.

It can be seen that by the designed adaptive algorithm, both the output error and parameter error will converge to 0 eventually, therefore, the estimate θ converge to θ^* , which achieves the goal of parameter estimation.

2.4 Preliminary Results and Discussion

To validate the accuracy of the clutch actuation system model and the effectiveness of the proposed adaptive estimation algorithm, simulation studies are performed in this section.

There are typically four vehicle operational modes: stationary, acceleration, deceleration and cruise. There is no doubt that no torque estimation is need when the vehicle is stationary; While then the vehicle is decelerating, it is very possible that the vehicle brake is applied, and the applied brake torque would be difficult to obtain; During vehicle cruise, it is also very possible that the vehicle operates in the 2WD mode. Therefore, only acceleration data is used for updating the touchpoint estimation since during acceleration period the transfer case clutch is engaged.

The measured input and output signals of the proposed model (2.19) are shown in Figure 2.7 (a) and Figure 2.7 (b), respectively. It is interesting to observe that the clutch actuation system is 'active' only between 5 and 10 second. Note that the actuator voltage is 'active' (or non-zero) only in this time frame (see Figure 2.7 (a)); and the cam stays stationary both before 5s and after 10s (see Figure 2.7 (b)). Thus, it is reasonable to only enable the estimation algorithm when the clutch actuation system is active in real-time. The associated trigger conditions will be discussed detailly in next Subsection. In this Subsection, for data completeness, the trigger conditions are not used.

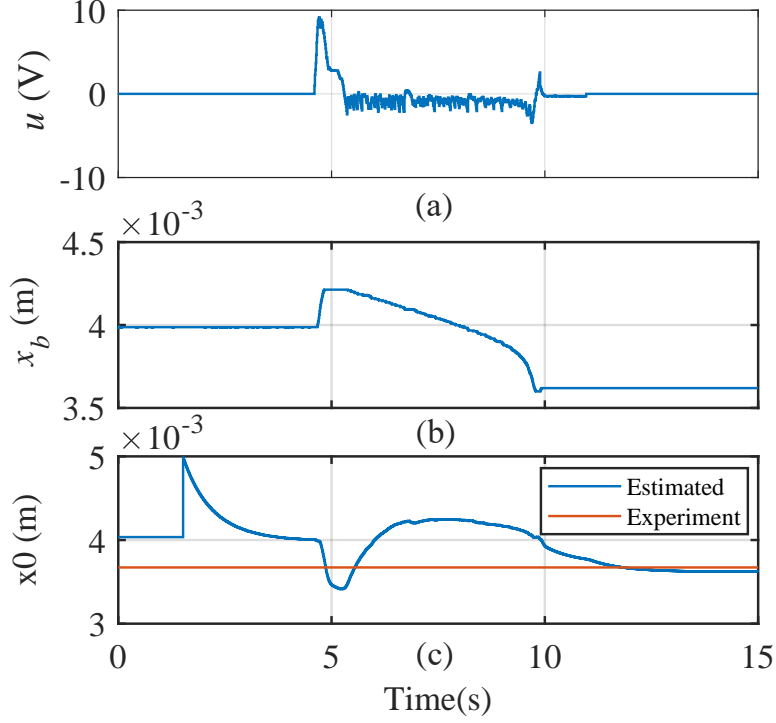


Figure 2.7: Touchpoint x_0 estimation results without friction. (a) applied input voltage of the clutch actuation system, (b) measured cam position, (c) estimated touchpoint x_0

Figure 2.7 (c) shows the x_0 estimation result, where the x_0 is changing quite complicated during the 'active' time. However, this changing rate is too fast compared with a physical clutch operation process, and contradicts with the assumption that x_0 is a constant at the time of estimation. Further examination of the actual cam position in Figure 2.7 (b) reveals that the chattering cam movement is a clear indication that there exists friction between the moving balls and the ball ramp while the clutch is 'active' in the physical system. Without a good friction model, the estimation result is not desirable. Therefore, it is crucial to take the friction effect between the balls and ball ramp into account for better estimation results.

Revisit equation (2.16), term d to be estimated is

$$d = \frac{k_c r_b \tan \beta}{i_s i_r \eta_r \eta_s \eta_p} (k_{br} b_{cam} + b_{br} - x_{ct}) \quad (2.27)$$

where no friction is considered. If consider the friction force between the moving balls and the ball

ramp, term d is modified to

$$d = \frac{k_c r_b \tan \beta}{i_s i_r \eta_r \eta_s \eta_p} (k_{br} b_{cam} + b_{br} - x_{ct} + \frac{F_f}{k_c}) \quad (2.28)$$

where F_f is the dry friction force to be determined. Denote $x'_{ct} = x_{ct} - \frac{F_f}{k_c}$, it is obvious that the estimation result in Figure 2.7(d) is actually x'_{ct} . Therefore, the actual touchpoint is

$$x_{ct} = x'_{ct} + \frac{F_f}{k_c} \quad (2.29)$$

For x_{ct} to be a constant (or almost a constant with friction effect), it would be reasonable to expect that the friction force is negative and positively proportional when the clutch is actively engaged between 5 and 10 second. In the following subsections, several friction models will be introduced in detail.

2.5 Friction Model Development

2.5.1 Coulomb Friction Model

A simple enough friction model is the Coulomb friction [39]. It describes the friction force between two contact surfaces as a constant and in the opposite direction of speed, and its magnitude is independent of speed magnitude. Figure 2.8 shows the typical relationship between Coulomb friction and motion speed graphically, where when the velocity is positive, the friction force is also positive and when the motion velocity is negative, it becomes negative force. It is modeled mathematically as

$$F_f = F_c \text{sgn}(v) \quad (2.30)$$

$$\text{sgn}(v) = \begin{cases} 1 & v > 0 \\ 0 & v = 0 \\ -1 & v < 0 \end{cases} \quad (2.31)$$

where F_f is the friction force; F_c is the Coulomb friction; v is the motion speed and $\text{sgn}(\cdot)$ is the sign function.

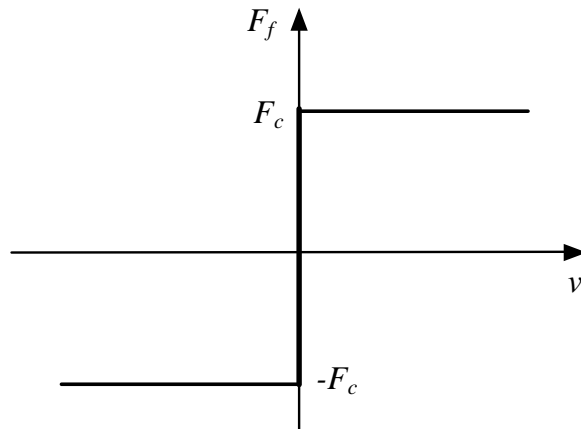


Figure 2.8: Graphical illustration of Coulomb friction model

Using the ball velocity in Figure 2.9 (a) to generate the Coulomb friction described by equation (2.30), and the friction force is shown in Figure 2.9 (b). During the clutch active period (5-10s), the Coulomb friction remains constant according to the Coulomb friction formula, which does not match the previous discussion of positively proportional requirement. Therefore, this friction model cannot represent the actual friction in the clutch actuation system. It is also noted that the measured ball velocity is not exactly at zero even when there is no active input voltage to the clutch actuation system(see Figure 2.7 (a) after 10s), which results in a non-zero friction when the clutch is inactive. This non-zero velocity is possibly mainly introduced by the measurement noise. Therefore, a good friction model also needs to take care of the measurement noise.

2.5.2 General Kinetic Friction Model

Another widely used friction model with more thorough friction description than the Coulomb model is the General Kinetic Friction (or GKF) model [40], [41], [42], [43] that is a combination of Coulomb friction, Stiction friction, Viscous friction and external force. Its relationship with respect to motion speed is shown in Figure 2.10 graphically.

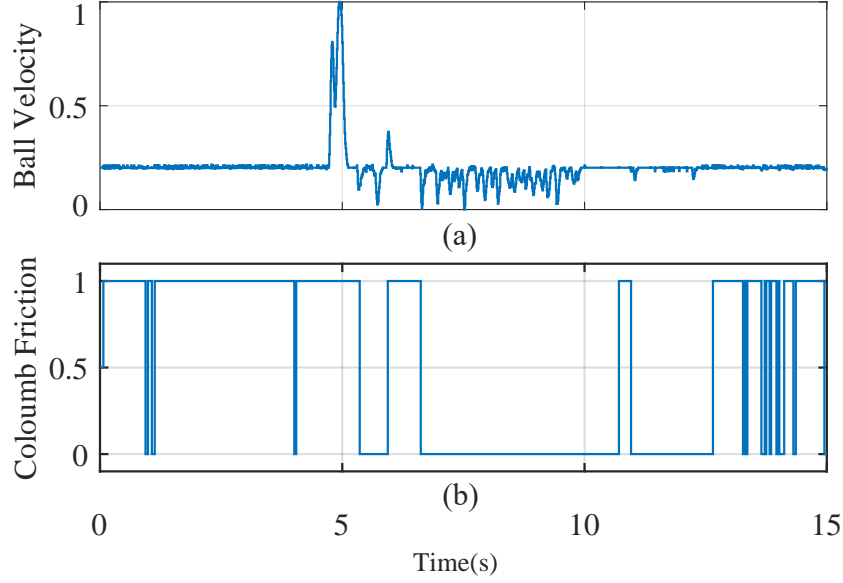


Figure 2.9: Performance evaluation of Coulomb Friction. (a) measured ball velocity. (b) Coulomb Friction

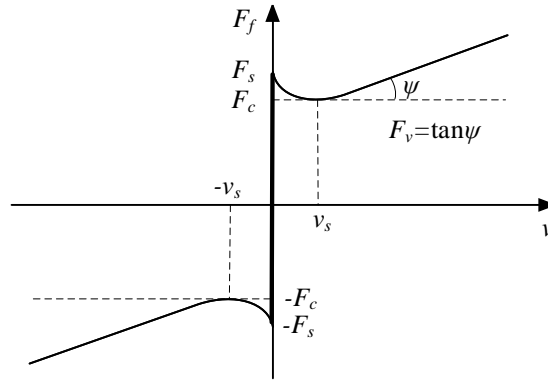


Figure 2.10: Graphical illustration of GKF model

The GKF is modeled mathematically as

$$F_f = \begin{cases} F_g & |v| > 0 \\ -F_e & |v| = 0, |F_e| < F_s \\ F_s \text{sign}(v) & |v| = 0, |F_e| \geq F_s \end{cases} \quad (2.32)$$

$$F_g = (F_c + (F_s - F_c)e^{-|\frac{v}{v_s}|^\delta}) \text{sign}(v) + F_v v$$

where F_f is the total friction force; F_c is the Coulomb friction; F_s is the Stiction friction; F_v is the slope of Viscous friction; F_e is the external force on the ball; v is the ball movement speed; v_s is

the Stribeck velocity to be calibrated; δ is the Stribeck coefficient, and typically has the value of 1 or 2.

The input of the friction model is still the ball velocity of the moving balls as described in Figure 2.9 (a), and the resulting general friction using friction model (2.32) is shown in Figure 2.11. The trend is similar to that of the Coulomb friction model that the friction is almost constant when the clutch is active. Also note that an almost constant nonzero velocity (see Figure 2.9(a)) can only result in an approximately constant nonzero friction by either Coulomb friction or GKF model.

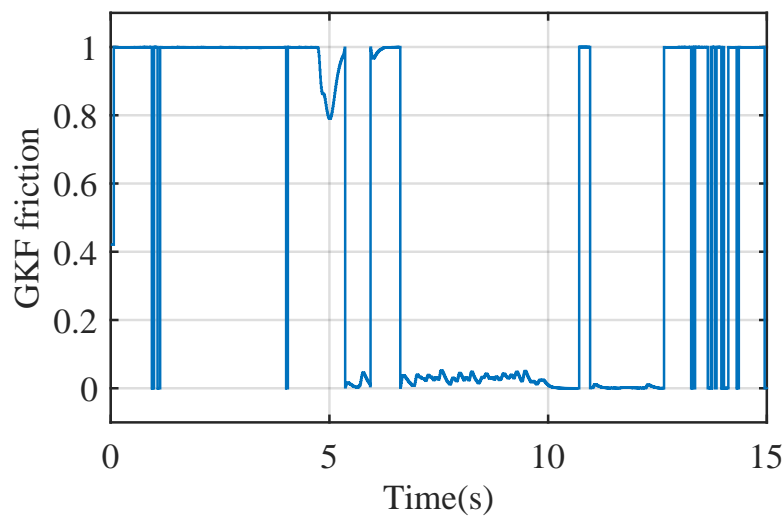


Figure 2.11: Friction force using GKF model

The fact is that the ball velocity (see Figure 2.9 (a)) is relatively small between 6 and 10 seconds comparing with that at the start of ball movement at around 5s. It is possible that between 6s and 10s, the velocity is so close to 0 that the friction could be static and should be described by the second equation in (2.32) instead of the kinetic friction given by the first equation in (2.32). However, due to the measurement noise, the measured velocity can never be exactly zero, which results in the friction force cannot take in the form of the second equation in (2.32). Therefore, modification is needed for the GKF friction model for practical applications.

2.5.3 Modified General Kinetic Friction Model

In this section, a threshold of low velocity v_0 is proposed for the Modified General Kinetic Friction (or MGKF) model. That is, the comparison with zero in equation (2.32) is replaced by v_0 . The marked region in Figure 2.12 illustrates the effect of the threshold. Within the threshold region, the friction is static. The advantages for this are two-fold: firstly, it overcomes the discontinuity of friction force at zero-velocity encountered in either the Coulomb or GKF friction model; and secondly, it avoids the need of detecting exact zero-velocity in the presence of measurement noise in case the actual friction is static.

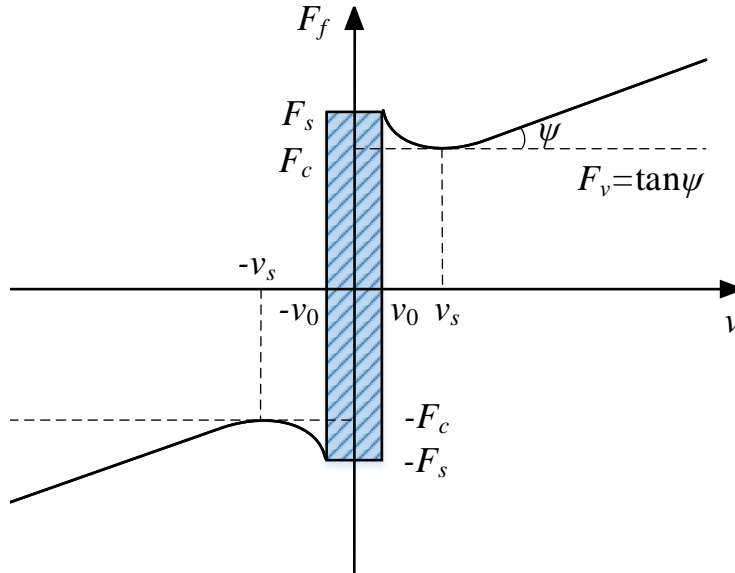


Figure 2.12: Graphical illustration of MGKF model

The MGKF model is described mathematically by the equation below.

$$F_f = \begin{cases} F_g & |v| > v_0 \\ -F_e & |v| \leq v_0, |F_e| < F_s \\ F_s \text{sign}(v) & |v| \leq v_0, |F_e| \geq F_s \end{cases} \quad (2.33)$$

$$F_g = (F_c + (F_s - F_c)e^{|\frac{v}{v_s}|^\delta}) \text{sign}(v) + F_v v$$

where v_0 is the introduced velocity threshold to be calibrated and all the other parameters are defined before. Note that the main purpose of introducing v_0 is to deal with the difficulty of

detecting exact zero-velocity in the presence of speed measurement noise. As a result, the choice of v_0 is largely dependent on the noise level of the actual speed sensor. For this study, v_0 was chosen to be 5×10^{-4} m/s.

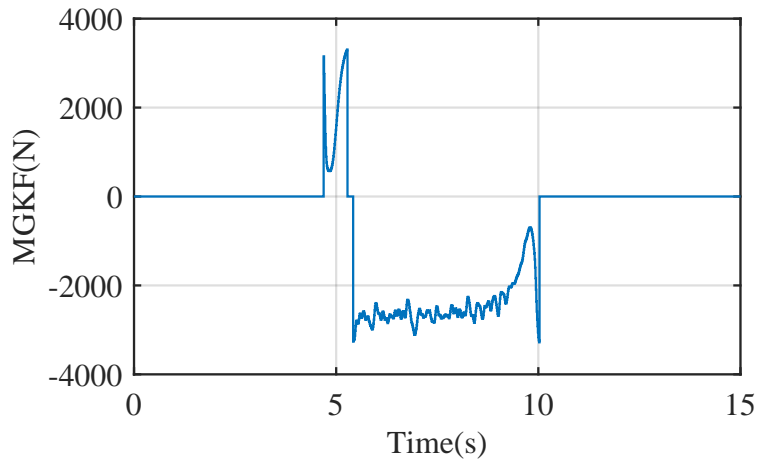


Figure 2.13: Friction Force using MGKF model

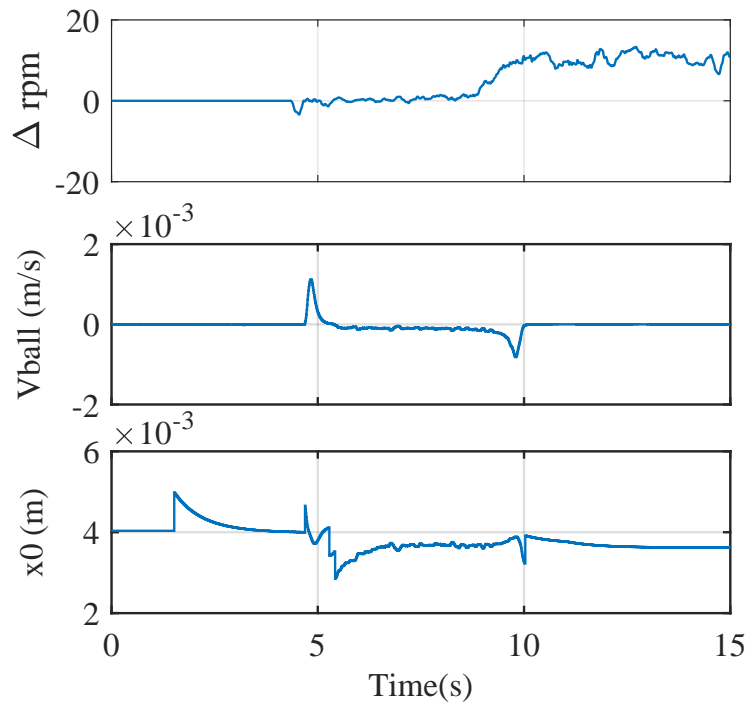


Figure 2.14: Performance evaluation of MGKF model. (a) clutch Δ rpm; (b) ball velocity; (c) estimated x_0 with MGFK model

Figure 2.13 shows the friction force using MGKF model for the same ball velocity. It increases slightly in a linear way and its magnitude is negative when the clutch is active, which matches well with early discussion. Figure 2.14 (a) shows the clutch slip speed while the transfer case is operating. It shows that when the clutch starts to engage (around 5s), there is no slip in the clutch, which can be assumed to be overtaken. And then starting around 7s, the clutch Δrpm starts to increase, indicating the clutch starts to slip. Starting from around 9s, the clutch is disengaged, and there exists almost constant speed difference between clutch pack. Figure 2.14 (b) shows the measured ball velocity under the control voltage u . The initial speed increase corresponds to the sudden increase of ball position at around 5s as shown in Figure 2.15 (b). And the final speed increase in the opposite direction also corresponds to the ball position drop at around 10s as shown in Figure (2.15) (b). Figure 2.14 (c) shows the associated estimation of total touchpoint displacement x_{ct} using equation (2.33), it is desirable that the x_{ct} is almost a constant when the clutch is active between 7s and 9s. However, in the duration from 5s to 7s and from 9s to 10s, the x_0 estimation is not accurate. For the duration from 5s to 7s, since the clutch is in the overtaken condition, it is very possible that the spring between clutch pack works in the nonlinear region due to the sharp increase of actuation force, which is different from the linear spring assumption as described in equation (2.11). For the duration from 9s to 10s, it can be concluded that the balls fall down to the point where there is no contact between the ball and the clutch pack, which means that the clutch is disengaging, and there is no load torque exerted on the clutch actuation system. In this sense,, the dynamics of the system has changed, which leads to an inaccurate estimation. In summary, the clutch slip duration is the desired period for x_{ct} estimation. As a result, the MGKF model is adopted and the clutch slip duration is the targeting period in the next session for experimental validation.

2.6 Algorithm Evaluation and Validation

In this section, the proposed algorithm is validated through multiple data from testing vehicles. And also they are compared with the results using the existing direct detection method, where the direct detection results are obtained also from the vehicle tests. Estimation Results obtained using

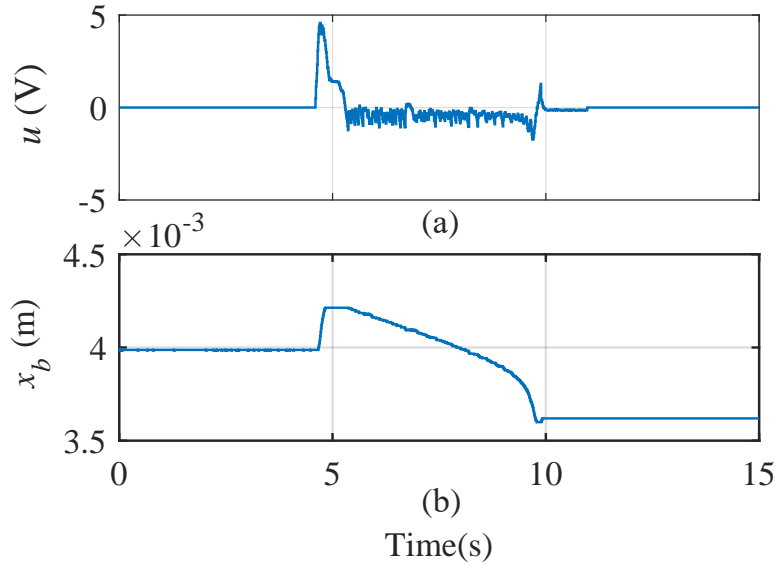


Figure 2.15: Touchpoint x_0 estimation results without friction. (a) input voltage (b) output ball position

the proposed method are based on the motor control voltage and measured cam position from the same data set collected for the direct detection method.

2.6.1 Two Acceleration Data Set Validation

Figures 2.16 and 2.17 shows the results of touchpoint displacement x_{ct} estimation, along with the associated signals. Figure 2.16 (a) is the corresponding vehicle speed profile, which shows clearly that the vehicle goes through two complete acceleration operations. Figure 2.16 (b) presents the input voltage of the clutch actuator motor and Figure 2.16 (c) shows the corresponding ball position. Note that in this study, the algorithm enabling trigger is not used, and the interested duration would only be the complete acceleration duration, i.e., from 19s to 30s and from 143s to 150s.

Figure 2.17 (a) shows the clutch slip speed while the transfer case clutch is engaged, and Figure 2.17 (b) presents the ball velocity. Figure 2.17 (c) shows the final estimation result of the touchpoint displacement x_{ct} . Since the two acceleration performance are similar, the first acceleration data can be used to analyze the estimation performance in detail.

Figure 2.18 (a) is the clutch slip speed Δrpm during the first acceleration. Similar to the results

reported in Figure 2.14, the clutch first operates in the overtaken condition (from 19s to 21s), and then the clutch starts slipping as the Δrpm increases, and finally the clutch will be disengaged. The resulted touchpoint x_{ct} estimation is also similar to the results in Figure 2.14, where the clutch slip condition provides good estimation performance.

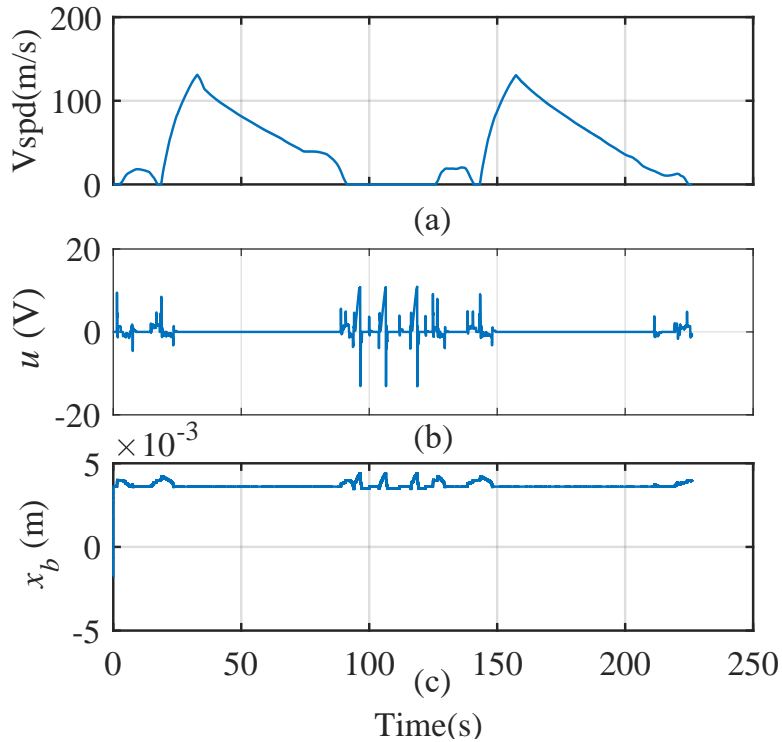


Figure 2.16: Two acceleration data validation, the plots are corresponding to (a) vehicle speed (b) clutch actuation input voltage (c) ball position

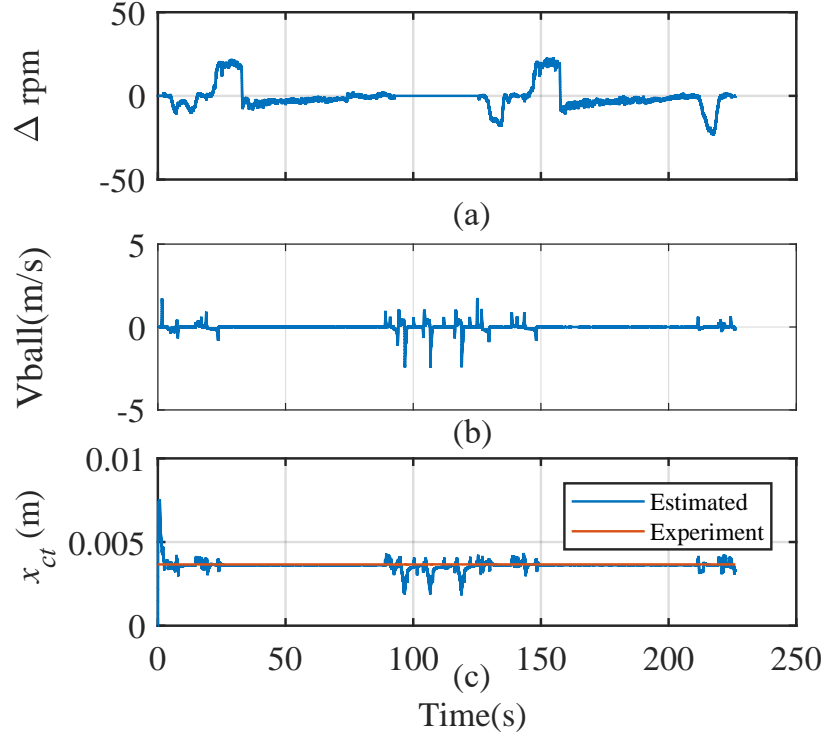


Figure 2.17: Two acceleration data validation, the plots are corresponding to (a) clutch Δ rpm (b) ball velocity (c) estimated touchpoint displacement x_{ct}

2.6.2 Two Acceleration Data Validation with Trigger Condition

In previous Subsection, the estimation is performed with the complete measured data. However, estimation results show that only the clutch slip condition provides reasonable estimation. Therefore, in this section an estimation trigger is proposed to select desired duration for real-time estimation. The detailed trigger conditions are listed in Table 2.1. When all the conditions are met, the estimation will be enabled. Several cases will be discussed to validate the effectiveness of estimation with trigger condition based on the MGKF model.

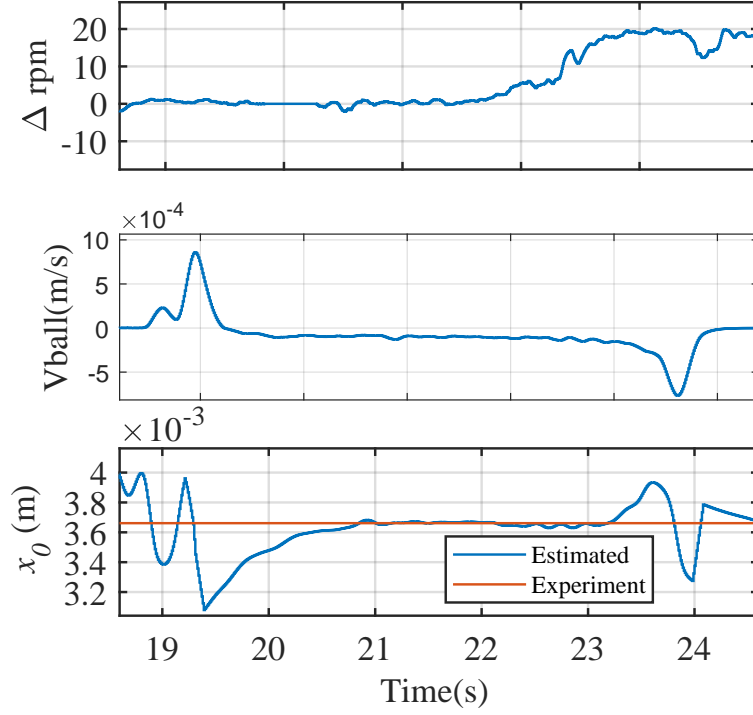


Figure 2.18: Two acceleration data validation, results for the first acceleration, the plots are corresponding to (a) clutch Δrpm (b) ball velocity (c) estimated touchpoint displacement x_{ct}

Table 2.1: Estimation trigger conditions

Parameters	Conditions	Unit
Vehicle Speed (v)	$v > v_0$	m/s
Input Voltage(u)	$u \in [u_0 0]$	V
Ball Velocity (v_b)	$v_b \in [v_{b0} 0]$	m/s
Ball displacement(x_p)	$x_p > x_{c0}$	m
Motor Brake (B_m)	$B_m = 0$	-
Vehicle Cornering(C_v)	$C_v < w_0$	degree
Vehicle Brake (B_v)	$B_v = 0$	-
Clutch Slip Speed (Δrpm)	$\Delta_l < \Delta\text{rpm} < \Delta_u$	rpm

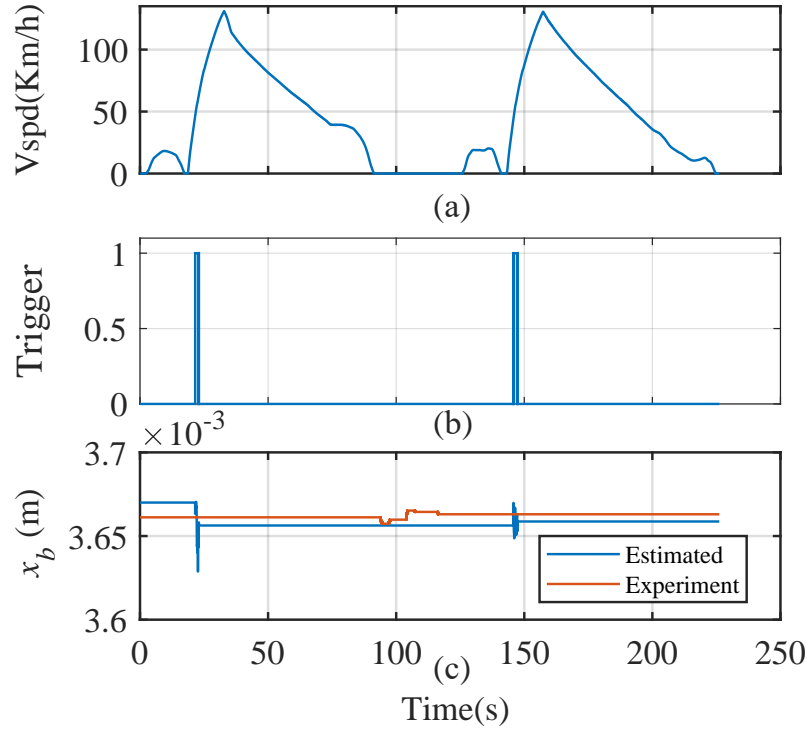


Figure 2.19: Two acceleration data validation with trigger condition, the plots are corresponding to (a) vehicle speed (b) trigger condition (c) estimated touchpoint displacement x_{ct}

Figure 2.19 (b) shows the estimation results under the trigger condition, it is obvious that the trigger is only enabled during the small period specified by the conditions in Table 2.1. And if the trigger conditions are not satisfied, the previous estimation touchpoint x_{ct} will be used as the estimation output. Figure 2.19 (c) is the estimated touchpoint with a specified initial value. It can be seen that the estimated touchpoint is very close to the experiment measured one. The estimation error is within 0.5% along the time series.

In order to show the effectiveness of proposed algorithm with trigger conditions, several more comparisons with experiment measured results are presented in Figures 2.20 and 2.21. It can be seen that in both cases, the estimation is only enabled for a small period when vehicle is accelerating, filtering out the undesired data. On the other hand, the x_b estimation results indicate the estimation accuracy. In Figure 2.20 (c), the max error is around 1% while in the Figure 2.21 (c) the max error is just only around 0.5%.

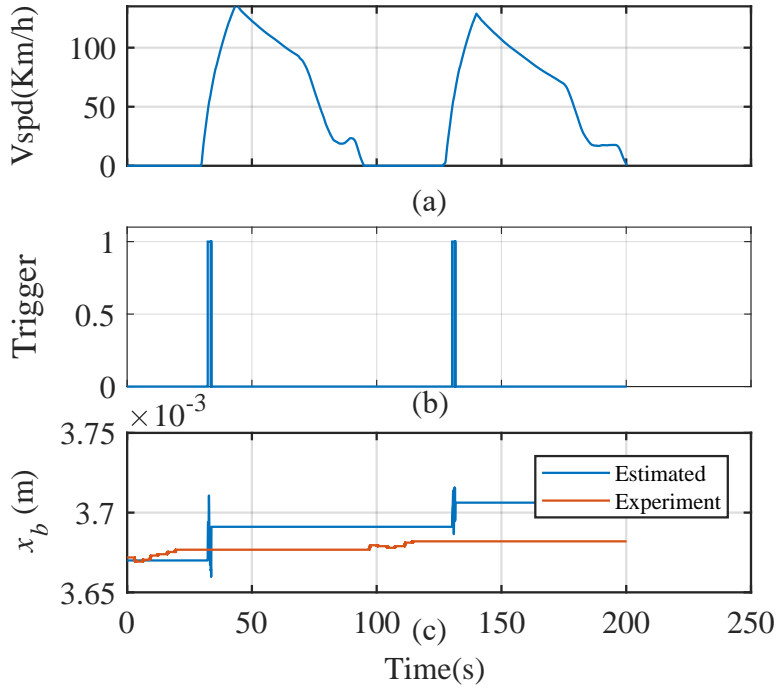


Figure 2.20: Two acceleration data 1 validation with trigger condition, the plots are corresponding to (a) vehicle speed (b) trigger condition (c) estimated touchpoint displacement x_{ct}

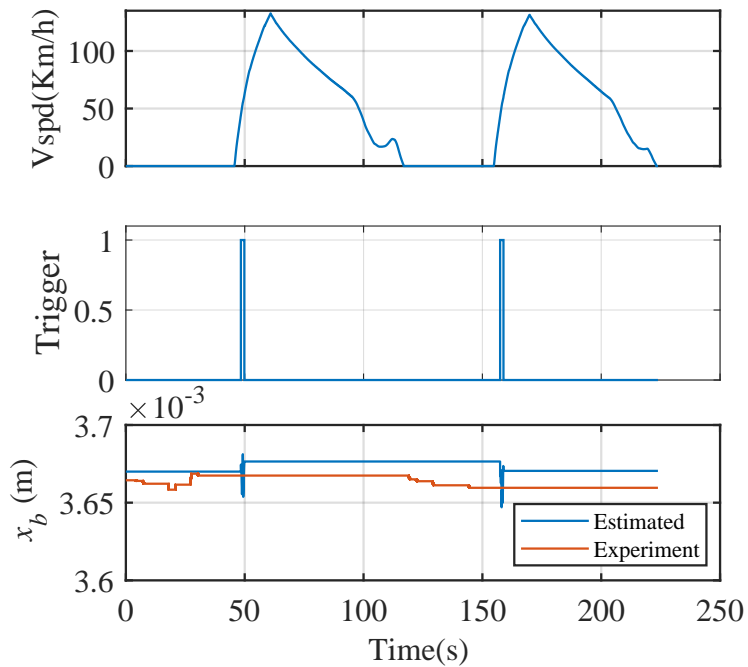


Figure 2.21: Two acceleration data 2 validation with trigger condition, the plots are corresponding to (a) vehicle speed (b) trigger condition (c) estimated touchpoint displacement x_{ct}

2.6.3 Multiple Acceleration Data Validation with Trigger Condition

Figure 2.22 shows the touchpoint estimation algorithm with multiple acceleration data, i.e., multiple clutch engagement operations. It can be observed that the touchpoint obtained from adaptive estimation algorithm is much more robust than that from current production method. And also the mean value of the adaptive estimated touchpoint is close to that of the production method. Further comparison of these two approaches can be seen from Table 2.2. The results can be interpreted in two ways: first, the accuracy metric is evaluated by the mean value of multiple touchpoints and the adaptive estimated touchpoint achieves 0.06% relative error, which confirms its estimation accuracy; second, the touchpoint robustness can be characterized by the standard deviation that is 0.28% for the adaptive estimation and 1.07% for the current production one, indicating that the model-based adaptive estimation is more robust than the current production method.

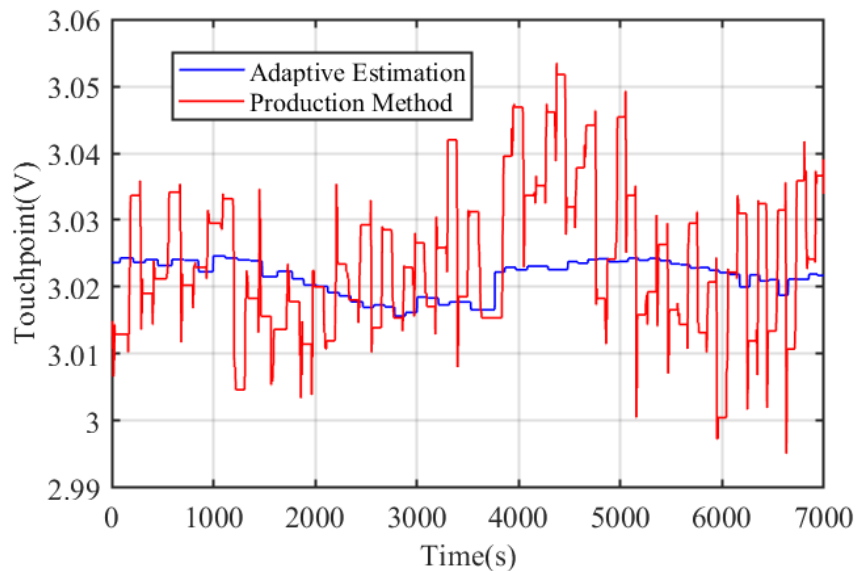


Figure 2.22: Multiple acceleration data validation with trigger condition

Metrics	Results	Conclusions
Accuracy metric (mean value)	production: 3.024V adaptive: 3.022V	$\frac{ x_{ad}-x_{pro} }{x_{pro}} = 0.06\%$
Robustness metric (standard deviation)	production: 1.07% adaptive: 0.28%	The adaptive SD is smaller

Table 2.2: Touchpoint Estimation Results Comparison

2.6.4 Adaptiveness of the Adaptive Estimation Algorithm

Current touchpoint displacement estimation is performed on a medium-wear clutch. Note that typically the clutch aging (wear) rate is very small. Therefore, it will be difficult to validate the adaptation of adaptive estimation algorithm to different stage of wearing.

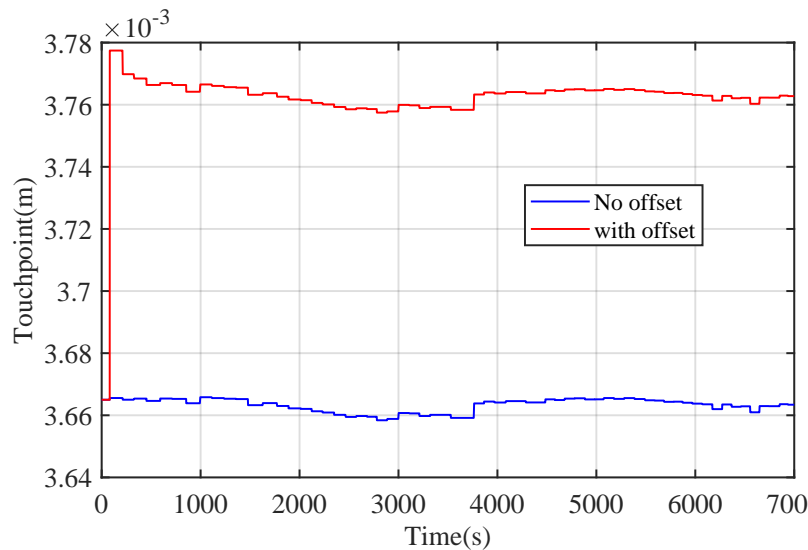


Figure 2.23: Demonstration of Adaptiveness of Adaptive Estimation Algorithm

However, according to the experimental results that several factors may render the touchpoint displacement to change, the adaptation can be check with these factors. One such factor is the cam position sensor drift. It is noted from the experimental data that a 0.12V sensor drift in the cam position measurement will introduce around 0.1mm offset in the touchpoint displacement. To evaluate this sensor drift, an additional 0.12V is added to the measured cam position, and the

resulting touchpoint displacement is shown in Fig. 2.23, indicating that the touchpoint displacement do offset around 0.1mm matching with what is expected. Therefore, the adaptation capability is validated.

2.7 Conclusions

In conclusion, the following are achieved in this chapter:

1. A clutch actuation system model is developed for transfer case and its clutch actuation system;
2. The adaptive estimation algorithm using normalized gradient method, along with the modified friction model, is proposed and developed;
3. The simulation results using experiment data show that the proposed algorithm is accurate, and the comparison between the proposed and existing direct detection method exhibits that the proposed method is more robust than the existing one. Furthermore, the adaptation capability to system change is validated by matching the desired performance of the estimation algorithm.

CHAPTER 3

INTEGRATED TOUCHPOINT ESTIMATION AND POSITION TRACKING USING DEADBEAT ADAPTIVE BACKSTEPPING

3.1 Overview

3.1.1 Chapter Organization

In this chapter, instead of using the separated scheme for the desired clutch displacement control and touchpoint estimation, an integrated scheme is designed [44, 45], the structure of this chapter is shown in Figure 3.1. More specifically, given the reference signal, the integrated control and estimation are achieved by using the deadbeat adaptive backstepping technique. A Least-Squares estimation algorithm is first proposed to estimate the unknown system parameter, and then, the discrete-time backstepping control law is designed to guarantee the reference tracking, and at the same time, to achieve the deadbeat form of closed-loop system for fast convergence.

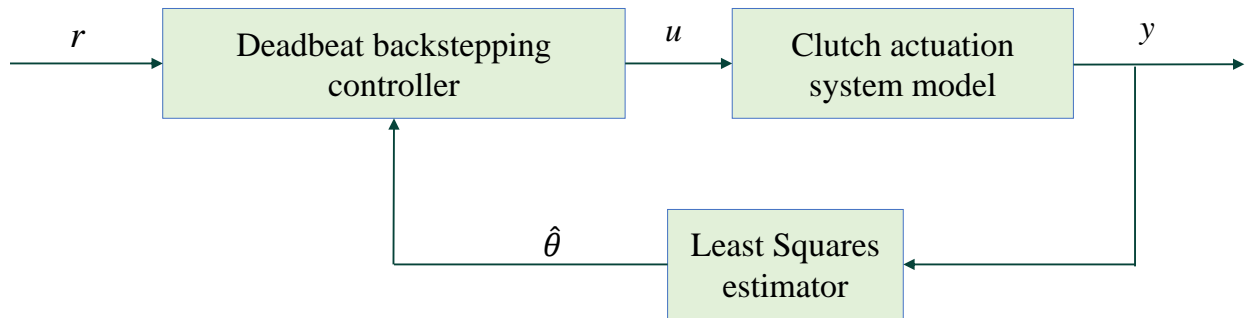


Figure 3.1: Chapter organization overview

3.1.2 Review of Backstepping Control

Model-based backstepping control technique is utilized due to its integrated architecture for estimating unknown system parameters and tracking reference simultaneously. In general, the backstepping

control technique designs a stabilizing controller at each stage of the control synthesis process for a special class of nonlinear systems. The stability of the closed-loop system is guaranteed at each design stage by the properly selected Lyapunov function [46]. The backstepping control scheme was initially developed in [47, 48, 49] to stabilize a class of nonlinear dynamic systems in a recursive way. References [50] and [51] present adaptive backstepping control approaches for continuous-time systems, resulting a globally stable closed-loop system as well as asymptotically reference tracking. In [52] and [53] the backstepping-based adaptive control was utilized for position tracking.

However, these controllers are designed in continuous-time domain [54]. In fact, for practical applications, discrete-time adaptive backstepping control is more desirable since it can be implemented exactly for real-time control. In [55], a second-order discrete-time backstepping controller was developed for a pumping station system and validated experimentally. However, there is not much earlier work for the discrete-time adaptive backstepping design. This is mainly due to the fact that the difference Lyapunov function in discrete-time domain does not obey the product rule used for the derivative of Lyapunov function in continuous-time domain. Thus, it is somehow difficult to find such a discrete-time linear Lyapunov function with respect to incremental variables. Therefore, the discrete-time adaptive backstepping scheme is more challenging in practical applications than that of the continuous-time case. However, note that the continuous-time scheme could be sensitive to signal noises due to the derivative operations in the backstepping control scheme, while the discrete-time scheme only uses the difference operation between two time steps and is more robust to the system noises. Also, it is worth to note that the discrete-time scheme is able to deal with rapid change of reference signal, which is another advantage over continuous-time case. Furthermore, the method, proposed in this paper, provides fast closed-loop system response by taking advantage of the deadbeat form, which is available only for discrete-time control.

In [56], the regulation problem using the discrete-time backstepping controller was addressed for both known and unknown chaos system parameters. Reference [57] adopted the backstepping procedure and designed a robust adaptive controller to reach the canonical form closed-loop system

so that global stability and global asymptotically tracking were achieved.

3.2 System Transformation for Backstepping Design

The backstepping design starts with the clutch actuation system. For convenience, the clutch actuation system is show here again in Figure 3.2. Although it is different from what is shown in Figure 2.2, they are essentially the same based on the physical clutch actuation system.

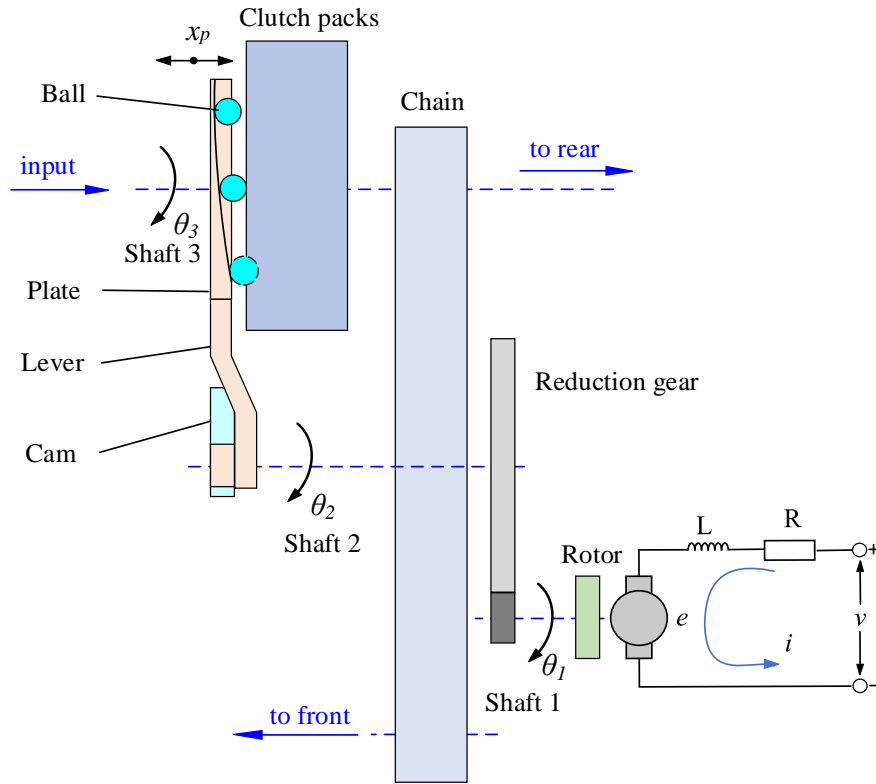


Figure 3.2: Transfer case clutch actuation system

Based on the modeling equations in Chapter 2, a system state-space model can be obtained below by choosing states as $x = [x_1, x_2, x_3]^T = [\theta_1, \dot{\theta}_1, \frac{K_e}{J_m} i]^T$, input as v , and output as $y = x_1$.

$$\begin{aligned}
 \dot{x}_1 &= x_2 \\
 \dot{x}_2 &= x_3 - \frac{b}{J_m} x_2 - \frac{h(x_1)}{J_m} - \frac{d}{J_m} \\
 \dot{x}_3 &= -\frac{K_e K_t}{J_m L} x_2 - \frac{R}{L} x_3 + \frac{K_e}{J_m L} u \\
 y &= x_1
 \end{aligned} \tag{3.1}$$

Note that term d to be estimated is the same as that in equation (2.16). However, the main difference between this system and the system (2.19) in Chapter 2 is that $h(x_1)$ in this system is kept as a nonlinear function due to the ability of dealing nonlinearity by the backstepping design.

The $h(x_1)$ function takes the form of

$$h(x_1) = \frac{k_c k_b g(x_1/i_r) r_b \tan \beta}{i_r i_s \eta_r \eta_s \eta_p} \quad (3.2)$$

and the function $g(\cdot)$ is the same as that in equation (2.5) and according to Figure 2.4, it can be fitted using a third order polynomial for either 4-H or 4-L range. Consider the case of 4-L range, in which the transfer case operates in most of the time, the function is fitted as:

$$g(p) = h_3 p^3 + h_2 p^2 + h_1 p + h_0 \quad (3.3)$$

where h_0 , h_1 , h_2 and h_3 are coefficients, and p is the variable.

This completes the nonlinear form of the clutch actuation system.

3.2.1 Parametric Semi-Strict Feedback Formulation

System (3.1) can be represented in a more general parametric semi-strict feedback form [58] as following.

$$\begin{aligned} \dot{x}_1 &= x_2 + g_1(x_1) + \theta^* f_1(x_1) \\ \dot{x}_2 &= x_3 + g_2(x_1, x_2) + \theta^* f_2(x_1, x_2) \\ \dot{x}_3 &= \beta(x)u + g_3(x_1, x_2, x_3) + \theta^* f_3(x_1, x_2, x_3) \\ y &= x_1 \end{aligned} \quad (3.4)$$

For the backstepping control to be utilized, the following assumption needs to be satisfied.

Assumption 2: f_i and g_i ($i = 1, 2, 3$) are known and continuously differentiable, and $\beta(x)$ is lower-bounded by a positive constant β_0 , i.e. $\beta(x) \geq \beta_0 > 0$.

From system (3.1), nonlinear functions in (3.4) are corresponding to the functions below.

$$g_1(x_1) = f_1(x_1) = 0, \theta^* = d$$

$$g_2(x_1, x_2) = -\frac{b}{J_m}x_2 - \frac{h(x_1)}{J_m}, f_2(x_1, x_2) = -\frac{1}{J_m},$$

$$\beta(x) = \frac{K_e}{J_m L}, g_3(x_1, x_2, x_3) = -\frac{K_e K_t}{J_m L}x_2 - \frac{R}{L}x_3, f_3(x_1, x_2, x_3) = 0.$$

where θ^* is the unknown term to be estimated. And it is obvious that the **Assumption 2** is satisfied.

3.2.2 Discretized Parametric Semi-Strict Feedback Formulation

This design will be in the discrete-time form so that we can take the advantage of the deadbeat closed-loop system. For a nonlinear system, the exact Linear Time Invariant system discretizing formula cannot be performed. Thus, Euler Approximation is used below.

$$\dot{x} = \frac{x(k+1) - x(k)}{T} \quad (3.5)$$

where T is the sampling period.

For simplicity, $g_1(x_1) = f_1(x_1) = 0$ and $f_3(x_1, x_2, x_3) = 0$ are ignored, and the resulting discrete time system is

$$\begin{aligned} x_1(k+1) &= x_1(k) + T x_2(k) \\ x_2(k+1) &= x_2(k) + T(x_3 + g_2(x_1, x_2) + \theta^* f_2) \\ x_3(k+1) &= x_3(k) + T(\beta(x)u + g_3(x_1, x_2, x_3)) \\ y &= x_1(k) \end{aligned} \quad (3.6)$$

Note that system (3.6) is still in the parametric semi-strict feedback form and will be used in the control design in the following section.

3.3 Deadbeat Adaptive Backstepping Algorithm Development

3.3.1 Non-Lyapunov-Function-Based Deadbeat Adaptive backstepping control design

During the control design process, no Lyapunov function is needed to guarantee the convergence as it is required in the traditional backstepping design. That is why it is called a Non-Lyapunov-Function-Based design.

The controller design is divided into two steps, where the first step is to design the adaptive parameter estimation law to update the unknown parameter and the second step is to design the actual control law u to track the reference signal.

Step 1: designing estimation law

Design the first auxiliary state z_1 and second auxiliary state z_2 , respectively, below.

$$z_1(k) = x_1(k) \quad (3.7)$$

$$z_2(k) = x_1(k) + Tx_2(k) \quad (3.8)$$

Propagating the auxiliary states one step ahead results

$$z_1(k+1) = x_1(k+1) = z_2(k) \quad (3.9)$$

$$\begin{aligned} z_2(k+1) &= Tx_2(k+1) + x_1(k+1) \\ &= T[Tx_3(k) + x_2(k) + Tg_2(x_1(k), x_2(k)) + \theta^*Tf_2] + z_2(k) \\ &= z_2(k) + T^2x_3(k) + Tx_2(k) + T^2g_2(x_1(k), x_2(k)) + \hat{\theta}T^2f_2 - \tilde{\theta}T^2f_2 \\ &= z_3(k) - \tilde{\theta}T^2f_2 \end{aligned} \quad (3.10)$$

where $\tilde{\theta}(k) = \hat{\theta}(k) - \theta^*$ is the parameter estimation error, and the third auxiliary state z_3 is designed as

$$\begin{aligned} z_3(k) &= z_2(k) + T^2x_3(k) + Tx_2(k) \\ &\quad + T^2g_2(x_1(k), x_2(k)) + \hat{\theta}T^2f_2 \end{aligned} \quad (3.11)$$

Rearranging equation (3.10) yields the following discrete-time linear parametric error model as follows.

$$\epsilon(k) = -\tilde{\theta}^T(k)\phi(k) \quad (3.12)$$

where $\epsilon(k) = z_2(k+1) - z_3(k)$ is the estimation output error and $\phi(k) = T^2f_2$ can be viewed as the regression vector.

The update law for the unknown parameter can be designed using the normalized Least-Squares estimation algorithm [38] below.

$$\hat{\theta}(k+1) = \hat{\theta}(k) + \frac{P(k)\phi(k)\epsilon(k)}{\kappa + (\phi(k))^T P(k)\phi(k)} \quad (3.13)$$

$$P(k+1) = P(k) - \frac{P(k)(\phi(k))(\phi(k))^T P(k)}{\kappa + (\phi(k))^T P(k)\phi(k)} \quad (3.14)$$

where κ is the designing parameter and $P(0) > 0$. To this point, the first step, namely, the parameter estimation is completed.

Step 2: designing control law

For tracking purpose, propagating the third auxiliary state z_3 at time step $k+1$ and considering the system equation (3.6) yield

$$\begin{aligned}
z_3(k+1) &= z_2(k+1) + T^2 x_3(k+1) + T x_2(k+1) \\
&\quad + T^2 g_2(x_1(k+1), x_2(k+1)) \\
&\quad + \hat{\theta}(k+1) T^2 f_2 \\
&= z_3(k) - \tilde{\theta}(k) T^2 f_2 + T^2 (T \beta u + x_3(k) + \\
&\quad T g_3(x_2(k), x_3(k))) + T x_2(k+1) + \\
&\quad T^2 \left(-\frac{b}{J_m} x_2(k+1) - \frac{h(x_1(k+1))}{J_m}\right) \\
&\quad + \hat{\theta}(k+1) T^2 f_2 \\
&= T^3 \beta u + T^2 x_3(k) + T^3 g_3(x_2(k), x_3(k)) \\
&\quad + z_3(k) + \left(T - \frac{b}{J_m} T^2\right) x_2(k+1) \\
&\quad - T^2 \frac{h(x_1(k+1))}{J_m} + \hat{\theta}(k+1) T^2 f_2 - \tilde{\theta}(k) T^2 f_2 \\
&= T^3 \beta u + T^2 x_3(k) + T^3 g_3(x_2(k), x_3(k)) \\
&\quad + z_3(k) + \left(T - \frac{b}{J_m} T^2\right) (T x_3(k) + x_2(k) \\
&\quad + T g_2(x_1(k), x_2(k)) + \theta^* T f_2) \\
&\quad - T^2 \frac{h(x_1(k+1))}{J_m} + \hat{\theta}(k+1) T^2 f_2 - \tilde{\theta}(k) T^2 f_2 \\
&= T^3 \beta u + T^2 x_3(k) + T^3 g_3(x_2(k), x_3(k)) \\
&\quad + z_3(k) + \left(T - \frac{b}{J_m} T^2\right) (T x_3(k) \\
&\quad + x_2(k) + T g_2(x_1(k), x_2(k)) + \hat{\theta} T f_2) \\
&\quad - T^2 \frac{h(x_1(k+1))}{J_m} + \hat{\theta}(k+1) T^2 f_2 \\
&\quad - \tilde{\theta}(k) T^2 f_2 - \tilde{\theta}(k) \left(T - \frac{b}{J_m} T^2\right) T f_2
\end{aligned} \quad (3.15)$$

Design the control input u as

$$\begin{aligned}
u = & -\frac{1}{T^3\beta}(T^2x_3(k) + T^3g_3(x_2(k), x_3(k))) \\
& + z_3(k) + (T - \frac{b}{J_m}T^2)(Tx_3(k) + x_2(k)) \\
& + Tg_2(x_1(k), x_2(k)) + \hat{\theta}(k)Tf_2 \\
& - T^2\frac{h(x_1(k+1))}{J_m} + \hat{\theta}(k+1)T^2f_2 - r(k+3)
\end{aligned} \tag{3.16}$$

and convert equation (3.15) to

$$z_3(k+1) = r(k+3) - \tilde{\theta}(k)(2 - \frac{b}{J_m}T)T^2f_2 \tag{3.17}$$

where $r(k)$ is the reference signal assumed to be known and bounded. By implementing the designed control u (3.16) into plant system (3.6), the closed-loop system eventually becomes

$$\begin{aligned}
z_1(k+1) &= z_2(k) \\
z_2(k+1) &= z_3(k) - \tilde{\theta}(k)T^2f_2 \\
z_3(k+1) &= r(k+3) - \tilde{\theta}(k)(2 - \frac{b}{J_m}T)T^2f_2
\end{aligned} \tag{3.18}$$

The system can be expressed in a more compact form below:

$$\begin{aligned}
z(k+1) &= A_z z(k) + B_z r(k+3) + \Phi(k) \\
y(k) &= C_z z(k)
\end{aligned} \tag{3.19}$$

where matrix $A_z = \begin{bmatrix} 0 & 1 & 0 \\ 0 & 0 & 1 \\ 0 & 0 & 0 \end{bmatrix}$ is deadbeat; $B_z = \begin{bmatrix} 0 \\ 0 \\ 1 \end{bmatrix}$; $\Phi(k) = E\tilde{\theta}(k)$, $E = \begin{bmatrix} 0 \\ -1 \\ -(2 - \frac{b}{J_m}T) \end{bmatrix} T^2 f_2$;
and $C_z = \begin{bmatrix} 1 & 0 & 0 \end{bmatrix}$.

3.3.2 Stability and Convergence Analysis

For the closed-loop system (3.19), reference $r(k)$ serves as the system input, and the transfer function from $r(k)$ to $y(k)$ can be expressed as

$$G(z) = C_z(zI - A_z)^{-1}B_z \tag{3.20}$$

The stability of transfer function $G(z)$ is guaranteed since all the eigenvalues of A_z are at zero, which is inside the unit circle. As a result, any bounded reference signal $r(k)$ leads to a bounded output $y(k)$. Therefore, to proceed with the stability analysis for system (3.19), the reference can be set to 0, i.e., $r(k) = 0$, and the closed-loop system reduces to

$$\begin{aligned}
z(k) &= A_z z_{k-1} + \Phi(k-1) \\
&= A_z (A_z z_{k-2} + \Phi(k-2)) + \Phi(k-1) \\
&= A_z^2 z_{k-2} + A_z \Phi(k-2) + \Phi(k-1) \\
&\vdots \\
&= A_z^k z(0) + \sum_{i=0}^{k-1} A_z^i \Phi(k-1-i)
\end{aligned} \tag{3.21}$$

Due to the special deadbeat structure of matrix A_z in (3.19), for $i = 3, 4, \dots, k-1$,

$$A_z^i = 0 \tag{3.22}$$

Therefore, for $k \geq 3$, equation (3.21) can be further reduced down to

$$\begin{aligned}
z(k) &= A_z^2 \Phi(k-3) + A_z \Phi(k-2) + \Phi(k-1) \\
&= A_z^2 E \tilde{\theta}(k-3) + A_z E \tilde{\theta}(k-2) + E \tilde{\theta}(k-1)
\end{aligned} \tag{3.23}$$

For $z(k)$ to be bounded, the sequence $\tilde{\theta}(k)$ should be bounded, which is guaranteed by the Least-Squares estimation algorithm and the proof is shown below.

A Lyapunov function for the Least-Squares estimation algorithm is defined as

$$V(k) = \tilde{\theta}(k) P(k)^{-1} \tilde{\theta}(k) \tag{3.24}$$

Note that the above Lyapunov function is used to prove the convergence of the Least-Squares algorithm in equations (3.12) and (3.13), and not for the non-Lyapunov function-based backstepping control design.

Subtracting θ^* from both sides of (3.13) leads to

$$\tilde{\theta}(k+1) = \tilde{\theta}(k) - \frac{P(k) \phi(k) \phi(k)^T \tilde{\theta}(k)}{\kappa + (\phi(k))^T P(k) \phi(k)} \tag{3.25}$$

and combining it with equation (3.14) yields

$$\tilde{\theta}(k+1) = P(k+1)P(k)^{-1}\tilde{\theta}(k) \quad (3.26)$$

which leads to the following difference Lyapunov function

$$\begin{aligned} \Delta V(k) &= V(k+1) - V(k) \\ &= (\tilde{\theta}(k+1) - \tilde{\theta}(k))P(k)^{-1}\tilde{\theta}(k) \\ &= -\frac{\epsilon(k)^2}{\kappa + (\phi(k))^T P(k)\phi(k)} \leq 0 \end{aligned} \quad (3.27)$$

Since $\Delta V(k)$ is non-positive, it can be concluded that $V(k)$ is bounded, and therefore $\tilde{\theta}(k)$ is bounded. This concludes that $z(k)$ is bounded. To show that $z(k)$ converges to 0 when k goes to infinity, or equivalently

$$\lim_{k \rightarrow \infty} z(k) = 0 \quad (3.28)$$

for any bounded initial condition $z(0)$, the following lemma from [59] is needed.

Lemma 1: *If the signal $\phi(k)$ is persistently exciting, the Least-Squares estimation algorithm described in equations (3.13) and (3.14) guarantees that $\lim_{k \rightarrow \infty} \|\tilde{\theta}(k)\|_2 = 0$.*

Since $\phi(k)$ is a non-zero scalar defined in equation (3.12) once the sampling period T is determined for a discrete-time system, there always exist $\delta > 0$ and $\alpha > 0$ such that over the time interval $[\sigma, \sigma + \delta]$

$$\int_{\sigma}^{\sigma+\delta} \phi^T(t)\phi(t)dt \geq \alpha I \quad (3.29)$$

for any $\sigma > t_0$. Hence, signal $\phi(k)$ is persistently exciting. Furthermore, the convergence of estimation error $\tilde{\theta}(k)$ leads to $\lim_{k \rightarrow \infty} z(k) = 0$, which can be clearly observed from equation (3.23).

Theorem 1: If Lemma 1 is satisfied, all closed-loop system states are bounded, and its output tracks the reference signal.

Proof: Since $\tilde{\theta}$ converges to 0 in finite steps k , beyond step k , $\tilde{\theta}(k) = 0$, which implies that

$\Phi(k + 1) = 0$. Equation (3.19) becomes

$$\begin{aligned} z_1(k + 1) &= z_2(k) \\ z_2(k + 1) &= z_3(k) \\ z_3(k + 1) &= r(k + 3) \end{aligned} \tag{3.30}$$

It is obvious that $z_1(k)$ tracks $r(k)$ in this case. And for any bounded $r(k)$, $z_1(k)$, $z_2(k)$ and $z_3(k)$ are also bounded. Note that, different from the traditional backstepping design, in this design architecture, $z_1(k)$, $z_2(k)$ and $z_3(k)$ are not tracking error terms for different states, but the same tracking signal at three consecutive steps. In addition, due to this property and deadbeat design of system (3.19), the effect of any external disturbance will last for no more than three steps. As a result, the algorithm is robust to the external disturbance.

In comparison with the algorithm described in reference [57], where the closed-loop system is designed in the controller canonical form below.

$$z(k + 1) = Mz(k) + by_m(k + n) + \Psi(k + 1) + e(k + 1) \tag{3.31}$$

where system matrix M is in the controller canonical form, and detailed $\Psi(k + 1)$ and $e(k + 1)$ expressions are not listed here. Let matrix M be

$$M = \begin{bmatrix} 0 & 1 & 0 \\ 0 & 0 & 1 \\ -m_1 & -m_2 & -m_3 \end{bmatrix} \tag{3.32}$$

which has the same dimension as A_z in our deadbeat design. For the convergence analysis of $z(t)$, let the reference $y_m(k + n) = 0$ and define $\Theta(k + 1) = \Psi(k + 1) + e(k + 1)$, equation (3.31) reduces to

$$z(k + 1) = Mz(k) + \Theta(k + 1) \tag{3.33}$$

The solution of $z(k)$ is

$$z(k) = M^k z(0) + \sum_{j=0}^{k-1} M^j \Theta(k - 1 - j) \tag{3.34}$$

For the control canonical form matrix M , if the elements $[m_1 \ m_2 \ m_3] \neq 0$, namely M is different from the deadbeat form of A_z , for any non-zero initial condition $z(0)$, the response $M^k z(0)$ with given initial condition $z(0)$ for $t \geq 3$ will not vanish. Considering also the estimation error in Θ , $z(k)$ cannot converge to 0 within 3 steps in general. Thus, based on the analysis of deadbeat design, it is obvious that the deadbeat design converges faster than the algorithm in reference [57].

Note that the convergence analysis can easily be extended to n dimensional A_z or M , in this case A_z can converge in at most n steps while M cannot.

Another restriction of the canonical form of matrix M in (3.32) is that the tracked signal depends on not only the reference signal but also the choice of m_i ($i = 1, 2, 3$). From reference [57] the tracking error satisfies

$$\sum_{\tau=t_0}^{t-1} |y(\tau) - \frac{1}{K} y_m(\tau)| \leq \beta_1 + \beta_2 0(\epsilon, \epsilon_\theta)(t - t_0) \quad (3.35)$$

where $K = 1 + \sum_{i=1}^n |m_i|$, β_1 and β_2 are constants, and $0(\epsilon, \epsilon_\theta)(t - t_0)$ is a function such that $\lim_{\epsilon \rightarrow 0, \epsilon_\theta \rightarrow 0} 0(\epsilon, \epsilon_\theta)(t - t_0) = 0$. Therefore, the tracking error depends on the locations of the poles of matrix M . While according to Theorem 1, the deadbeat design can track the reference robustly.

A simple example is used to show the influence of choices for m_i . Consider equations (3.19) and (3.31) without any estimation error, and choose the first set of m_i at $m_1 = -0.216, m_2 = 1.08$ and $m_3 = -1.8$ so that all the closed-loop system poles are at 0.6, which is inside the unit circle, the second set of m_i at $m_1 = -0.027, m_2 = 0.27$ and $m_3 = -0.9$ so that all the closed-loop system poles are at 0.3, and the third set of m_i ($i = 1, 2, 3$) equal to 0. The reference is chosen as $r = 1$. The simulation response is shown in Figure 3.3. It can be seen that on one hand, when the closed-loop system poles are at 0, the deadbeat design is identical to the canonical design, therefore their convergence rate are the same; on the other hand, the convergence rate of the deadbeat design is faster than the canonical designs when their poles are not all at 0; furthermore, the deadbeat design tracks the reference exactly, while the canonical designs converge to a value different from the reference. Note that the closer to 0 the closed-loop system poles are, the more accurate the tracking

can be achieved.

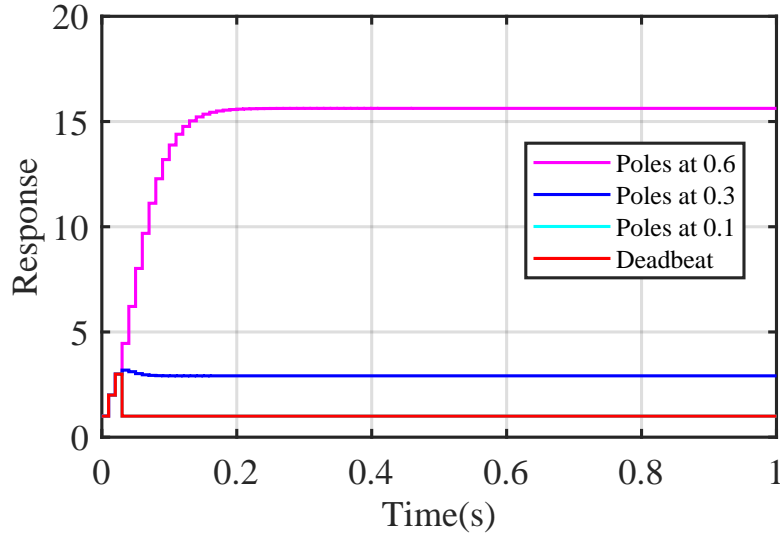


Figure 3.3: Comparison of canonical and deadbeat designs

3.4 Results Performance Evaluation

The motor parameters are provided in Table 3.1. The reference signal r is from vehicle experiment. The initial condition for the control algorithm is chosen as $x = [r(1), 0, 0]^T$. For the canonical design, the designing parameters m_i ($i = 1, 2, 3$) are selected so that the poles of matrix M are at 0.5, 0.5, 0.5 to show the validity of the deadbeat design. For simulation purpose, the unknown x_0 is assumed to be $1e-4$ m. Sampling time is selected to be 0.01s.

Table 3.1: DC Motor Parameters

Parameters	Value	Unit
Inertia J_m	7×10^{-5}	Kgm^2
Damping b_1	1.17×10^{-3}	Nms
Resistance R	0.25	Ω
Inductance L	0.495×10^{-3}	H
Torque Constant K_e	0.036	Nm/A
Back-EMF Constant K_m	0.036	Vs/rad

3.4.1 Reference Signal: 2WD Case

The reference position signal is shown as the blue line in Fig 3.4. The reference starts at some point where the ball is in contact with the clutch, transmitting torque to the front shaft, and then falls back to the steady-state where no torque is transmitted to the front shaft, which is equivalent to the 2WD (2-Wheel-Drive) situation.

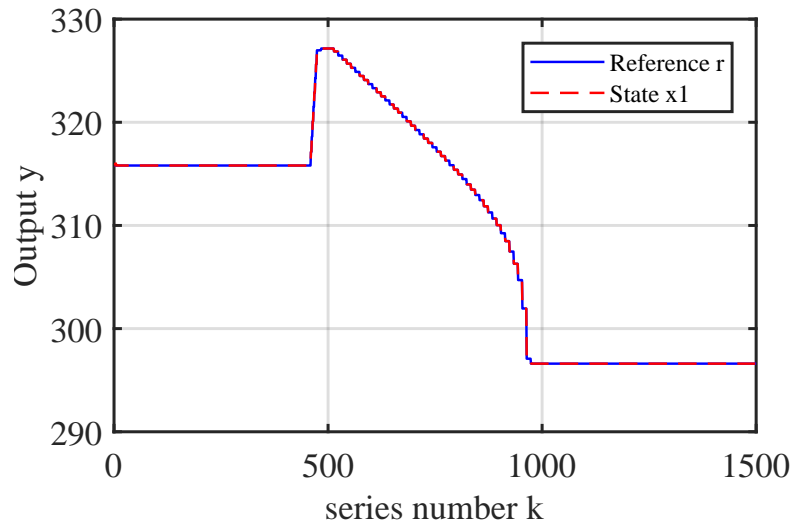


Figure 3.4: Tracking for deadbeat design

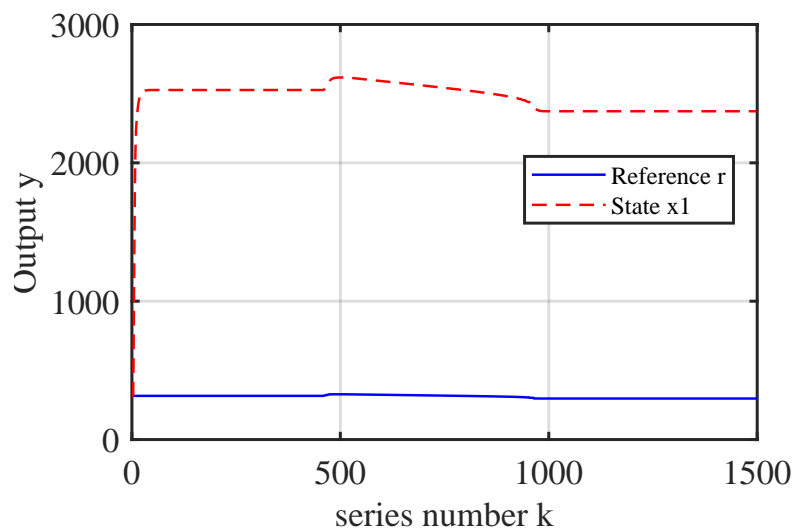


Figure 3.5: Tracking for canonical design

Figure 3.4 shows the output tracking for the deadbeat design and Figure 3.5 for the canonical

design. It is clear that the deadbeat design tracks the reference signal exactly while the canonical design cannot due to the three non-zero design parameters m_1 , m_2 , and m_3 . Figure 3.6 shows the closed-loop state responses for the deadbeat design and Figure 3.7 for the canonical design. Note that different from the traditional backstepping design, the states in the closed-loop system are not tracking errors but actual tracking signal at three consecutive steps. The simulation results show that the states in both designs are convergent. But after careful examination, it reveals that the deadbeat design converges at step 6 while the canonical design converges at around step 20, indicating that the deadbeat design converges faster. For the unknown term estimation, both designs use the same update law, the result shown in Figure 3.8 exhibits fast convergence with no oscillations. The control effort for the deadbeat design is shown in Figure 3.9. Note that the recorded reference (see Figure 3.4) was sampled at 10 Hz and then the signal is resampled at 100 Hz (the controller sample frequency), the signal has a small step change every 100 ms, which could cause chattering in control signal. To eliminate the chattering caused by low sample frequency of the reference signal, a low-pass filter is applied to the resampled reference signal to smooth the sampled reference signal.

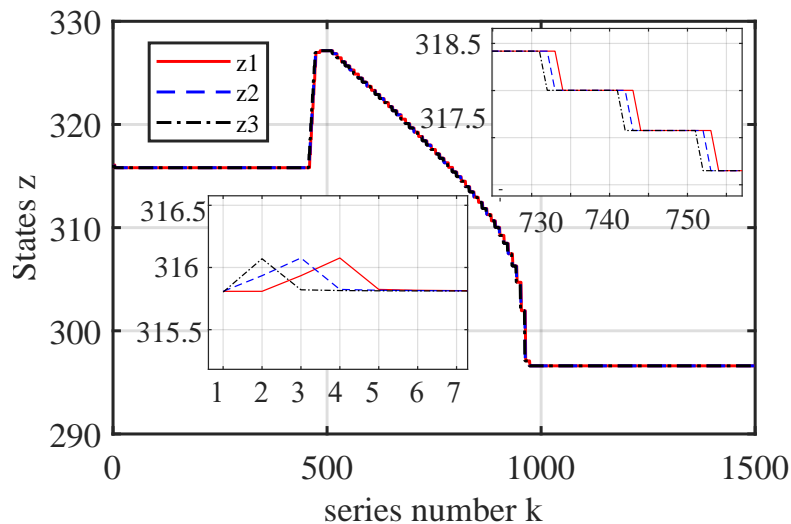


Figure 3.6: States for deadbeat design

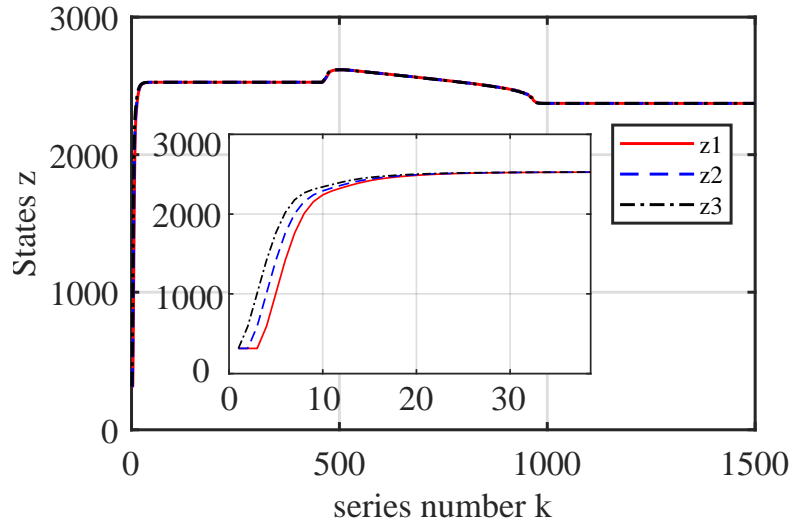


Figure 3.7: States for canonical design

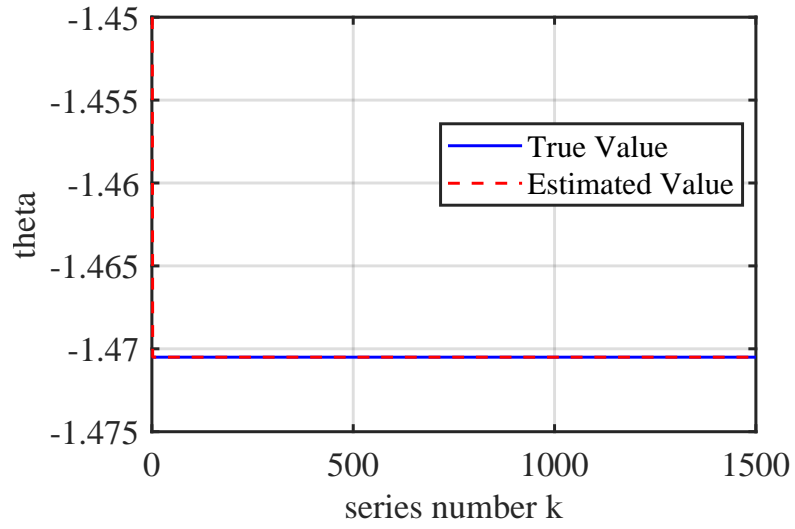


Figure 3.8: Unknown term estimation

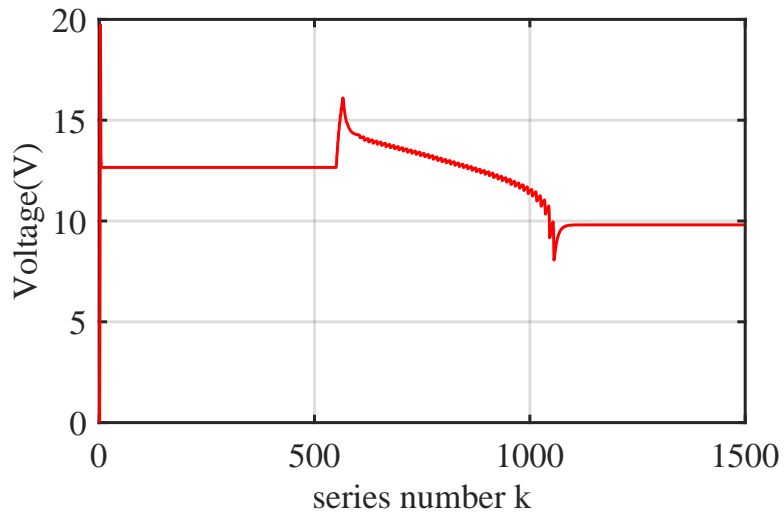


Figure 3.9: Control effort

3.4.2 Reference Signal: 4WD Case

In this case, the steady-state of reference position is kept at the point where there is certain amount of torque transmitted to the front shaft, which corresponds to the 4WD (4-Wheel-Drive) mode. The reference signal is shown as the blue line in Figure 3.10.

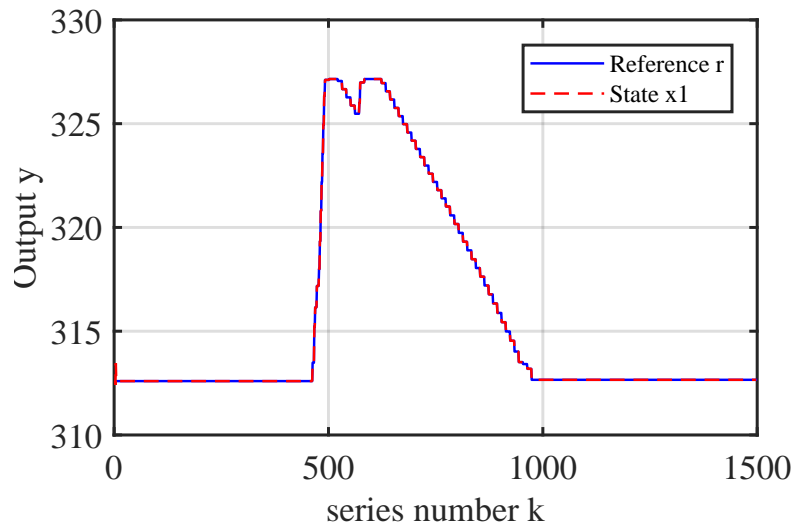


Figure 3.10: Reference tracking

The convergence trends are similar to that of the previous case. Figure 3.10 shows the tracking

performance and it is obvious that the output also tracks the reference. Figure 3.11 shows the closed-loop states responses and again the three states are the same signal at three different time steps. Figure 3.12 is the control effort to achieve the aforementioned performance.

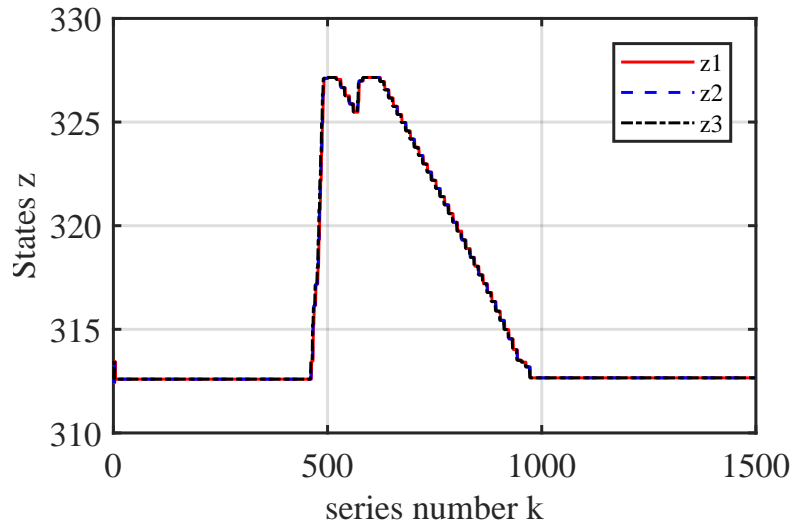


Figure 3.11: Closed-loop States estimation

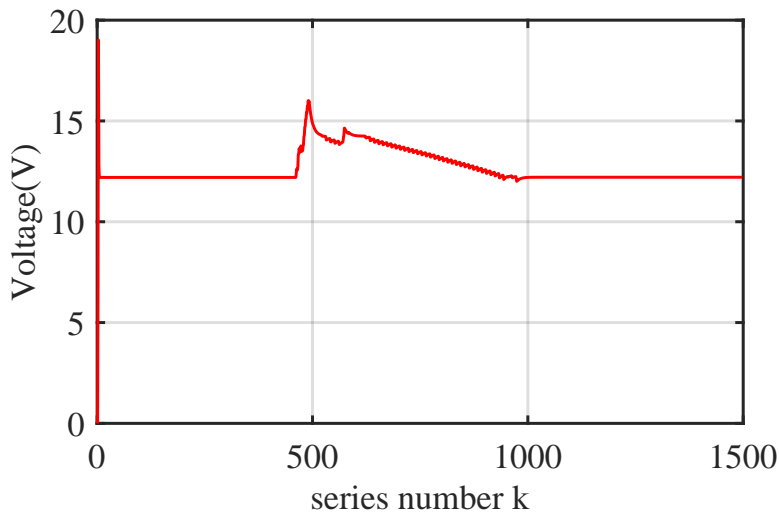


Figure 3.12: Control effort for 4WD case

3.5 Conclusions

In conclusion, the following are achieved in this chapter:

1. The clutch actuation system model is first transformed to a parametric semi-strictly form in preparation for backstepping control design;
2. The integrated scheme is achieved by two steps: first step designs the estimation law to estimate the unknown parameter and the second step designs the control law so that the output of close-loop system tracks the desired reference clutch displacement; The stability of closed-loop system is guaranteed by the post-design Lyapunov function analysis, and the fastest convergence rate is realized due to the deadbeat design.
3. The integrated design scheme is validated using different reference signals corresponding to different vehicle mode (2WD or 4WD) and also compared with that of the canonical design.

CHAPTER 4

CLUTCH TORQUE MODELING AND VALIDATION UNDER VARIOUS CLUTCH OPERATION CONDITIONS

4.1 Overview

4.1.1 Chapter Organization

In this chapter, the vehicle traction force (or clutch torque) is estimated. Several models are proposed to deal with the challenges stated in the chapter of Introduction. First, the effective tire radius model with vehicle acceleration compensation is proposed; Second, the vehicle speed estimation model is proposed by considering the vehicle and tire tracking force dynamics; Lastly, a torque estimation model under different clutch operational conditions is proposed, where the clutch operational condition is determined by the clutch slip speed. The comparison of estimated and measured torques shows the validity of proposed estimation model.

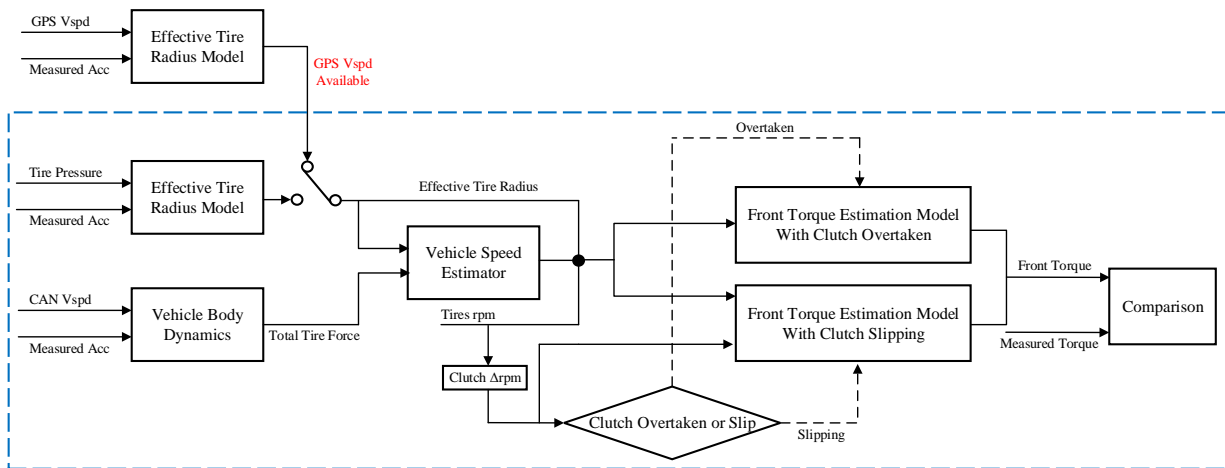


Figure 4.1: Chapter organization overview

4.1.2 Review of Clutch Torque Estimation

A well-known solution for transmission clutch torque estimation is via the vehicle propulsion system dynamics between the IC engine to vehicle tires for 2WD systems, where the clutch is located right after the IC engine[60], [61], [62], [63], [64]. While for 4WD systems with a transfer case (see Figure 4.2), since the transmission output torque is split into solid-connected rear tires and soft-connected front tires through transfer case clutch and the actual torque distribution ratio between front and rear tires is typically unknown, it is challenging to estimate the transfer case clutch torque.

This chapter proposes to estimate the transfer case clutch torque based on both vehicle longitudinal and tire dynamics. That is, estimating the clutch torque based upon the estimated front tire traction force. Although tire magic formula (TMF) proposed in [23] is widely used to model the longitudinal force characteristics, the nonlinearity nature of this formula could make the estimation problem over-complicated since under normal vehicle operations tire characteristics is close to linear. Therefore, the tire longitudinal force is assumed to be linear, that is, the longitudinal force is a linear function of tire slip ratio, which depends heavily on vehicle longitudinal speed and effective tire radius [65].

Many methods, including direct and indirect ones, are available to obtain vehicle speed in real-time. One of the direct methods is the well-known GPS measurement [66], [67]. However, limited by technology and cost, highly accurate GPS devices may not be equipped in all production vehicles. The indirect estimation method is usually based on the vehicle dynamic models whose complexity varies case-by-case for different applications. Reference [68] presented a complete vehicle model, including longitudinal, lateral and yaw dynamics, to estimate the vehicle speed along with many other vehicle parameters using a dual-extended Kalman filter. While reference [69] employs a bicycle model to estimate vehicle states and tire stiffness simultaneously. In this paper, the bicycle model is adopted due to its simplicity since this work is aiming at real-time applications in future. However, different from these references, this dissertation estimates the vehicle speed from the measured acceleration and the associated longitudinal tire forces. Detailed estimator architecture

can be found in Section 4.3.1.2. Note that all these estimation models depend on the accuracy of effective tire radius used in the tire longitudinal or lateral forces as part of the vehicle dynamics model.

As a matter of fact, many literature assume effective tire radius to be constant [24]. However, on one hand, the tire effective radius may change with tire inflation pressure [70] over time since tire pressure is closely related to the tire vertical stiffness; on the other hand, when a vehicle is accelerating or braking, the pitch motion along the lateral axis of vehicle may change the normal force distribution to front and rear tires, leading to variation of effective tire radius. As a result, it is proposed to estimate the effective tire radius in real-time. Reference [71] estimates the effective tire radii and rolling resistance forces in real-time based on a quarter-car model by designing nonlinear high-gain and sliding-mode observers and the proposed method is validated through simulation and experimental studies. In reference [72], the tire radius along with the vehicle trajectory was estimated based on GPS measurements using a marginalized particle filter. However, these approaches not only require complex system models but also expensive measurement devices that may not be available for production vehicles. Therefore, this paper utilizes a simple tire model as a function of tire pressure and vehicle acceleration, that are easily available through measurements, to estimate the effective tire radius. Detailed effective tire radius model can be found in Sections 4.3.1.3.

Another, yet important aspect to address is the effect of clutch operation conditions to the vehicle speed estimation due to the unique architecture of IC engine-powered 4WD propulsion system (see Figure 4.2). Note that in this architecture rear tires are always in solid connection with the transmission output shaft through transfer case, while the front tires connects to the transmission output shaft through transfer case clutch. When the clutch is overtaken, the connection is solid; and when the clutch slips, the connection is soft and there is certain slip speed transmits to the front tires from the transfer case clutch, making the front tire speed different from the rear tire speed. Therefore, this paper proposes to compensate this slip effect in the front tires when the clutch slips, and the tire slip model makes the overtaken case as a special case when slip speed equal to zero;

see Section 4.3.3 for details.

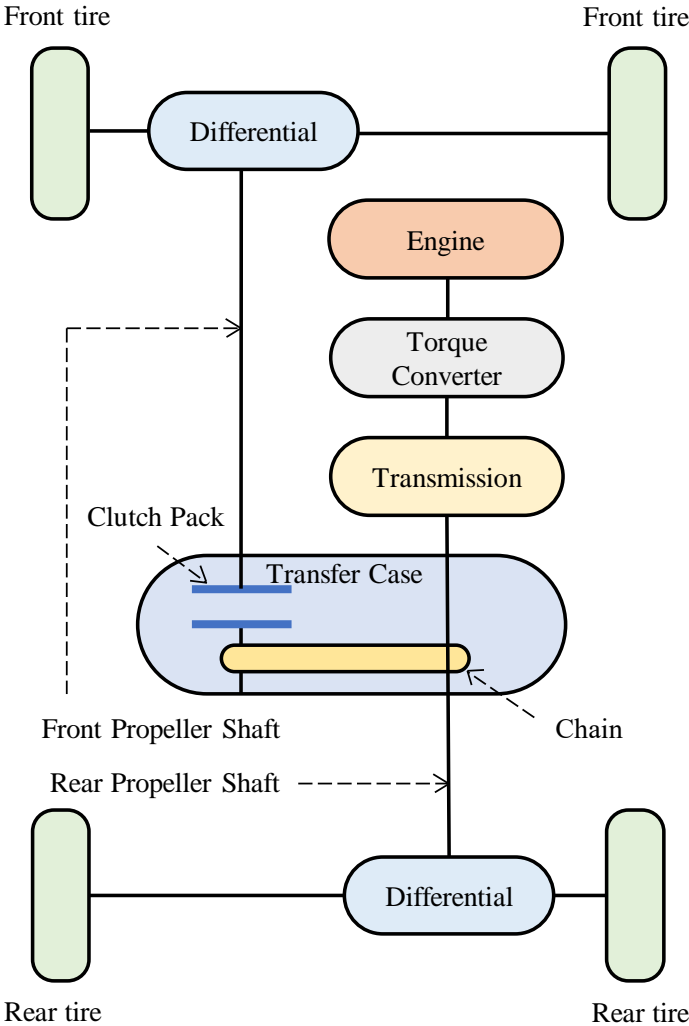


Figure 4.2: 4WD vehicle system overview

4.2 Clutch Torque Model Flow Chart

In this chapter, three clutch torque models are concerned, where the clutch torque model 1 (CTM-1) is a baseline model, the clutch torque model 2 (CTM-2) provides vehicle acceleration compensation to the developed effective tire radius model under clutch overtaken condition, and the clutch torque model 3 (CTM-3) deals with clutch slip condition based on CTM-2 model by taking clutch slip effect into account. Note that CTM-2 model is a special case of CTM-3 with zero

slip speed. The detailed modeling work is presented in Sections 4.3 and 4.4 .

Before diving into these estimation models, the process of estimating the clutch torque is summarized in Figure 4.3 as follows.

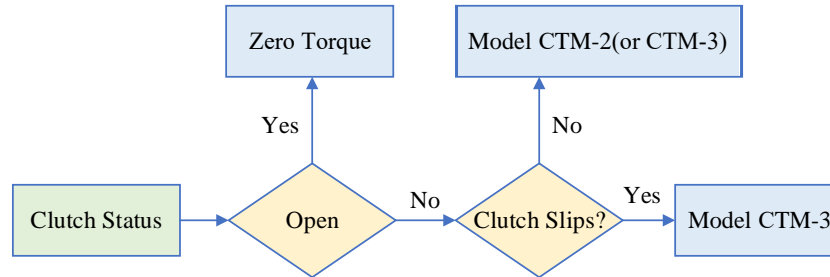


Figure 4.3: Clutch torque estimation flow chart

Step 1: Determine the clutch status. If it is open, the clutch output torque is zero;

Step 2: If the clutch is overtaking (see detailed condition in equation (4.21) of Section 4.3), proceed to the clutch torque model using CTM-2 (or CTM-3 with slip speed equals to zero);

Step 3: If the clutch is slipping, proceed to the clutch torque model using CTM-3.

4.3 Clutch Torque Modeling

From Figure 4.2, it is obvious that modeling the clutch torque is equivalent to model the tires traction torque, since front tires traction torque is directly connected to the clutch torque, and once the clutch torque becomes available, the rear tire traction torque would be easily obtained, assuming that the total torque from transmission is known. In the following section of this chapter, the notation of clutch torque model is used instead of traction torque.

When the clutch is disengaged, clutch output torque is zero, and therefore, no torque estimation is needed in this case. As a result, this paper focuses on the torque model development when the clutch is engaging. For an engaged clutch, there are two operational modes: slip and overtaken. Different clutch torque models will be developed to accommodate the condition changes.

4.3.1 Baseline Clutch Torque Model (CTM-1)

4.3.1.1 Tire dynamics

Note that transfer case clutch of target 4WD vehicle shown in Figure 4.2 acts as a torque distributor between the front and rear tires, and this dissertation estimates the clutch torque from tires backward to the clutch. As a result, clutch torsional damping effect is not considered.

When the clutch is engaged, the torque generated by the clutch is transmitted to the front wheels through the front propeller shaft. Assuming that there is no mechanical loss for the clutch driven components and the front propeller shaft is solid, the torque transmitted by the clutch should equal to the front propeller shaft torque, namely,

$$T_c = T_f \quad (4.1)$$

where T_c is clutch output torque and T_f is the torque transmitted by front propeller shaft.

The front propeller shaft torque drives the front tires through the front differential. The tire dynamics below links the front propeller shaft torque to the front tires.

$$T_f i_{fd} = J_f \dot{w}_f + F_f r_{ef} \quad (4.2)$$

where J_f is the front-tire inertia; w_f is the front-tire rotational speed; i_{fd} is the front differential ratio; F_f is the front-tire longitudinal force; and r_{ef} is the effective front-tire radius.

The relationship between tire longitudinal force and slip ratio is typically nonlinear and symmetric to the origin as shown in Figure 4.4. The longitudinal force increases to a peak as the slip ratio changes from zero to the threshold $|\lambda_0|$, and then decreases as the tire slip ratio continues increasing. The tire slip ratio is defined below with respect to different vehicle conditions.

$$\lambda_i = \begin{cases} \frac{r_{ei} w_i - v}{r_{ei} w_i}, & \text{acceleration} \\ \frac{r_{ei} w_i - v}{v}, & \text{brake} \end{cases} \quad (4.3)$$

where λ_i is tire slip ratio; i is either 'f' for front tire or 'r' for rear tire; and v is the vehicle longitudinal speed. This dissertation mainly concerns with the acceleration condition.

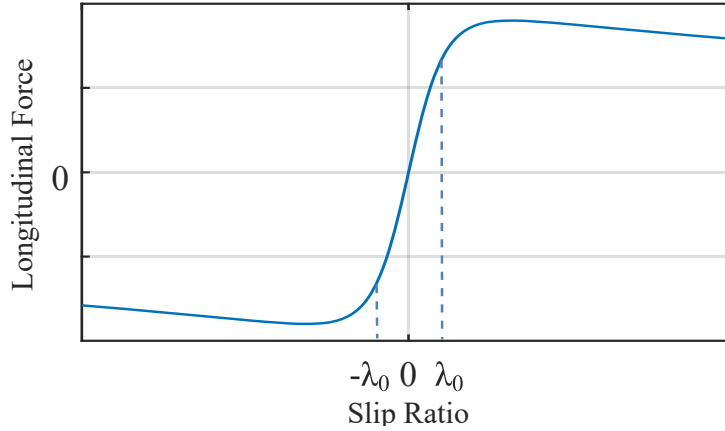


Figure 4.4: Longitudinal force vs slip ratio

Note that within range $|\lambda| \leq \lambda_0$ as shown in Figure 4.4, longitudinal force increases linearly with tire slip ratio. Therefore, for small tire slip ratio, longitudinal force can be approximated by

$$F_i = C_i \lambda_i, \quad |\lambda_i| \leq \lambda_0 \quad (4.4)$$

where C_i is the corresponding front or rear tire longitudinal stiffness and can be calibrated as constant.

Note that in equation (4.2), the longitudinal force term is a dominating factor for the traction torque T_f . Therefore, it is desired to have an accurate tire longitudinal force F_f , which depends largely on accurate vehicle longitudinal speed and effective tire radius according to equations (4.3) and (4.4).

4.3.1.2 Vehicle Speed Model

Although vehicle longitudinal acceleration can be measured with reasonable accuracy using the vehicle accelerometer sensor, the vehicle longitudinal speed obtained by direct integration of longitudinal acceleration is usually not accurate due to sensor signal drift. Alternatively, for certain production vehicles, the vehicle speed could be calculated using GPS (global position system) measurements with certain accuracy even though the estimated vehicle speed could be polluted by the measurement noise. While for those vehicles without the GPS, it is indispensable to estimate vehicle speed.

A possible solution of estimating vehicle speed is via vehicle body dynamics. Since the developed algorithm needs to be implementable in real-time, a simple vehicle model, neglecting the lateral and yaw vehicle dynamics, is desired. Consider the free body diagram of vehicle in Figure 4.5, according to the Newton's second law, the longitudinal vehicle dynamics can be obtained as following

$$m\dot{v} = F - F_a - F_{ro} - mg \sin \theta \quad (4.5)$$

where m is the vehicle mass; F is total longitudinal force; F_a is the air drag force; F_{ro} is tire rolling resistance force; g is gravity acceleration constant; and θ is road grade angle.

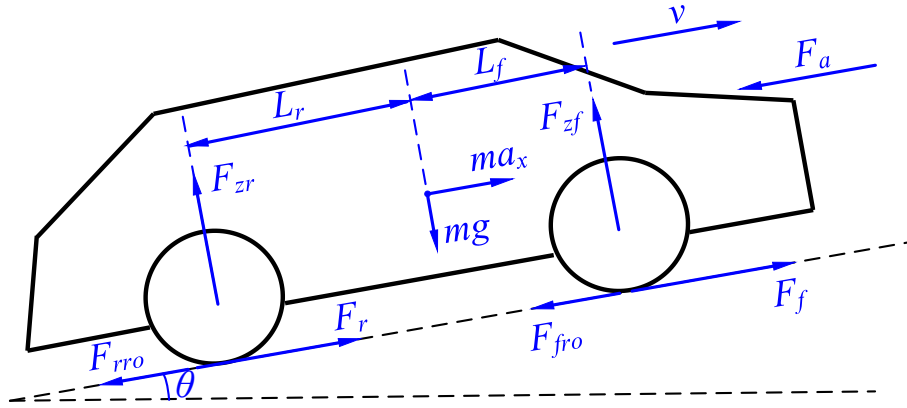


Figure 4.5: Vehicle Free Body Diagram

The air drag force can be approximated using

$$F_a = \frac{1}{2} C_a \rho_a A_a v^2 \quad (4.6)$$

where C_a is the air drag coefficient; ρ_a is air density; and A_a is the vehicle front section area.

The tire rolling resistance force is approximated by one of the empirical formulae [73] as a function of vehicle speed below.

$$F_{ro} = (a_r + b_r v^2) mg \quad (4.7)$$

where a_r and b_r are empirical coefficients to be calibrated.

Note that the measured vehicle longitudinal acceleration usually contains road grade information, and can be represented by

$$a_x = \dot{v} + g \sin \theta \quad (4.8)$$

where a_x is the measured vehicle longitudinal acceleration.

Therefore, combining equations (4.5) to (4.8), the total longitudinal force is

$$F = ma_x + F_a + F_{ro} \quad (4.9)$$

On the other hand, when the slip ratio condition $|\lambda_i| \leq \lambda_0$ is satisfied, equations (4.3) and (4.4) provide another approach to obtain the total longitudinal force below.

$$F_f + F_r = C_f \frac{r_{ef} w_f - v}{r_{ef} w_f} + C_r \frac{r_{er} w_r - v}{r_{er} w_r} \quad (4.10)$$

where F_f and F_r are front and rear tire longitudinal forces, respectively; and w_i ($i = f, r$) are the average speed of the corresponding wheels. Note that a bicycle model is used in this model.

By letting equation (4.9) equal to equation (4.10), the vehicle speed can be calculated as

$$v = \frac{(C_f + C_r - F)r_{ef}r_{er}w_fw_r}{C_fr_{er}w_r + C_r r_{ef}w_f} \quad (4.11)$$

The advantage of this vehicle speed model is that the estimated vehicle speed is confined to the four tires, thus it reflects the actual vehicle speed.

4.3.1.3 Effective Tire Radius Model

In fact, there are several ways of calculating the tire effective radius. One possible way is to calculate the ratio between vehicle longitudinal speed and wheel rotational speed when the vehicle is coasting down, since in this case tires are in free rolling. However, when the vehicle speed is not available, this approach may not be practical.

An alternative solution is to make use of tire pressure information, which now is available for most of production vehicles. According to reference [70], the effective tire radius is derived as

$$r_{ei} = r_{wi} - \frac{z_i}{3} \quad (4.12)$$

where i stands for f or r (meaning front or rear tire), respectively; r_{ei} is the effective tire radius; r_{wi} is the undeformed tire radius; and z_i is the deformation displacement of tires. Figure 4.6 shows the corresponding tire radius parameters.

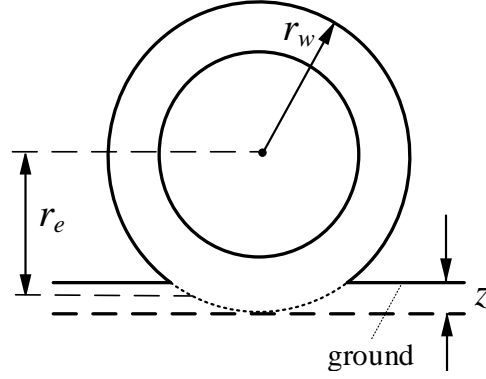


Figure 4.6: Tire radius diagram

The tire deformation z_i can be obtained by the tire normal force

$$z_i = \frac{F_{zi}}{k_{it}} \quad (4.13)$$

where F_{zi} represents front or rear tire normal force; and k_{it} represents front or rear tire vertical stiffness.

Although tire normal forces may change due to pitch motion during vehicle acceleration or braking, for this model, the pitch motion of the vehicle is neglected. Therefore, according to Figure 4.5, the tire normal force is the same as that when the vehicle is static, and can be obtained by Newton's second law below.

$$F_{zf} = \frac{L_r}{L_f + L_r} mg \quad (4.14)$$

$$F_{zr} = \frac{L_f}{L_f + L_r} mg \quad (4.15)$$

where L_f and L_r are the distance between front axle to center of gravity and rear axle to center of gravity, respectively.

An empirical formula was proposed to relate tire vertical stiffness with tire inflation pressure and tire parameters [74] as follows.

$$k_{it} = t_p a_i p_{it} + b_i$$

$$t_p = \sqrt{(-0.004AR + 1.03) \left(\frac{S_N AR}{50} + D_R \right) S_N} \quad (4.16)$$

where a_i and b_i are coefficients for a specific tire to be calibrated; p_{it} represents front or rear tire inflation pressure; t_p is the lumped tire parameters; AR is the aspect ratio of tires; S_N is the section width of tires; and D_R is the tire rim diameter.

Equations (4.12) to (4.16) provide formula to obtain the effective tire radius from tire pressure that can be summarized below.

$$r_{ei} = f(p_{it}), \quad i = r, f \quad (4.17)$$

where $f(\cdot)$ represents the conversion function.

In summary, equations (4.2), (4.3), (4.4), (4.11) and (4.17) complete the clutch torque (T_c) calculation. For simplicity in remaining sections, this baseline model is denoted as Clutch Torque Model 1 (CTM-1).

4.3.2 Overtaken-Clutch Torque Model (CTM-2)

However, CTM-1 was proved to be inaccurate for calculating the clutch output torque. Therefore, modifications are needed to improve the torque calculation accuracy using CTM-1.

As a matter of fact, during acceleration, the pitch motion introduced by acceleration may redistribute the normal forces on the tires, which would change the tire deformation, and further leading to the change of tire effective radius and making it different from that when vehicle is coasting down or static. In this sense, the tire normal forces in equations (4.14) and (4.15), neglecting the pitch motion seems unreasonable. Although re-deriving the normal forces including the pitch motion may be a possible solution, it makes the modeling process more complicated. An alternative approach is to compensate the effective tire radius directly using vehicle acceleration.

The compensated effective tire radius takes the following form:

$$r_{eic} = \begin{cases} r_{ei} - \Delta r & \text{accelerating} \\ r_{ei} & \text{coasting down} \end{cases} \quad i = r, f \quad (4.18)$$

where r_{eic} is the compensated front or rear effective tire radius; and the compensation term Δr takes a general quadratic form below:

$$\Delta r = n_{i1}a_x^2 + n_{i2}a_x + n_{i3} \quad (4.19)$$

where n_{i1} , n_{i2} and n_{i3} are coefficients to be calibrated and may vary for different types of tires.

The quadratic form of compensation term is inspired by three facts. The first is that deviation of calculated clutch torque using CTM-1 from the measured clutch torque during vehicle accelerating is nonlinear; see Figure (4.7) (d) for signals between 10 and 17s. The second fact is that the tire deformation due to vehicle acceleration can be understood as energy transformation, and energy term usually takes a quadratic form. Lastly, a cubic compensation form is also studied, however, its performance is worse than that of quadratic form (see Section 4.4.2 for detailed discussions). As a result, cubic and higher order compensation forms are not considered.

Therefore, with acceleration compensation to the effective tire radius, equations (4.2), (4.3), (4.4), (4.11) and (4.18) complete clutch torque (T_c) model under clutch overtaken condition. For simplicity, this model is denoted as Clutch Torque Model 2 (CTM-2).

4.3.3 Slip-Clutch Torque Model (CTM-3)

Even though CTM-2 works well under the clutch overtaken condition, it does not provide satisfactory clutch torque results when it comes under clutch slip condition. As a result, this subsection establishes a modified model based on CTM-2 to deal with the clutch slip.

Under clutch overtaken condition, the front propeller shaft connects firmly to the transmission through transfer case clutch, while in the clutch slip stage, there are speed difference between the driving and driven clutch disks. The speed difference is defined as Δrpm , and can be calculated by

$$\Delta rpm = w_r i_{rd} - w_f i_{fd} \quad (4.20)$$

where i_{fd} and i_{rd} are front and rear differential ratio, respectively. In the investigated vehicle, they are equal.

Note that due to the measurement noises of w_i ($i = f, r$), even though the clutch is overtaken, Δrpm may not be exactly 0. Therefore, it is reasonable to introduce a threshold to determine the clutch overtaken condition. That is, if the following condition

$$|\Delta rpm| \leq \Delta_0 \quad (4.21)$$

is satisfied, the clutch is assumed to be overtaken and otherwise slip, where the threshold is calibrated to be $\Delta_0 = 5 rpm$.

If equation (4.21) does not hold, meaning the clutch is slipping, based on equation (4.20), the linear slip speed in the front tires due to the clutch slip can be calculated by

$$\Delta v_f = \frac{1}{2} r_{efc} i_{fd} \Delta rpm \quad (4.22)$$

where Δv_f is the linear slip speed of front tires, and other variables are defined previously.

The actual front tires linear speed with slip speed compensation under clutch slip condition is then changed to

$$v_{fc} = r_{efc} w_f + \Delta v_f \quad (4.23)$$

where v_{fc} is the compensated front tire speed.

The speed estimation formula (4.11) is then corrected to the following form under clutch slip condition.

$$v_c = \frac{(C_f + C_r - F) v_{fc} r_{erc} w_r}{C_f r_{erc} w_r + C_r v_{fc}} \quad (4.24)$$

where v_c is the compensated vehicle speed.

The front tire force in equation (4.10) is then replaced by

$$F_{fc} = C_f \frac{v_{fc} - v_c}{v_{fc}} \quad (4.25)$$

where F_{fc} is the compensated front tire force.

Eventually, the front torque is derived to be

$$T_{fc}^{i_{fd}} = J_f \dot{w}_f + F_{fc} r_{efc} \quad (4.26)$$

where T_{fc} is the slip compensated front torque.

Therefore, with clutch slip speed correction to front tires under the clutch slip condition, equations (4.18), (4.20), (4.24), (4.25) and (4.26) complete the model for clutch torque (T_c) under slip condition. For simplicity, this model is denoted as Clutch Torque Model 3 (CTM-3).

4.4 Overtaken-Clutch Torque Model Validation

This subsection focuses on clutch torque model validation under overtaken condition, while in the next subsection validation under clutch slip condition is investigated. The necessary parameters of the targeted vehicle are shown in Table 4.1. Due to project sponsors confidential requirements, only necessary data (error comparison data) is shown in the rest of section.

Practically, the transfer case clutch engages when vehicle is accelerating, and intuitively, the clutch torque can be calculated only when the clutch is engaged. Therefore, the clutch torque model validation is confined to the condition when vehicle is accelerating.

Note that the measured T_f for validation purpose in the following sections refers to the front propeller shaft torque obtained from torque sensor measurement. The tire rotational speed w_i is measured by production wheel speed sensors and vehicle acceleration a_x is measured by a production accelerometer.

4.4.1 Overtaken-Clutch Torque Results with CTM-1

Figure 4.7 shows the clutch torque results of first data set with vehicle acceleration from 0 to 25 m/s using CTM-1. Figure 4.7 (a) shows the vehicle speed from the proposed speed estimator described in equation (4.11). It can be seen that the estimated vehicle speed is very close to the measured vehicle speed. Figure 4.7 (b) shows the clutch slip speed Δrpm . Criteria in equation

Table 4.1: Parameters of targeted vehicle

Parameters	Value	Parameters	Value
$i_{fd} \& i_{rd}$	3.09	$J_f (kg \cdot m^2)$	1.6
$m (kg)$	2949	$C_a \rho_a A_a$	0.7965
a_v	0.0136	b_v	$5.18e^{-7}$
$C_f \& C_r$	$2.5e^5$	t_p	507.94
a_i	$4.5e^{-4}$	b_i	3.45

(4.21) confirms the overtaken operation condition. Figure 4.7 (c) shows the vehicle brake pedal signal and Figure 4.7 (d) shows the clutch torque result. One thing to note is that there is almost no torque oscillation in the measured T_f , which confirms that the torsion vibration effect can be ignored. Between 7 and 10s, although the measured torque is increasing, the torque calculation is not started yet since vehicle brake is applied and the vehicle is static. When the vehicle is accelerating (10-17s), there exists considerable error between the estimated and measured clutch torque, while the clutch torque matches perfectly with the measured torque when the vehicle is coasting down (after 17s). This phenomenon motivates to calculating the torque using CTM-2 with modification in the effective tire radius during acceleration period since vehicle speed estimation (4.11) also depends on the effective tire radius.

4.4.2 Overtaken-Clutch Torque Results with CTM-2

Particularly, in this paper, the coefficients of the compensation term for the front effective tire radius is calibrated to be $n_{f1} = 3 \times 10^{-4}$, $n_{f2} = 0$ and $n_{f3} = 0$ since energy term usually only contains the quadratic part. While for the rear effective tire radius the compensation coefficients are set to $n_{rj} = 0$ ($j = 1, 2, 3$), since whichever the vehicle mode is (4WD or 2WD), the rear tires always receive driving torque, indicating that acceleration may not have that much effect for rear tires. The effect of compensating rear effective tire radius will be discussed in the next subsection.

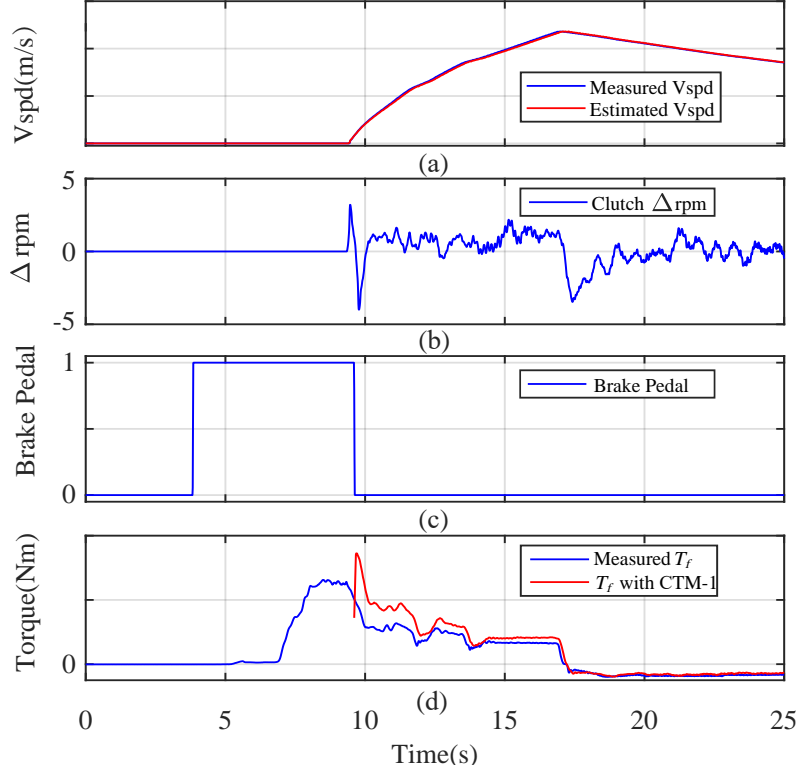


Figure 4.7: Clutch torque results with CTM-1 under clutch overtaken condition: (a) Vehicle speed estimation; (b) Clutch slip Δrpm ; (c) Brake pedal status; (d) Clutch torque result.

As a result, the compensated effective tire radius in this paper takes the following form.

$$r_{efc} = \begin{cases} r_{ef} - 3e^{-4}a_x^2 & \text{accelerating} \\ r_{ef} & \text{coasting down} \end{cases} \quad (4.27)$$

$$r_{erc} = r_{er}$$

Figure 4.8 shows the clutch torque results using CTM-2. Figure 4.8 (a) is the vehicle longitudinal acceleration, which shows clearly that the vehicle experiences three phase: static (0-10s), acceleration (10-17s) and coast down (after 17s). Figure 4.8 (b) shows the compensated front effective tire radius with its comparison to the original effective tire radius. Due to the transformation of mechanical energy to deformation energy, the acceleration compensated effective radius is less than the radius of non-accelerating one. Figure 4.8 (c) presents the vehicle speed estimation, which is still very close to the measured one. Figure 4.8 (d) shows the clutch torque comparison using different approaches. It is obvious that CTM-2 improves the clutch torque accuracy significantly

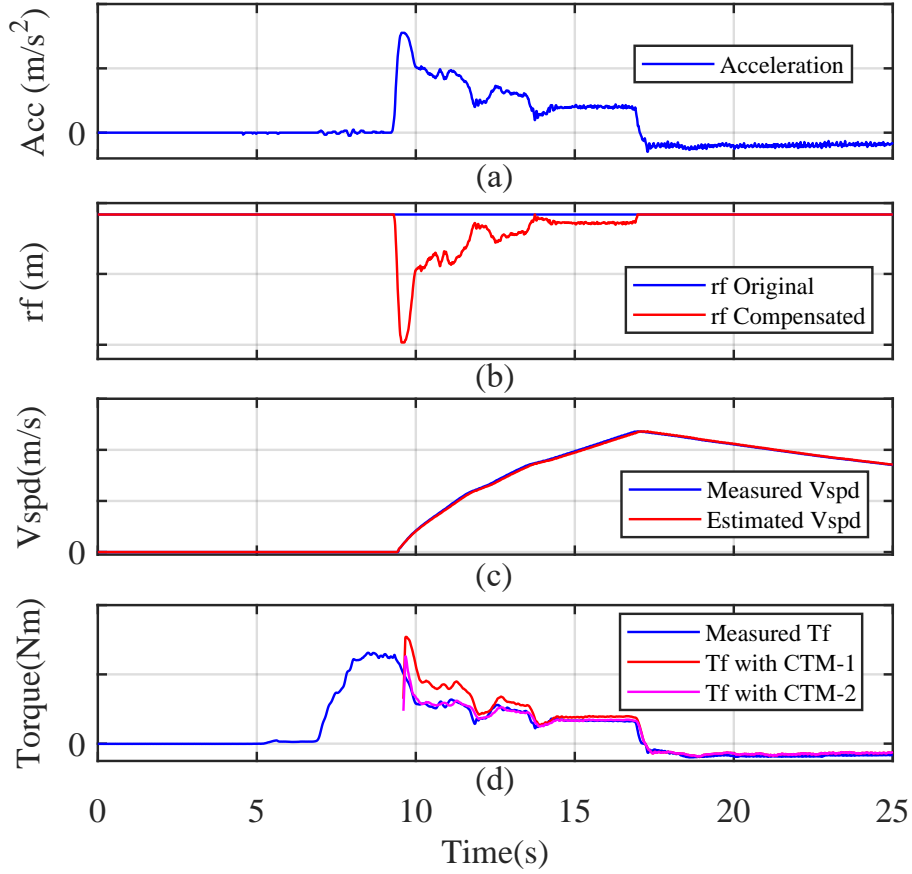


Figure 4.8: Clutch torque results with CTM-2 under clutch overtaken condition: (a) Vehicle longitudinal acceleration; (b) Front effective tire radius comparison; (c) Vehicle speed estimation; (d) Clutch torque result.

comparing to CTM-1. Some numerical evaluation are presented below.

Define the absolute error(*AbsErr*) by the equation below.

$$AbsErr = |T_{fj} - T_{mea}| \quad (4.28)$$

where T_{mea} is the measured clutch torque and j in T_{fj} equals to 1, 2 or 3 that corresponds to the estimated clutch torque using CTM-1, CTM-2 or CTM-3.

The relative error percentage(*RelErr%*) is calculated by the equation below.

$$RelErr\% = \frac{|T_{fj} - T_{mea}|}{T_{mea}} \times 100 \quad (4.29)$$

Furthermore, the root mean square error percentage (*RMSE%*), defined below, is also an estimation

performance index.

$$RMSE\% = \sqrt{\frac{1}{n} \sum_{q=1}^n (RelErr^2)} \quad (4.30)$$

where n is the total number of active data points. In the investigated case, only the duration of vehicle accelerating accounts for the total number of active data points.

Figure 4.9 summarizes the clutch torque error with respect to the measured clutch torque under clutch overtaken condition using CTM-1 and CTM-2, respectively.

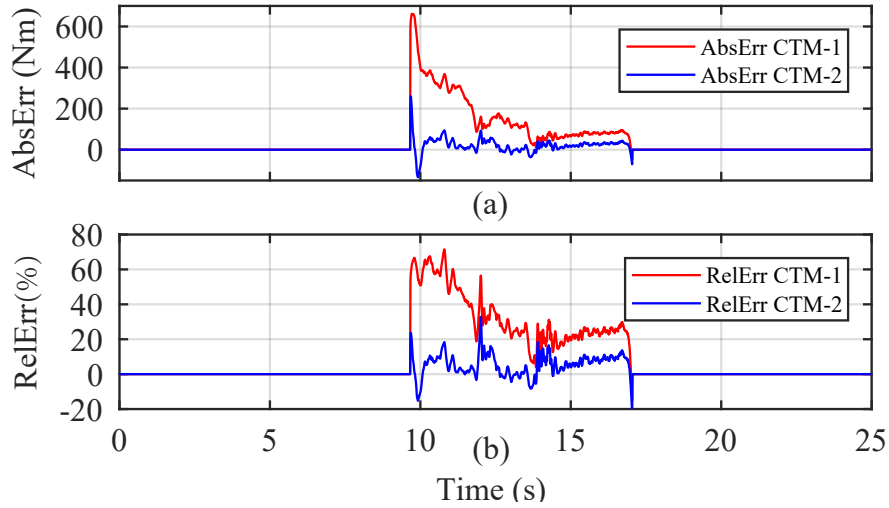


Figure 4.9: Error analysis under clutch overtaken condition: (a) Absolute error; (b) Relative percentage error.

Figure 4.9 (a) compares the absolute errors of CTM-1 and CTM-2. It can be seen that the absolute error using CTM-1 is fairly large, especially with high vehicle acceleration (see Figure 4.8 (a) near 10s). The maximum absolute error using CTM-1 reaches to around 650 N·m. However, with the acceleration compensation to the front effective tire radius using CTM-2, the absolute error during the entire acceleration period decreases to within 80 N·m with an 88% reduction over CTM-1. Figure 4.9 (b) compares the relative percentage error. Due to the large absolute error of CTM-1, the maximum relative error of CTM-1 is around 60%, while the maximum relative error of CTM-2 is less than 10% for fixed gear operation and around 20% under gear-shifting. The gear shift periods can also be found in Figure 4.8 (a).

The calculated $RMSE\%$ of CTM-1 is 23.3%, while the $RMSE\%$ of CTM-2 is 5.46% (a 27% reduction). From this perspective, the CTM-2 performs much better than CTM-1 for the clutch torque calculation.

As a matter of fact, cubic compensation form ($r_{efc} = r_{ef} - b_f a_x^3$) has also been studied with three b_f values ($0.5e^{-4}$, $0.6e^{-4}$, $0.7e^{-4}$), the resulting torque $RMSE\%$ values are 10.16%, 9.19%, 9.4%, respectively, and they are much larger than the quadratic form result of 5.46%. Increasing (decreasing) b_f from $0.7e^{-4}$ ($0.5e^{-4}$) leads to over-compensated (under-compensated) tire radius, causing even larger torque estimation error. As a result, the cubic form compensation was not adopted.

Furthermore, two additional data sets are used to validate the developed model shown in Figure 4.10, where the $RMSE\%$ for data set 2 is 4.69% during vehicle acceleration (12.5-23.5s) and the $RMSE\%$ for data set 3 is 6.43% (7-13s).

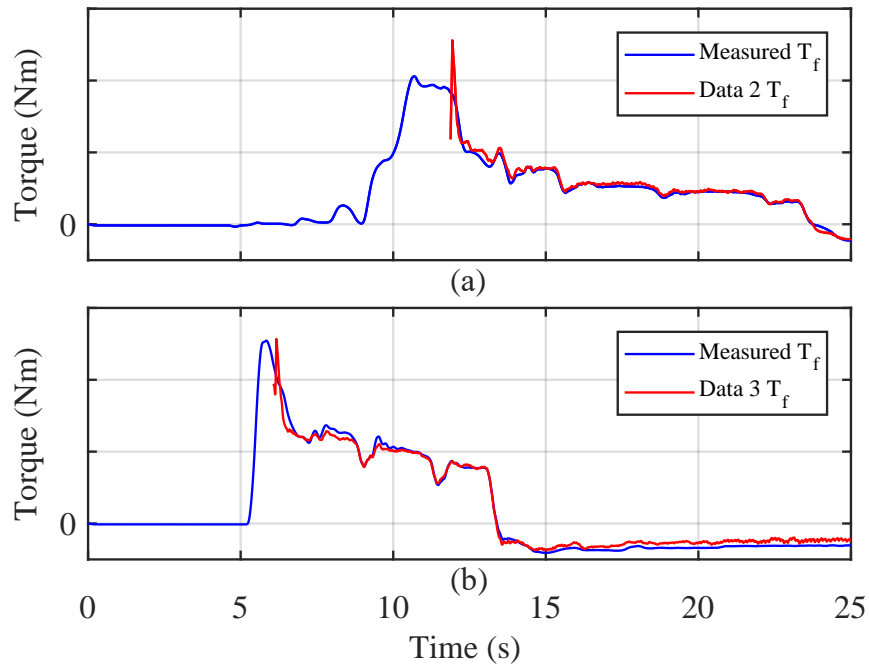


Figure 4.10: Other data sets torque validation: (a) Data 2 validation; (b) Data 3 Validation.

4.4.3 Rear Effective Tire Radius Analysis

In this subsection, the influence of acceleration compensation coefficients for rear effective tire radius is analyzed.

Equation (4.27) indicates not to compensate the rear effective tire radius with vehicle acceleration in this paper. As a matter of fact, although the clutch torque in equation (4.2) does not depend on the rear effective tire radius directly, the rear effective tire radius may affect the vehicle speed accuracy according to equation (4.11). As a result, an accurate rear effective tire radius may improve the accuracy of clutch torque.

Consider replacing the rear effective tire radius as

$$r_{erc} = r_{er} - n_{r1}a_x^2 \quad (4.31)$$

where n_{r1} is the acceleration compensation coefficient for rear effective tire radius. Selecting $n_{r1} = -2 \times 10^{-4}$, 0 and 2×10^{-4} , respectively, the associated influence of the compensation coefficient on clutch torque is shown in Figure 4.11, where Figure 4.11 (a) shows the variation of rear effective tire radius with different compensation coefficients and Figure 4.11(b) compares the measured clutch torque and the calculated clutch torque with different compensation coefficients. Using equation (4.30), RMSE% values resulted from estimated torque with compensation coefficients (n_{r11} , n_{r12} and n_{r13}) with respect to the measured torque within the interested region (vehicle acceleration between 10 and 16.8s) are calculated to be 14.01%, 2.15% and 18.44%, respectively. Therefore, it can be concluded that with $n_{r12} = 0$, the calculated clutch torque matches best with the measured clutch torque. As a result, it is reasonable to adopt the rear effective tire radius as proposed in equation (4.27).

4.5 Slip-Clutch Torque Model Validation

In Section 4.4, the CTM-2 is proved to be feasible under clutch overtaken condition. This section investigates the clutch torque model when the clutch is slipping.

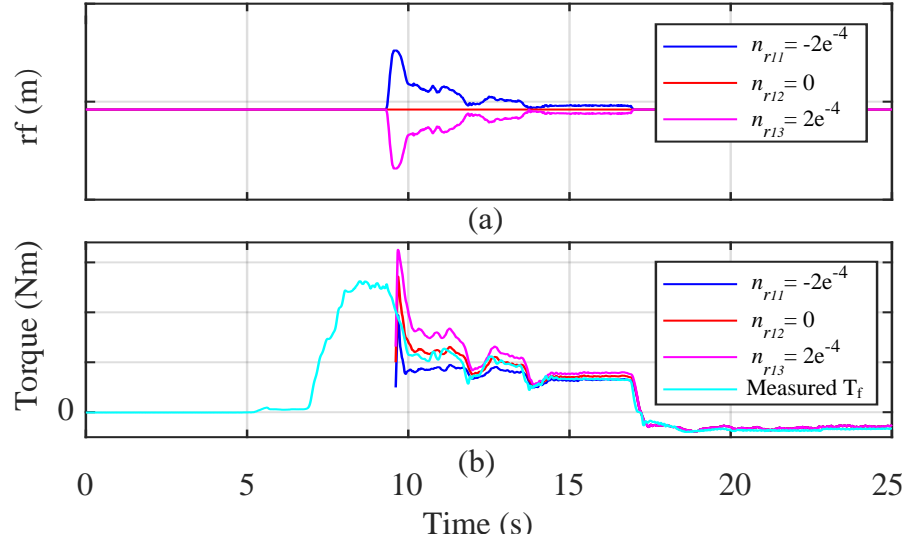


Figure 4.11: Influence of rear effective tire radius compensation with CTM-2 under clutch overtaken condition on clutch torque estimation: (a) Rear effective tire radius with different compensation coefficients; (b) Clutch torque with different compensation coefficients.

4.5.1 Slip-Clutch Torque Results with CTM-2

Figure 4.12 presents the clutch torque results with CTM-2 under clutch slip condition. Figure 4.12 (a) is the vehicle speed estimation using equation (4.11) with clutch slip-speed compensation, which shows the same matching trend as that under clutch overtaken condition. Figure 4.12 (b) shows the clutch slip speed. According to criteria (4.21), the clutch is overtaken between 20 and 30s except the spike at around 23s, which could be caused by potholes on the road, and it is slipping between 30 and 38s. Figure 4.12 (c) indicates that the calculated torque matches quite well under clutch overtaken condition but there exists considerable error when the clutch is slipping. Note that the duration of spike leads to an abnormal operational period (around 0.3s), and the estimated torque shows that it is able to re-track the measured torque once the operating condition becomes normal.

Therefore, the torque estimation model CTM-2 may not be suitable when the clutch is slipping. A possible reason for this is that when the clutch is overtaken, both front and rear propeller shafts are in solid connection with the transmission, while when the clutch is slipping, the front propeller shaft does not connect firmly with the transmission through the transfer case clutch. As a result, the clutch slip effect is transmitted from the clutch to front tires. This leads to the evaluation of

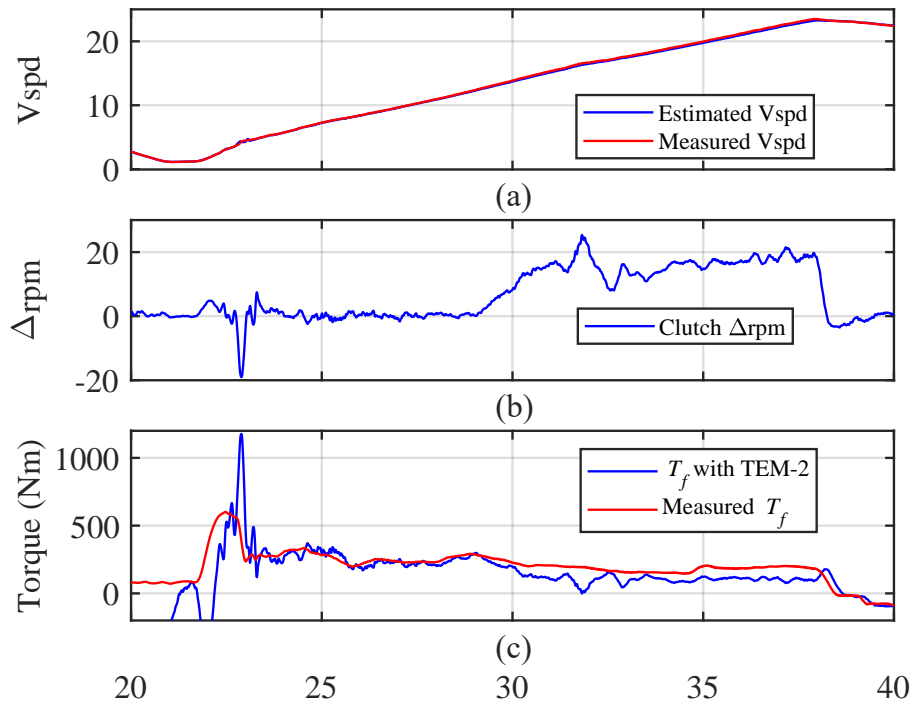


Figure 4.12: Clutch torque results with CTM-2 under clutch slip condition: (a) Vehicle speed estimation; (b) Clutch slip speed Δrpm ; (c) Torque result.

CTM-3 model in the next subsection.

4.5.2 Slip-Clutch Torque Results with CTM-3

Figure 4.13 presents the clutch torque with slip speed compensation to the front tires under clutch slip condition. Figure 4.13 (a) is the vehicle speed estimation with estimator (4.24) and Figure 4.13 (b) presents the resulting torque comparison. It is obvious that CTM-3 improves the clutch torque accuracy significantly comparing with CTM-2.

Figure 4.14 summarizes the error analysis of the clutch torque performance with respect to the measured clutch torque under slip condition, where $AbsErr$, $RelErr$ and $RMSE\%$ are defined in equations (4.28), (4.29) and (4.30) with j in T_{fj} equals 2 or 3, meaning the estimated clutch torque using CTM-2 or CTM-3.

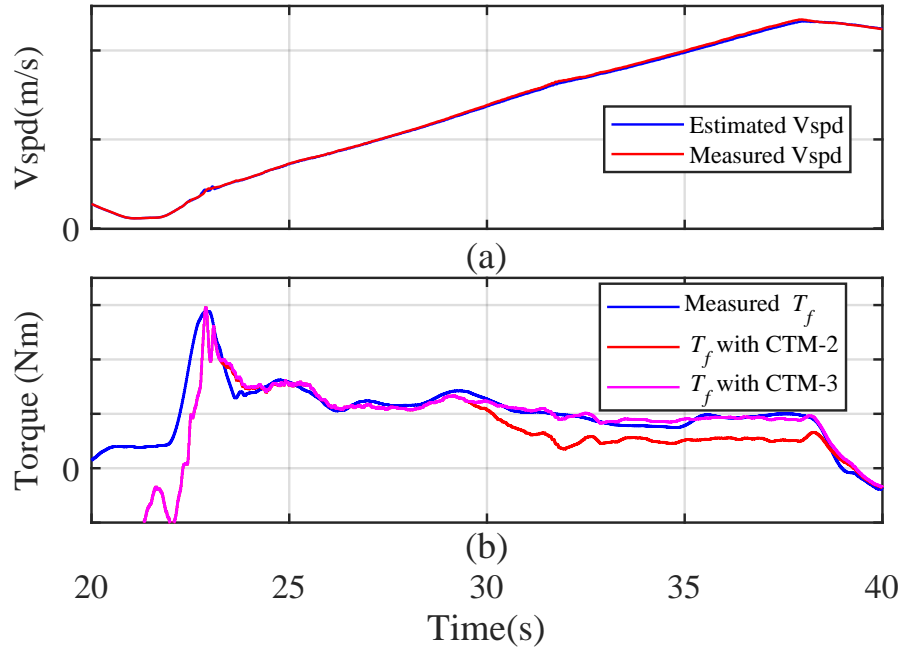


Figure 4.13: Clutch torque results with CTM-3 under clutch slip condition: (a) Vehicle speed estimation; (b) Torque result.

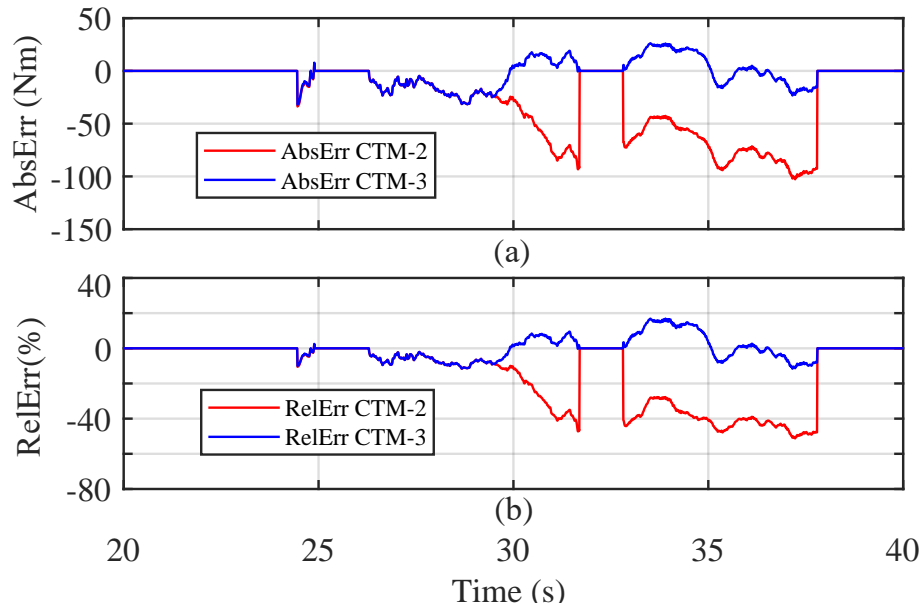


Figure 4.14: Error analysis under clutch slip condition: (a) Absolute error; (b) Relative percentage error.

Estimation results are obtained using an estimation trigger to rule out those data points under unmodeled transmission gear shifting and/or large tire slip operational condition(s). In Figure 4.14

(a), it is noted that under overtaken condition (between 23.5 and 30s), the absolute errors using both slip and overtaken models are the same (within 30 Nm), which is consistent with the claim that the overtaken condition is a special case of slip condition with clutch slip speed less than Δ_0 (see inequality (4.21)). However, when the clutch slips, the maximum AbsErr using CTM-2 surges to 100 Nm, while the AbsErr using CTM-3 remains within 30 Nm. Figure 4.14 (b) compares the corresponding relative errors. The maximum RelErr% using CTM-3 over the entire overtaken and slip conditions falls within 20%, while it is around 40% for CTM-2 when the clutch slips.

Further calculation of the RMSE% reveals that the RMSE% is 26.4% for CTM-2 and 6.8% for CTM-3. Therefore, the slip speed compensation to the front tires in CTM-3 improves the clutch torque estimation performance over CTM-2 significantly.

Table 4.2: Estimation error summary

Clutch condition	Model	<i>RMSE%</i>
Overtaken only	CTM-1	23.3%
	CTM-2	5.46%
Overtaken + slip	CTM-2	26.4%
	CTM-3	6.8%

The *RMSE%* for the clutch torque performance under both clutch overtaken and slip condition using different models are summarized in Table 4.2. The results indicate that CTM-3 provides torque accuracy with *RMSE%* error of 6.8%. In summary, when the clutch works under overtaken only condition, either CTM-2 or CTM-3 (by setting slip speed equal to 0) can be used to estimate clutch torque. While when the clutch operates under slip stage, CTM-3 needs to be utilized for accurate clutch torque estimation.

4.6 Conclusions

In conclusion, the following are achieved in this chapter:

1. The nominal clutch torque estimation model, i.e. the TEM-1 is first established and evaluated

with experimental data, which shows that the the estimated torque does not track the measured ones;

2. The compensation of vehicle acceleration to the effective tire radius is proposed to obtain the TEM-2 torque estimation model, which turns out to be more accurate than the TEM-1 under the clutch overtaken condition;
3. However, the TEM-2 model does not perform well when it comes under clutch slip condition, therefore, another slip speed compensation is proposed to the front tires under this situation, it turns out that the torque can be well tracked with the modified model.

CHAPTER 5

CLUTCH TORQUE ESTIMATION USING AN EXTENDED KALMAN FILTER WITH UNKNOWN INPUT

5.1 Overview

5.1.1 Chapter Organization

In this chapter, in order to deal with the issue of measurement and process noises presented in the system for clutch output torque estimation, the Kalman filter based estimation algorithm is applied. First of all, based on the clutch output torque model proposed in Chapter 4 dealing with different modeling challenges, the integrated clutch output torque estimation model is summarized suitable for both clutch overtaken and slip condition; Second, the system transformation is performed so that the estimation of clutch output torque is equivalent to develop an unknown input observer; This is solved by using the Extended-Kalman filter, where the unknown system states and unknown input are formed into an extended unknown vector and solved by minimizing the estimation error. The comparison of the clutch output torque under different operational conditions shows the advantage of this EKF-UIO algorithm.

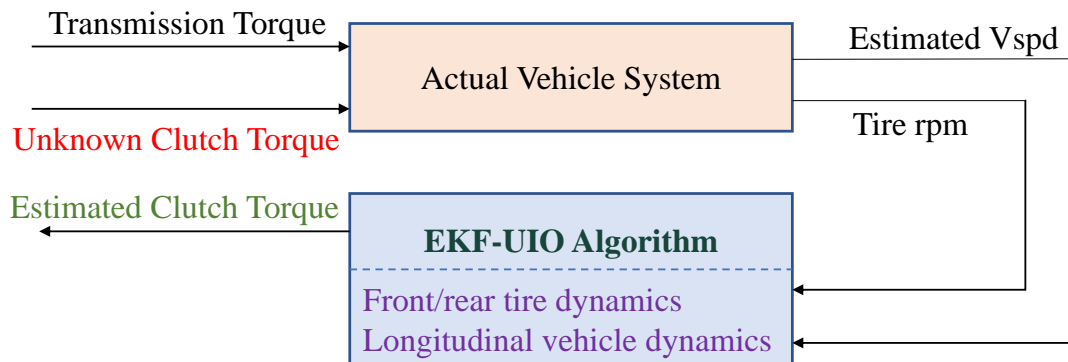


Figure 5.1: Chapter organization overview

5.1.2 Review of Unknown input Observer

Based on the propulsion architecture shown in Figure 5.2, this paper utilizes a backward vehicle propulsion system model to capture the clutch output torque; and the estimation of clutch output torque is formulated as an unknown system input estimation problem. Section 5.3 presents the details of system transformation and problem formulation.

For systems with unknown inputs, the unknown estimation is usually proceeded jointly with system state estimation. As a matter of fact, several solutions have been proposed. One common practice is to decouple the system states and unknown inputs so that system states can be estimated first by minimizing the variance of states estimation error and subsequently the unknown input can be estimated [75, 76, 77, 78, 79, 80]. The major restriction of this approach is that it only works for linear systems and the rank of system output matrix should be greater than that of unknown input matrix. Another solution is to treat the unknown inputs as disturbances and utilizes traditional Kalman Filter to minimize estimation error variance with certain state constraints [81, 82, 83] to obtain the state and unknown input estimations. However, this approach could be complicated when the number of state constraints increases. Therefore, a third solution is proposed to form an extended state vector containing both system states and unknown inputs so that an unconstrained optimization problem minimizing the extended state estimation error can be solved using the Extended Kalman Filter [84, 85, 86, 87, 88] to achieve simultaneous estimation of system states and unknown inputs. The main limitation of this approach is that the number of measurements needs to be greater than the number of unknown inputs. Furthermore, there are several innovative solutions to estimate the unknown inputs. Reference [89] designs a novel yet simple unknown input observer based on an ideal invariant manifold to estimate effective engine torque. Reference [90] proposes a Differential Neural Network (DNN) algorithm to achieve robust estimation of the exogenous unknown inputs. This paper, given the facts that the 4WD vehicle propulsion system model is nonlinear and the number of measurements is greater than the number of unknown inputs, adopts the unknown input algorithm based on the Extended Kalman Filter (EKF-UIO) proposed in [84] to estimate the clutch output torque. Detailed EKF-UIO algorithm description is summarized in Section 5.4.

5.2 4WD Vehicle Propulsion System Model

Figure 5.2 shows a typical propulsion system architecture of an Internal Combustion (IC) engine-powered 4WD vehicle. This dissertation uses a backward model from vehicle body and tire dynamics to transfer case for clutch output torque estimation. Note that the front propeller shaft is in either soft (when clutch slips) or solid (when clutch is overtaken) connection with the transmission output shaft through a chain. Therefore, torque model is different for slip and overtaken cases. However, this paper utilizes a unified clutch torque model developed in [91], and a brief model summary is provided below.

5.2.1 Tire dynamics

The transmission output torque, which is assumed to be known since the engine torque is measured and the torque ratio from engine to transmission is provided, is split into front and rear traction torque. And the front (rear) propeller shaft torque drives the front (rear) tires through the front (rear) differential (see Figure 5.2). The torque relationship can be summarized as

$$T_{to} = T_f + T_r \quad (5.1)$$

$$J_f \dot{w}_f = T_f i_{fd} - F_{fc} r_{fef} \quad (5.2)$$

$$J_r \dot{w}_r = T_r i_{rd} - F_r r_{ref} \quad (5.3)$$

$$F_{fc} = C_f \lambda_f = C_f \frac{v_{fc} - v_c}{v_{fc}} \quad (5.4)$$

$$F_r = C_r \lambda_r = C_r \frac{r_{ref} w_r - v_c}{r_{ref} w_r} \quad (5.5)$$

where $i = f$ or r , meaning front or rear tire; T_{to} is the known transmission output torque; J_i is the tire inertia; w_i is the tire rotational speed; T_i is propeller shaft torque; i_{id} is the differential ratio; F_{fc} and F_r are the front and rear tire longitudinal force, respectively; C_i is tire longitudinal stiffness and can be calibrated as constants for $|\lambda_i| \leq \lambda_0$ as shown in Figure 5.3, typical threshold of λ_0 is around 0.05 ~ 0.1 [92]; v_{fc} is the compensated front tire linear speed defined in equation (5.9); r_{ief} is the effective tire radius; and v_c is the vehicle longitudinal speed defined next.

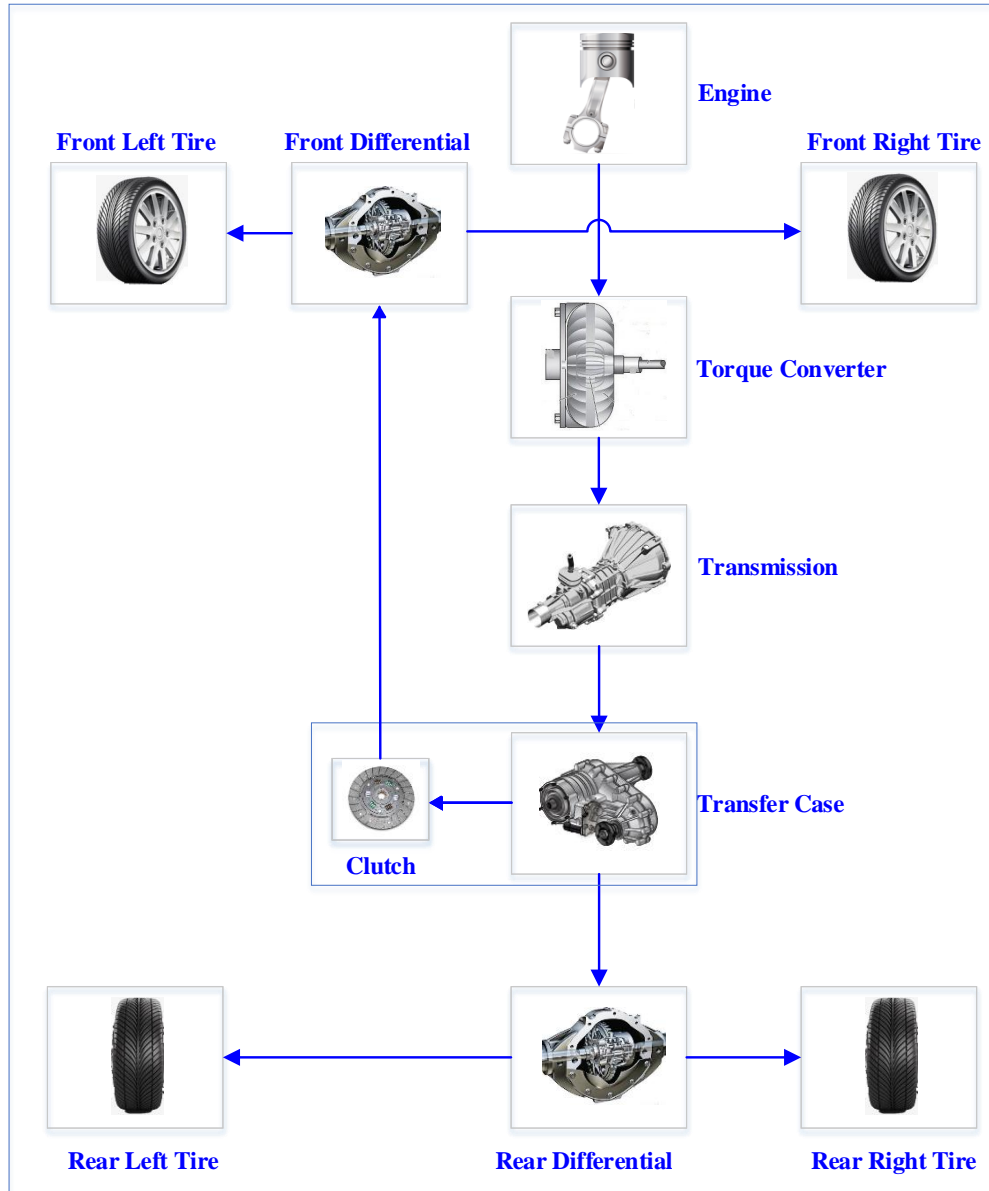


Figure 5.2: 4WD vehicle propulsion system architecture

5.2.2 Vehicle Speed Model

According to the Newton's second law, the longitudinal vehicle dynamics can be obtained as following

$$\begin{aligned}
 m\dot{v}_c &= F - F_a - F_{ro} - mg \sin \theta \\
 F_a &= \frac{1}{2} C_a \rho_a A_a v_c^2 \\
 F_{ro} &= (a_r + b_r v_c^2) mg
 \end{aligned}
 \tag{5.6}$$

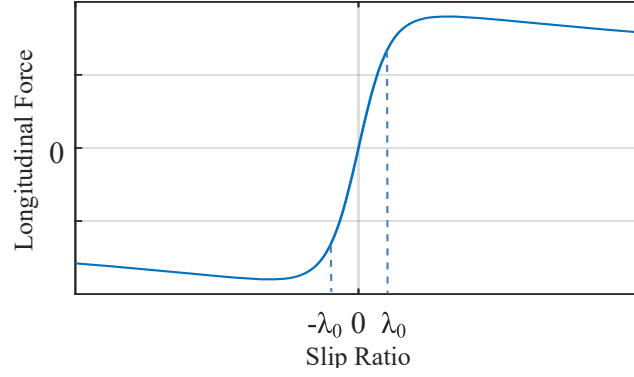


Figure 5.3: Longitudinal force vs slip ratio

where m is the vehicle mass; C_a is the air drag coefficient; ρ_a is air density; A_a is the vehicle front section area; a_r and b_r are empirical coefficients to be calibrated [73]; g is gravity acceleration constant; and θ is road grade.

On the other hand, the total longitudinal force can be obtained as below.

$$F = F_{fc} + F_r \quad (5.7)$$

Consolidating equations (5.4) to (5.7), the vehicle speed can be calculated by

$$v_c = \frac{(C_f + C_r - F)v_{fc}r_{ref}w_r}{C_f r_{ref}w_r + C_r v_{fc}} \quad (5.8)$$

where the front tire linear speed v_{fc} is given by

$$v_{fc} = r_{fef}w_f + \Delta v_f \quad (5.9)$$

$$\Delta v_f = \frac{1}{2i_{fd}} r_{fef} \Delta r_{pm} \quad (5.10)$$

$$\Delta r_{pm} = w_r i_{rd} - w_f i_{fd} \quad (5.11)$$

Note that Δr_{pm} is speed difference between two clutch disks. And if the following condition is satisfied,

$$|\Delta r_{pm}| \leq \Delta_0 \quad (5.12)$$

the clutch is assumed to be overtaken and otherwise slip, where the threshold Δ_0 is calibrated to be 5 rpm due to the existence of measurement noise,

Equation (4.23) introduces front tire linear speed compensation Δv_f to deal with slip clutch situation, making overtaken-clutch a special case with $\Delta rpm = 0$. As a result, it is a unified model for different clutch operation conditions. More details are presented in reference [91].

5.2.3 Effective Tire Radius Model

The effective tire radius is modeled as

$$\begin{aligned} r_{ei} &= r_{wi} - \frac{z_i}{3} \\ r_{ief} &= r_{ei} - n_1 a_x^2 \end{aligned} \quad (5.13)$$

where r_{ei} is the nominal effective tire radius; r_{wi} is the undeformed tire radius; z_i is the deformation displacement of tires relating to the corresponding tire pressure p_{it} ; n_1 is the calibrated compensation coefficient; and a_x is the vehicle longitudinal acceleration.

5.3 System Transformation

Choose the system state vector as $x = [w_f, w_r, v_c]^T$, system unknown input as $u_1 = T_f$, known input as $u_2 = T_{to}$ and $u = [u_1, u_2]^T$, system output as $y = [w_f, v_c]^T$. With the help of forward Euler approximation formula of sampling period T_s , the propulsion system under clutch overtaken condition ($\Delta rpm = 0$) can be transformed into a more general nonlinear discrete form as below.

$$\begin{aligned} x_{k+1} &= f(x_k, u_k) + w_k \\ y_k &= C_k x_k + v_k \end{aligned} \quad (5.14)$$

where indices $k + 1$ and k are the corresponding time step; $f(x_k, u_k)$ is the discretized nonlinear system governing function, whose detailed description can be found in equation (AA.3) in Appendix A; x is an n -dimension state vector; u contains q -unknown and p -known system inputs; y is r -

dimension measurement vector with $C_k = \begin{bmatrix} 1 & 0 & 0 \\ 0 & 0 & 1 \end{bmatrix}$.

Note that the system process noise w_k and output measurement noise v_k are considered in the discretized system, and they are assumed to be zero mean. Since process noise usually models parameter uncertainties or unmodeled dynamics, while measurement noises are more related to

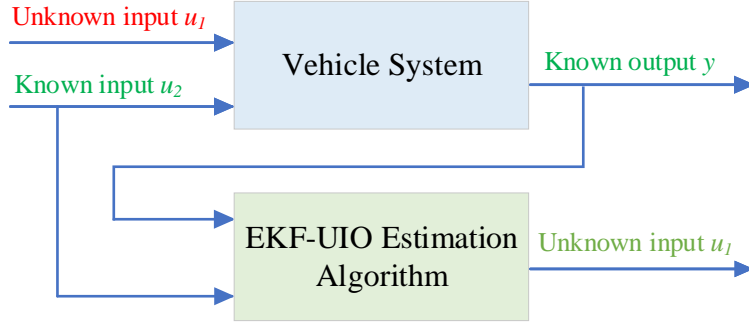


Figure 5.4: Estimation Algorithm Diagram

measurement sensor accuracy, they are assumed to be mutually independent. Therefore, the following equations are satisfied.

$$\begin{aligned}
 E(w_k) &= 0; & E(w_k w_k^T) &= W_k & E(w_{k_1} w_{k_2}^T) &= 0 \\
 E(v_k) &= 0; & E(v_k v_k^T) &= V_k & E(v_{k_1} v_{k_2}^T) &= 0 \\
 E(w_{k_1} v_{k_2}) &= 0 & & & k_1 \neq k_2 &
 \end{aligned} \tag{5.15}$$

where $E(\cdot)$ denotes the expectation operation of the corresponding term; W_k and V_k are the covariance matrix of w_k and v_k , respectively, k_1 and k_2 are different step indices.

Problem Formulation: Estimating the unknown input u_1 with p -known inputs u_2 and r -measured outputs y at each time step. The estimation diagram is summarized in Figure 5.4.

5.4 Extended Kalman Filter based Unknown Input Observer

Based on the system preparation and problem formulation described in Section 5.3, the unknown input observer based on Extended Kalman Filter is adopted to realize the goal.

Since the system governing equation is nonlinear, it is first linearized along the estimated states (\hat{x}) and unknown input (\hat{u}_1) trajectories using Taylor Expansion as below.

$$f(x_k, u_k) \approx \hat{f} + A_k(x_k - \hat{x}_k) + B_k(u_{1,k} - \hat{u}_{1,k}) \tag{5.16}$$

$$\hat{f} = f(\hat{x}_k, \hat{u}_{1,k}) \tag{5.17}$$

$$A_k = \left[\frac{\partial f(x_k, u_k)}{\partial x_k} \right] \Bigg|_{x_k = \hat{x}_k, u_{1,k} = \hat{u}_{1,k}} \tag{5.18}$$

$$B_k = \left[\frac{\partial f(x_k, u_k)}{\partial u_{1,k}} \right] \Big|_{x_k = \hat{x}_k, u_{1,k} = \hat{u}_{1,k}} \quad (5.19)$$

where \hat{x}_k is the estimate of true states x_k and $\hat{u}_{1,k}$ is the estimate of unknown input $u_{1,k}$ at time step k ; $f(x_k, u_k)$ is the true governing function; \hat{f} is an estimate of $f(x_k, u_k)$ at the estimated states (\hat{x}_k) and unknown input ($\hat{u}_{1,k}$); A_k and B_k are the linearized system and input matrices. The resulting linearized system is presented below.

$$x_{k+1} = A_k x_k + B_k u_{1,k} + \bar{u}_k + w_k \quad (5.20)$$

$$y_k = C_k x_k + v_k$$

$$\bar{u}_k = \hat{f} - A_k \hat{x}_k - B_k \hat{u}_{1,k} \quad (5.21)$$

Detailed A_k and B_k representations for the target vehicle are derived in Appendix B.

The optimal estimate of states (\hat{x}_k) and unknown input ($\hat{u}_{1,k}$) is achieved by minimizing the cost function J_k , which is the summation of square errors between measured output y_m and estimated output $C\hat{x}_m$ ($m = 1, 2, \dots, k$) over the cumulative time steps as below.

$$J_k = \bar{\Delta}_k^T Z_k \bar{\Delta}_k \quad (5.22)$$

where Z_k is a $(rk \times rk)$ weighting matrix; $\bar{\Delta}_k = [\Delta_1^T, \dots, \Delta_k^T]^T$ is the stacked up rk -error vector; and $\Delta_m = y_m - C\hat{x}_m$ is the r -dimension output error vector at each time step m ($m = 1, 2, \dots, k$).

Define the extended unknown state vector as

$$X_{un,k} = [x_k^T, u_{1,1}^T, u_{1,2}^T, \dots, u_{1,k}^T]^T \quad (5.23)$$

Note that the stacked up error vector $\bar{\Delta}_k$ can be represented as a function of extended unknown vector $X_{un,k}$ as below after some manipulations.

$$\bar{\Delta}_k = Y_k - A_{e,k} X_{un,k} \quad (5.24)$$

where $Y_k = [(y_1 - \hat{u}_{1,1})^T, \dots, (y_k - \hat{u}_{1,k})^T]^T$ and $A_{e,k} = \begin{bmatrix} \hat{L}_k & N_k \\ \hat{H}_k & 0_{r \times q} \end{bmatrix}$. More detailed derivation of $\bar{\Delta}_k$ as a function of $X_{un,k}$ and descriptions of matrix $A_{e,k}$ as well as its entries can be found in [84].

The problem is therefore transformed to obtain the optimal extended state estimation $\hat{X}_{un,k}$ of $X_{un,k}$, given the cumulative cost function in equation (5.22). This can be solved by setting the partial derivative of the cost function J_k with respect to $X_{un,k}$ to 0, i.e. $[\partial J_k / \partial X_{un,k}] = 0$. And the solution, $\hat{X}_{un,k}$, is the optimal estimate of $X_{un,k}$ expressed below.

$$\hat{X}_{un,k} = Q[A_{e,k}^T Z_k Y_k], \quad Q = [A_{e,k}^T Z_k A_{e,k}]^{-1} \quad (5.25)$$

According to [84] and [86], the existence condition for matrix Q requires **number of measured output (r) should be greater than number of unknown input (q), namely, $r > q$.**

For the EKF-UIO estimation algorithm to be implementable in real-time, a recursive solution of estimated $\hat{X}_{un,k}$, namely estimated states (\hat{x}_k) and unknown input ($\hat{u}_{1,k}$), is desired. Detailed recursive derivation can be referred to reference [84] and the recursive solution is summarized as follows.

Step 0: Initialization

Initialization of the algorithm at time step $k = 0$

$$\begin{aligned} \hat{x}_0 &= E(x_0), \quad \hat{u}_{1,0} = E(u_1), \quad K_{x,0} = K_{x0} \\ P_{xp,0} &= E[(x_0 - \hat{x}_0)(x_0 - \hat{x}_0)^T] \\ U_{u_1,0} &= E[(u_1 - \hat{u}_{1,0})(u_1 - \hat{u}_{1,0})^T] \end{aligned} \quad (5.26)$$

where P_{xp} is the state prediction gain matrix; U_{u_1} is the gain matrix for the unknown input u_1 ; and K_x is the state correction gain matrix.

Step 1: Prediction

The predicted states and outputs are given by

$$x_{p,k} = f(\hat{x}_k, \hat{u}_{1,k}) \quad (5.27)$$

where $x_{p,k}$ is the predicted state vector.

Step 2: Gain computation

Note that there are three gain matrices, namely state correction gain matrix $K_{x,k}$, state prediction gain matrix $P_{xp,k}$, and unknown input gain matrix $U_{u,k}$ to be calculated at time step k for the next

time step $k + 1$. The recursive solutions for each gain matrix are displayed below.

$$\begin{aligned}
P_{xp,k+1} &= A_k P_{x,k} A_k^T + W_k \\
K_{x,k+1} &= P_{xp,k+1} C_k^T [V_{k+1} + C_k P_{x,k+1} C_k^T]^{-1} \\
U_{u_1,k+1} &= [B_k^T C_k^T V_{k+1}^{-1} (I_r - C_k K_{x,k+1}) C_k B_k]^{-1}
\end{aligned} \tag{5.28}$$

Note that there is difference between $P_{xp,k}$ and $P_{x,k}$, where $P_{xp,k}$ is the state prediction gain matrix at time step k and $P_{x,k}$ is the state update gain matrix at time step k . The recursive solution for state update gain matrix $P_{x,k}$ is presented in equation (5.31).

Step 3: Estimation correction

The estimated states (\hat{x}) and unknown input (\hat{u}_1) are updated for time step $k + 1$ based on the predicted states $x_{p,k}$, updated gains at time step k , predicted output \hat{y}_k and current measured outputs y by the following equations.

$$x_{k+1} = x_{p,k} + K_{x,k+1}(y_k - \hat{y}_k), \quad \hat{y}_k = C_k \hat{x}_k \tag{5.29}$$

$$\begin{aligned}
u_{1,k+1} &= U_{u_1,k+1} B_k^T C_k^T V_{k+1}^{-1} (I_r - C_k K_{x,k+1}) \\
&\quad \times [y_k - \hat{y}_k + C_k B_k u_{1,k}]
\end{aligned} \tag{5.30}$$

And the recursive solution of the state update gain matrix $P_{x,k}$ is described as follows.

$$\begin{aligned}
P_{x,k} &= (I_n - K_{x,k} C_k) [P_{xp,k} \\
&\quad + B_{k-1} U_{u_1,k} B_{k-1}^T (I_n - K_{x,k} C_k)^T]
\end{aligned} \tag{5.31}$$

Note that for the target 4WD vehicle propulsion system, both B_k and C_k are constant matrices and the estimation road map is summarized in Figure 5.5.

5.5 Experiment Validation

In this section, the experiment validation of the proposed EKF-UIO estimation algorithm under both clutch slip and overtaken conditions are performed, where the proposed EKF-UIO algorithm was developed and implemented in MATLAB/Simulink.

Note that due to confidential requirements of the project sponsor, only numerical improvement analysis are presented, and the actual values of each signal cannot be shown.

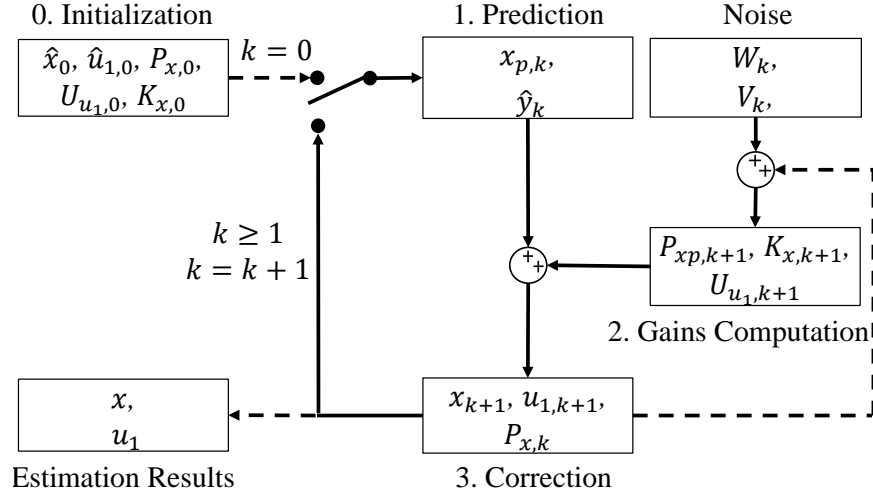


Figure 5.5: EKF-UIO Estimation Flow Diagram

Experiments are conducted in a proving ground. The tire rotational speed (w_i) is measured using a production wheel speed sensors and vehicle acceleration is measured by a production accelerometer. For validation purpose, the measured clutch torque (T_f) in the following sections is obtained from a torque sensor. The sampling time for the system discretization is select as 0.01s, which is the same as that of measured signals.

5.5.1 Model Initialization

Vector $x(0) = [0.01, 0.01, 0.01]^T$ represents the initial condition of the three states. Although the vehicle starts from static condition, the initial states cannot be set to 0 due to the fact that states appear in the denominator position in the system equations (see equation (AA.1) in Appendix A). Therefore, small values are used to avoid numerical issue. Scalar $u_1(0) = 0$ represents the initial value of unknown input. Matrix $W = \text{diag}[1, 1, 10]$ represents the processing noise, where w_1 and w_2 are assumed to be equal, meaning that the processing noise for front and rear tires are the same, and w_3 is larger since the road grade θ is not considered in the system equation (AA.1). $V = \text{diag}[1e^{-6}, 1e^{-6}]$ is the measurement noise matrix. Note that the processing noise is usually 10 times larger than the measurement noise. Matrix $P_{xp,0} = \text{diag}[1, 1, 1]$ denotes the initial values of states prediction gain matrix $P_{xp,k}$. $U_{u_1,0} = 0$ is the initial value of unknown input gain matrix

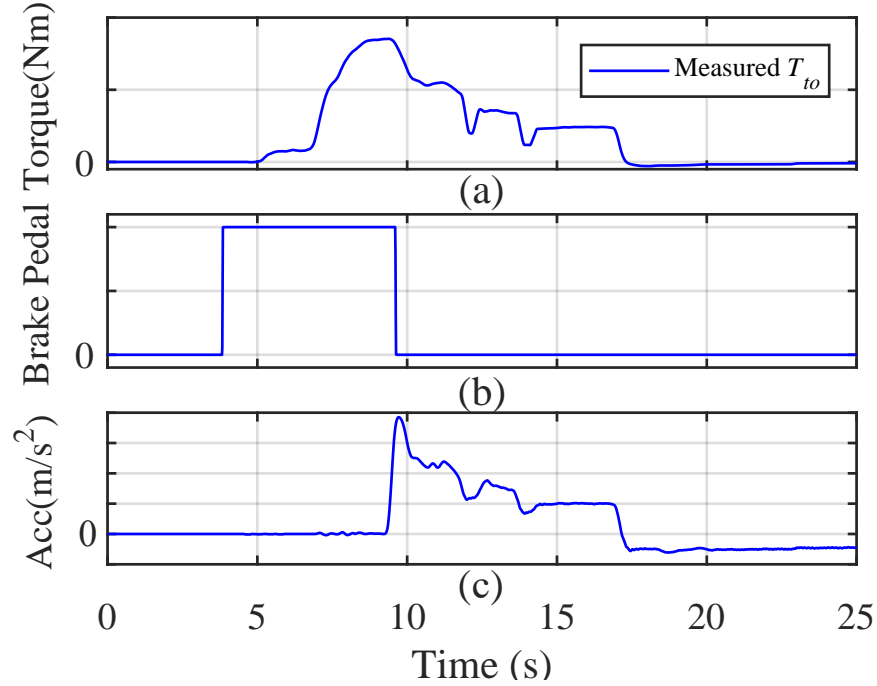


Figure 5.6: Known input u_2 for data set 1

and $K_{x,0} = \text{ones}(n, r)$ is the initial states correction gain matrix.

5.5.2 Overtaken-clutch Torque Estimation Validation

Particularly, under clutch overtaken condition, the indices for system variables described in equation (5.14) are fixed as the following: $n = 3$, $p = 1$, $q = 1$, $r = 2$. Since $r > q$, the existence of matrix Q is guaranteed.

Several experiment data sets are utilized to validate the proposed EKF-UIO algorithm under clutch overtaken conditions. Under the clutch overtaken condition, the known input is the transmission output torque T_{to} , which is shown in Figure 5.6 (a). This is obtained by multiplying the known engine torque to the measured total torque ratio between torque converter and transmission. Note that between 4 and 10s, although the transmission output torque starts building up, the brake pedal is fully applied so that the vehicle is static; see Figure 5.6 (b). The algorithm becomes active only when the vehicle is accelerating (or clutch is engaged), which can be identified from the positive vehicle acceleration shown in Figure 5.6 (c).

Figure 5.7 shows the resulting state estimation. It can be observed that both estimated front tire

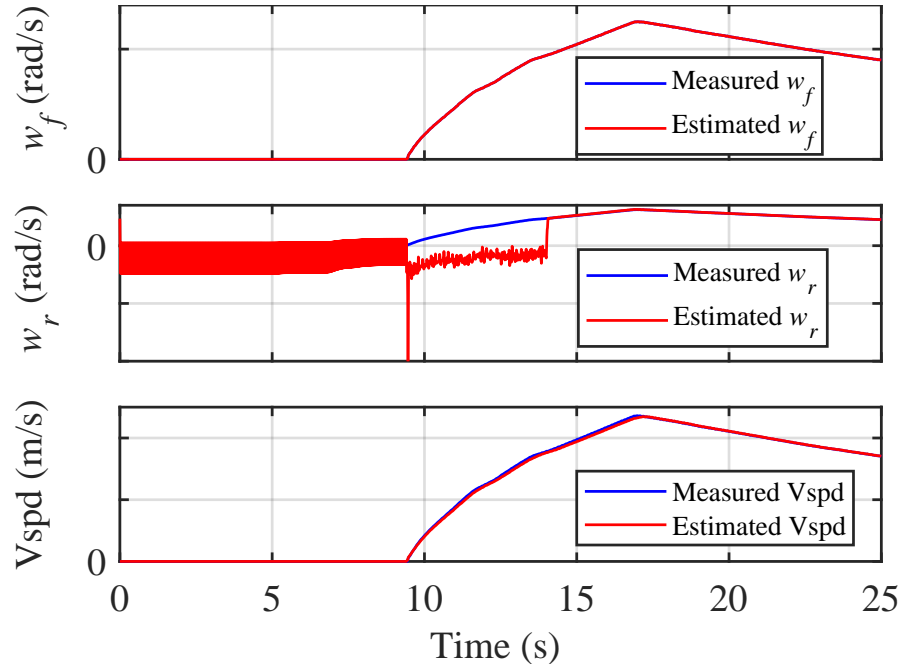


Figure 5.7: Estimated system states \hat{x} for data set 1

and the vehicle speeds track the measured ones well, while there exists some error in the rear tire speed.

Note that a simple longitudinal bicycle model, neglecting yaw and roll motion, is utilized to model the vehicle dynamics. From this point of view, the model is not accurate compared with actual vehicle system. Therefore, it would be reasonable to expect certain error in the estimated states using a simplified model. However, to deal with the modeling error, instead of re-deriving a more complex and accurate model, the key idea is to lump all the estimation error to a state that is not important in the estimation algorithm.

Remember that the goal of EKF-UIO algorithm is to estimate the unknown input (clutch torque), which is related more closely to the front tires than to the rear tires according to the configuration of propulsion system in Figure 5.2. Therefore, the output is chosen to be front tire speed and vehicle speed. The vehicle speed is obtained from the vehicle speed estimator in equation (5.8) since both front and rear tire speed signals are available. Figure 5.7 confirms that all the estimation errors are pushed to the rear tire speed in order to have an accurate estimation of unknown input. Therefore, even though there are some vibrations in rear tire speed, it does not affect the torque estimation as

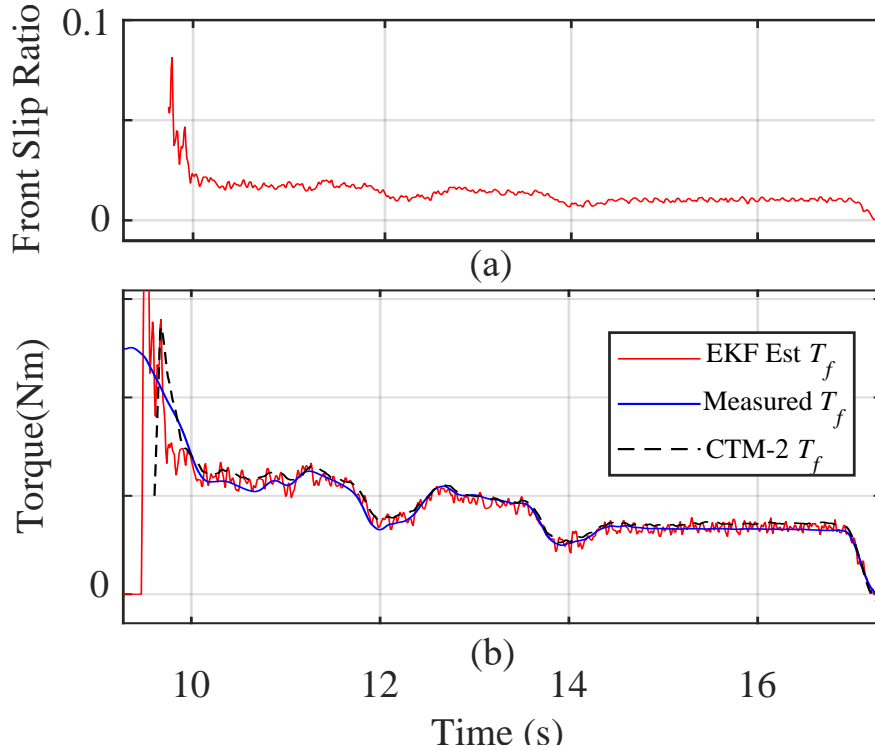


Figure 5.8: Front tire slip ratio and estimated system unknown input \hat{u}_1 for data set 1

shown in Figure 5.8. On the other hand, the accurate rear tire speed is also easily available through measurements, therefore, even though the estimated rear tire speed from EKF-UIO is inaccurate, the accurately measured rear tire speed can always be utilized for other applications in case it is needed.

Figure 5.8 (a) presents the front tire slip ratio result for the interested acceleration duration. It is obvious that the tire slip ratio is way below the threshold $\lambda_0 = 0.1$ as discussed before. Note that the rear tire slip ratio is similar to the front case and not shown here. Therefore, the assumption of constant tire stiffness holds in this case, and the linear tire force approximation is reasonable and accurate. Figure 5.8 (b) presents the unknown input validation results, where three clutch torque signals: measured torque using a torque sensor, EKF-UIO algorithm estimated torque, and CTM-2 torque which obtained from direct reverse calculation [91], are shown. Again, only vehicle acceleration period is considered, since typically the transfer case clutch only engage when vehicle is accelerating for improving traction torque performance. Between 9.5 and 10s, the vehicle just started moving and the tire slip is large, causing inaccurate tire longitudinal force. This further

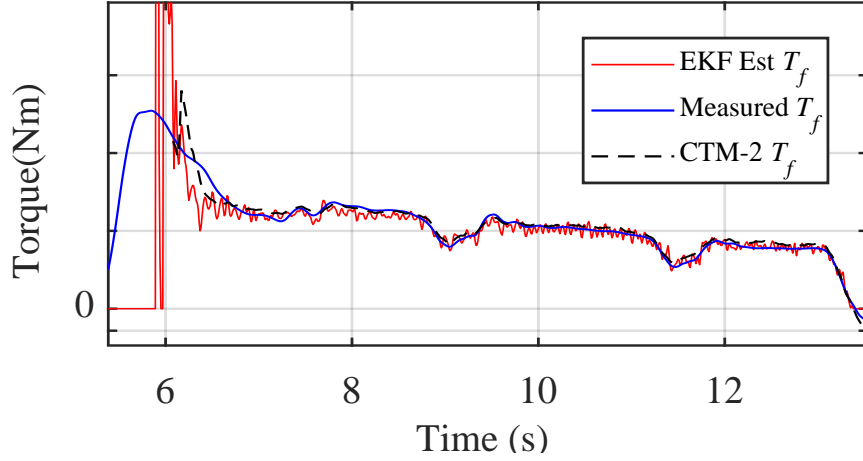


Figure 5.9: Estimated system unknown input \hat{u}_1 for data set 2

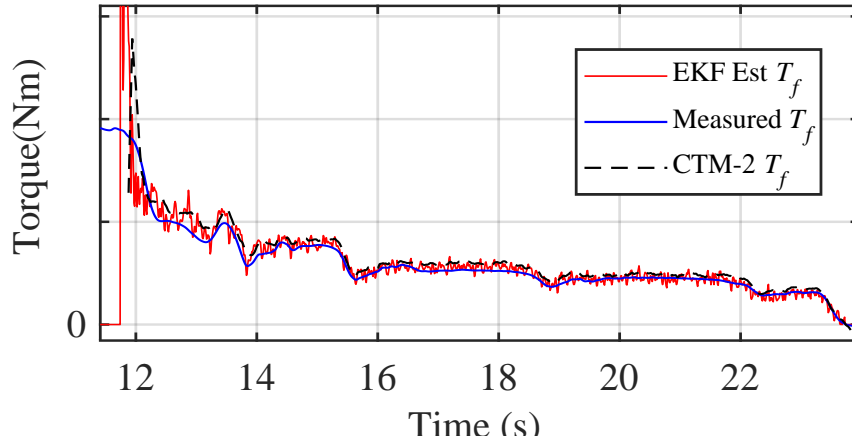


Figure 5.10: Estimated system unknown input \hat{u}_1 for data set 3

results in inaccurate clutch torque estimation as shown in the figure. However, when the vehicle runs at higher speed, the tire slip ratio becomes small so that the longitudinal force is accurate, leading to accurate clutch torque estimation between 10 and 16.8s. Both estimated torque values are close to the measured clutch torque, and the estimation error analysis is presented at the end of this section.

Figures 5.9 and 5.10 show two other experimental validation results. Since the state estimation results are similar to that of the first data set in Figure 5.7, they are not shown here. It can be observed that the unknown input estimation trend for the latter two data sets are also similar to the first data set.

For the estimation error analysis, two error evaluation indices are defined. The first one is

Table 5.1: Overtaken-estimation error summary

Data sets	Approach	$AMSE (Nm)$	$RMSE (\%)$
Data 1	EKF-UIO	3.75	1.10
	CTM-2	21.91	5.80
Data 2	EKF-UIO	8.00	1.02
	CTM-2	12.75	3.60
Data 3	EKF-UIO	12.75	3.60
	CTM-2	27.17	10.79

$AMSE$ (absolute mean square error), which is defined below,

$$AMSE = \sqrt{\frac{1}{n_d} \sum_{n_q=1}^{n_d} (|T_{fe} - T_{mea}|)^2}, \quad (5.32)$$

and the second index is $RMSE$ (relative mean square error) as defined below:

$$RMSE = \sqrt{\frac{1}{n_d} \sum_{n_q=1}^{n_d} \left(\frac{|T_{fe} - T_{mea}|}{T_{mea}} \right)^2} \quad (5.33)$$

where T_{fe} means the estimated clutch torque; T_{mea} means the measured clutch torque; and n_d is the total number of active data points and only acceleration duration accounts for the active data.

The estimation error are summarized in TABLE 5.1. It is obvious that comparing to the direct reverse calculation from CTM-2 model, both $AMSE$ and $RMSE$ with respect to the measured clutch torque are significantly reduced for all data sets using the proposed EKF-UIO estimation algorithm. Even in the worst case (Data set 3), the $AMSE$ is reduced by $15Nm$ and the $RMSE$ by 3.6% with a 7% improvement, comparing to CTM-2. Another important aspect is that there is no noise rejection feature in CTM-2 calculation, while EKF-UIO algorithm is relatively robust to measurement noises, and therefore leads to more accurate torque estimation results.

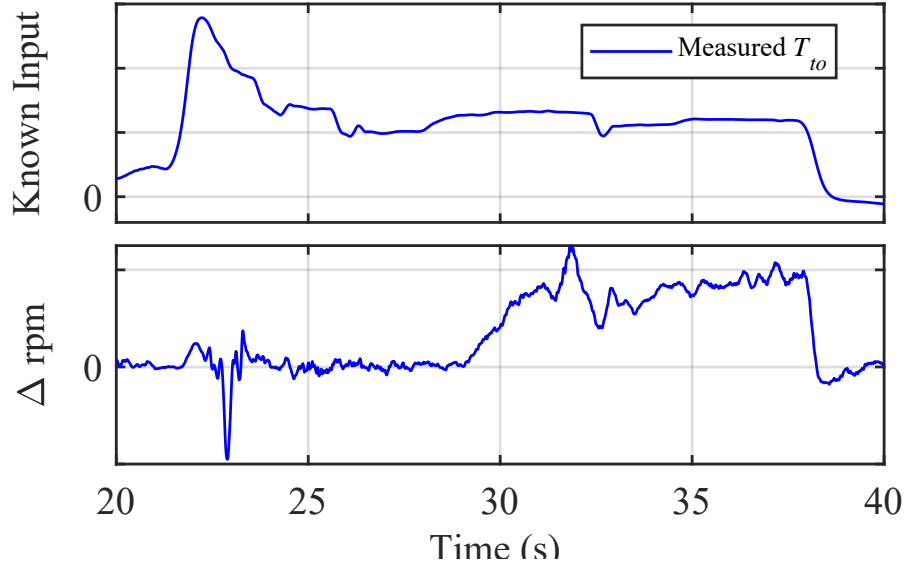


Figure 5.11: Known input and clutch Δrpm

5.5.3 Slip-clutch Torque Estimation Validation

This section performs the estimation validation under clutch slip condition. Since clutch slip speed Δrpm is vital for estimation under this condition, accurate Δrpm or equivalently front and rear tire speed measurements are desired. However, it is determined that the estimation error is lumped to rear tire speed in Section 5.5.2, as a result, the slip speed Δrpm obtained from the estimated rear tire speed is inaccurate, which may further lead to inaccurate clutch torque estimation.

However, as also discussed in Section 5.5.2 that both front and rear tire speeds are measured accurately, meaning that the accurate clutch slip speed Δrpm is available in real-time. The solution is to consider the Δrpm as another known input to the system, instead of relating it to the estimated system states. Therefore, under clutch slip condition, the system input vector becomes $u = [T_f, T_{to}, \Delta rpm]^T$. Therefore, the system for slip condition is slightly different from that of overtaken condition. For further implementation of the EKF-UIO algorithm for slip condition, similar procedures can be performed to that for the overtaken case. Due to page limitation, it is omitted in this paper.

Figure 5.11 presents the known input (transmission output torque) and the Δrpm under clutch slip condition. According to criteria in equation (4.21), the clutch is overtaken approximately

between 20 and 29s and is slipping between 29 and 38s. Figure 5.12 shows the state estimation results under this condition. Similar to the overtaken case, the front tire speed and vehicle speed match well with the measured ones, and all the estimation errors are lumped to the rear tire speed. The resulting unknown input (clutch torque) estimation is presented in Figure 5.13, where the EKF-UIO T_f is obtained from the modified system with two known inputs and CTM-3 T_f is the direct reverse calculation of clutch torque under slip condition [91]. Similarly, estimation results from both approaches match with the measured T_f . Further error calculation reveals that the EKF-UIO algorithm performs better than the direct CTM-3 model, where the $AMSE$ is reduced from $21.6Nm$ to $14.32Nm$ and $RMSE$ from 10.5% to 6.88% .

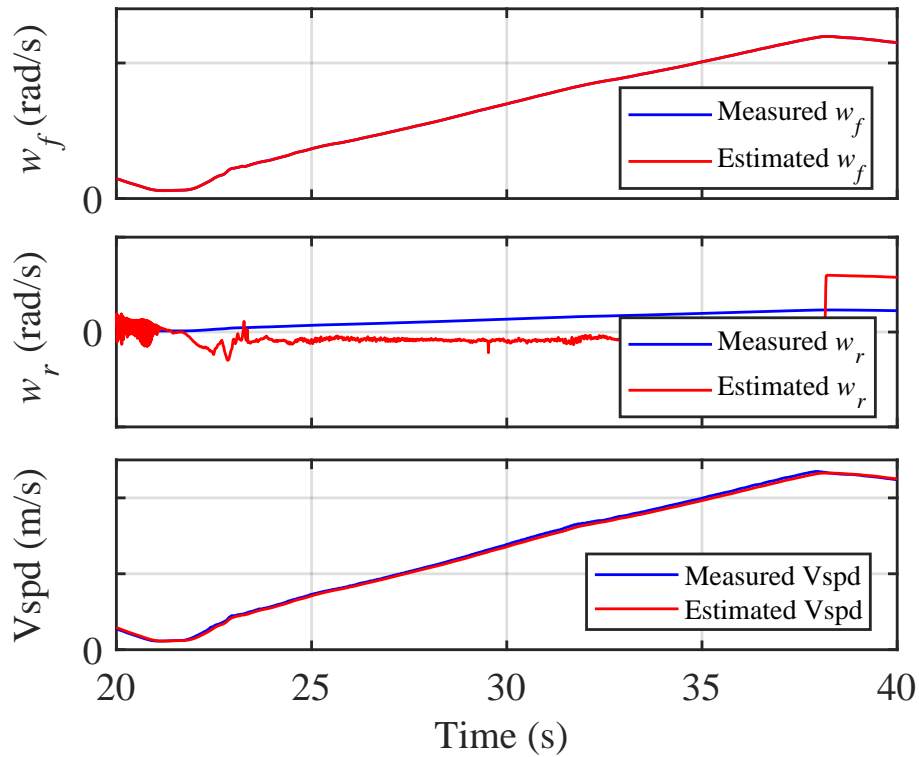


Figure 5.12: Estimated states under clutch slip condition

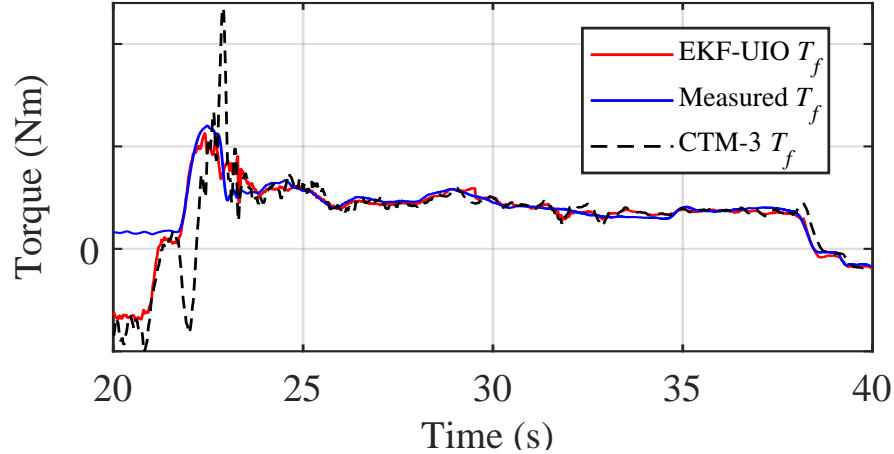


Figure 5.13: Estimated unknown input under slip condition

5.6 Conclusion

In conclusion, the following are achieved in this chapter:

1. Based on the clutch torque model in the Chapter 4, the clutch torque estimation problem is formulated into an unknown input estimation problem, which is solved with the help of extended Kalman filter, and the solution is a recursive one that is real-time implementable;
2. The effectiveness of the proposed algorithm is validated using experimental data under both clutch overtaken and slip condition. Note that the overtaken case is formulated as a two inputs (one unknown and one know) system while the slip case is formulated as a three inputs (one unknown and two known) system. The comparison shows that EKF estimated clutch torque is able to track the measured clutch torque well, and more importantly, the error performance (both AMSE and RMSE) is better than that obtained through the modeling approach as shown in Chapter 4, demonstrating EKF-UIO approach's advantage and effectiveness.

CHAPTER 6

CLUTCH FRICTION COEFFICIENT ESTIMATION VIA ADAPTIVE RECURSIVE LEAST-SQUARE LOOKUP TABLE

6.1 Chapter Overview

6.1.1 Chapter Organization

This chapter aims to estimate clutch surface friction coefficient based on the estimation results of clutch touchpoint from Chapter 2 and clutch output torque from Chapter 4. The idea is to first obtain the clutch surface friction coefficient from some sets of data, and use these results to establish a parameterized clutch surface friction coefficient model, which depends on the clutch slip speed. And further use other data sets to test the resulted lookup table (clutch surface friction coefficient vs. clutch slip speed) by comparing the resulting torque to a direct measured one.

The adaptive lookup table is established using a recursive Least-Squares (RLS) algorithm, based on the calculated clutch friction coefficient and clutch slip. Note that this will also depend on a predefined table nodes (x axis). The output of adaptive lookup table is the online updated table nodes (y axis) representing clutch surface friction coefficient corresponding to the predefined nodes.

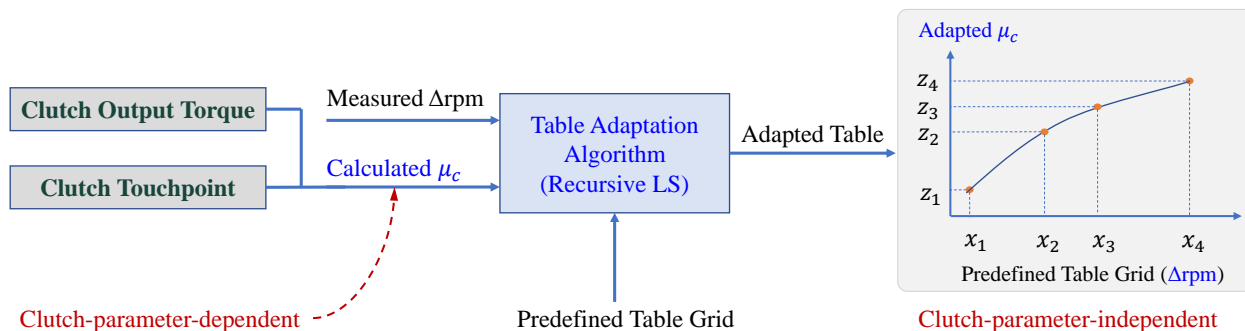


Figure 6.1: Real-time μ_c estimation flow

6.1.2 Review of Adaptive Lookup Table

As a matter of fact, the identification of the adaptive table nodes is a class of parameter identification problem, and multiple approaches exist for real-time estimation of parameters. However, due to the computational power limitation or model complexity for model-based design in current automotive industry, one of the most efficient ways is to use a lookup table [93], which requires that the desired parameter be parameterized with respect to certain easily available signals. In this chapter, it is proposed to relate the desired clutch surface friction coefficient to clutch slip speed only with a 1-D lookup table, since on one hand, factors such as clutch temperate, clutch wear have already been accounted for in the estimation of clutch touchpoint in our previous work [26]; on the other hand, clutch slip speed can be easily obtained from tire rotational speed; and further 1-D dimension lookup table is more computationally efficient than higher dimension ones.

In some applications, a static lookup table is used to cover the entire working range, such as transmission shifting lookup table. The established look-up table makes it possible to obtain the real-time values of system parameters, then gain-scheduling controllers can be designed [94],[95], [96]. However, more applications adopt adaptive lookup tables [97] [98] to deal with factors such as components aging, working condition variations. There are different lookup table adaptation methods. A common method with lowest computational requirement is the normalized least mean approach since it only stores the table grid values [99]. An alternative method is the recursive Least-Squares based algorithm, where the table nodes values are adaptively estimated to minimize the squared output estimation error based on available measurements. Reference [100] proposed a modified recursive Least-Squares algorithm with re-initializing of parameter covariance when the active table area changes for a 2-D lookup table. While in [101], an efficient recursive Least-Squares algorithm solved by Thomas algorithm for the identification of linear lookup table is proposed and validated with application to engine volumetric efficiency map. There are also Kalman filter based adaptation approaches. For instance, reference [102] proposed a constant Kalman filter gain for the table adaptation to reduce online computational burden with performance validation on a real engine. In [103], an EKF-based adaptive lookup table is proposed to generate an adaptive air

mass-flow map for a truck engine.

In this section, a 1-D lookup table of clutch surface friction coefficient (vertical axis) versus clutch slip speed (horizontal axis) is established, where the horizontal axis node is predefined and the vertical axis nodes are adaptively updated based on the efficient recursive Least-Squares algorithm in [101, 104].

6.2 Clutch Surface Friction Coefficient Model

From clutch perspective, clutch torque is usually related to the clutch surface friction coefficient, normal force of the engaged clutch disks, and clutch geometry parameters [17], which can be written specifically as

$$T_c = n_c \mu_c F_N R_{ceff} \quad (6.1)$$

where T_c is actual transmitted clutch torque; n_c is total number of engaged clutch contact surfaces and typically is fixed given a certain transfer case; μ_c is clutch surface friction coefficient; F_N is clutch normal force; and R_{ceff} is clutch disk mean effective radius.

Figure 6.2 shows the clutch disk geometry, and the clutch mean effective radius can be approximated by the simple equation below.

$$R_{ceff} = \frac{R_{ci} + R_{co}}{2} \quad (6.2)$$

where R_{ci} is the inner radius of clutch disk and R_{co} is the outer radius of the clutch disk.

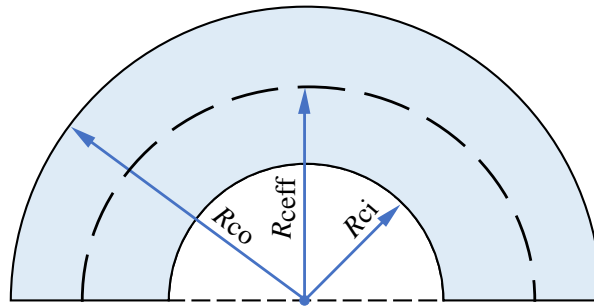


Figure 6.2: Clutch disk section view

Note that clutch surface friction coefficient is typically time-varying due to different operating condition and needs to be estimated in real-time. Rewrite equation (6.1), the clutch friction coefficient can be obtained by

$$\mu_c = \frac{T_c}{n_c F_N R_{ceff}} \quad (6.3)$$

Note that the clutch normal force F_N is obtained from Chapter 2 via the estimation of clutch touchpoint, and the clutch output torque is obtained from Chapter 4 through the tire and vehicle dynamics model.

6.3 Real-time Recursive Least-Squares Adaptive Lookup Table

6.3.1 Recursive Least-Squares based Adaptive 1-D Lookup Table Algorithm

Figure 6.3 shows the concept of recursive Least-Squares algorithm based 1-D adaptive lookup table[101]. In the horizontal axis, the predefined nodes are denoted as vector $\mathbf{x} = [x_1, x_2, \dots, x_n]^T$, and the corresponding table value in the vertical axis is denoted as vector $\Theta = [\Theta_1, \Theta_2, \dots, \Theta_n]^T$. The aim of the adaptive table is to estimate the table value Θ given the sets of known input-output($x - z$) so that a real-time updated lookup table $\Theta - x$ is obtained.

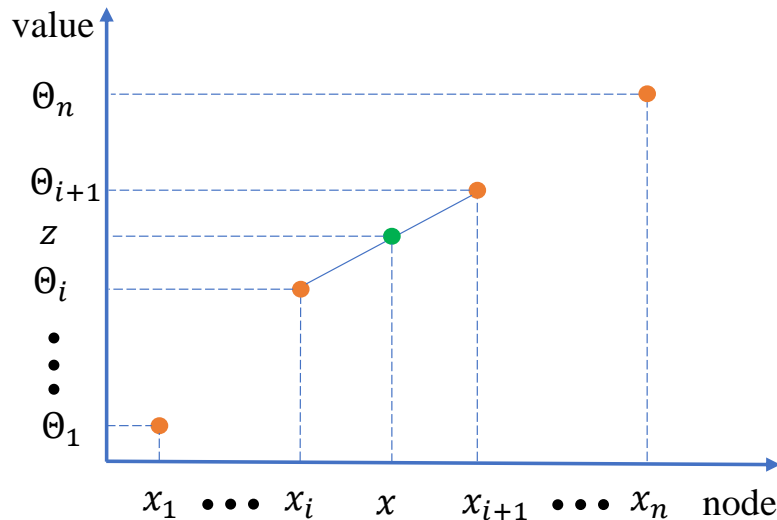


Figure 6.3: Illustrative diagram of 1-D lookup table

6.3.2 General 1-D Adaptive Table Structure

The first step is to determine the active node segment by comparing current x to the vector \mathbf{x} . If $x_i < x < x_{i+1}$ is satisfied, the active segment is $[x_i, x_{i+1}]$, and the normalized ratio is defined as

$$r(t) = \frac{x(t) - x_i}{x_{i+1} - x(t)} \quad (6.4)$$

The interpolated table value can then be expressed as

$$z(t) = [1 - r(t) \ r(t)] \begin{bmatrix} \Theta_i \\ \Theta_{i+1} \end{bmatrix} \quad (6.5)$$

Note that the above equation is true only for active segment with only two table values Θ_i and Θ_{i+1} .

And it can be rewrote as

$$z(t) = \phi(t)\Theta \quad (6.6)$$

where

$$\phi(t) = \begin{cases} 1 - r(t) & i^{th} \text{ element} \\ r(t) & (i + 1)^{th} \text{ element} \\ 0 & \text{elsewhere} \end{cases} \quad (6.7)$$

Therefore, for the cumulative k -step data, the generalized table adaptation model becomes

$$z = \Phi\Theta \quad (6.8)$$

where the regression vector is extended to have the following regression matrix

$$\Phi = \begin{bmatrix} 0, \dots, \phi(1), \dots, 0 \\ 0, \dots, \phi(2), \dots, 0 \\ \vdots \\ 0, \dots, \phi(k), \dots, 0 \end{bmatrix} \quad (6.9)$$

and vector Θ is to be estimated.

6.3.3 RLS Adaptive Table Algorithm

Model in equation (6.8) can be solved by the well-known recursive Least-Squares algorithm as follows.

$$\begin{aligned}\hat{\Theta}(t) &= \hat{\Theta}(t-1) + R^{-1}(t)\phi^T(t)[y(t) - \phi^T(t)\hat{\Theta}(t-1)] \\ R(t) &= \beta R(t-1) + \phi(t)\phi^T(t)\end{aligned}\tag{6.10}$$

Note that in the above equation, it is required to solve the inverse of matrix $R(t)$ at each time step, which is undesired. Therefore, generally speaking, to avoid the computation of inverse matrix of $R(t)$, define a matrix $P(t) = R^{-1}(t)$, by matrix inversion lemma, the following recursive solution can be obtained.

$$\begin{aligned}P(t) &= \frac{1}{\beta}(I - L(t)\phi^T(t))P(t-1) \\ L(t) &= \frac{P(t-1)\phi(t)}{\beta + \phi^T P(t-1)\phi(t)} \\ \hat{\Theta}(t) &= \hat{\Theta}(t-1) + L(t)[y(t) - \phi^T(t)\hat{\Theta}(t-1)]\end{aligned}\tag{6.11}$$

However, one of the main drawback of this formulation is the 'curse of dimension' for storing such $P(t)$ matrix, especially when the lookup table dimension increases. The way to solve this problem is to make use of the special structure of $\phi(t)$. Note that due to the particular structure of $\phi(t)$ as shown in equation (6.7), the active elements of $\phi(t)\phi^T(t)$ (0 in any other positions) is

$$\phi(t)\phi^T(t) = \begin{bmatrix} (1-r(t))^2 & r(t)(1-r(t)) \\ r(t)(1-r(t)) & r^2(t) \end{bmatrix}\tag{6.12}$$

which will further lead to a particular structure of $R(t)$ as shown in Figure 6.4.

6.3.4 Complete Road Map of Friction Coefficient Estimation

Further with the updated adaptive lookup table, other sets of measured clutch slip data are used to generating the clutch surface friction first, and then calculating the clutch torque, which is finally compared to a measured clutch torque to evaluate the table performance. The complete road map are summarized in Figure 6.5.

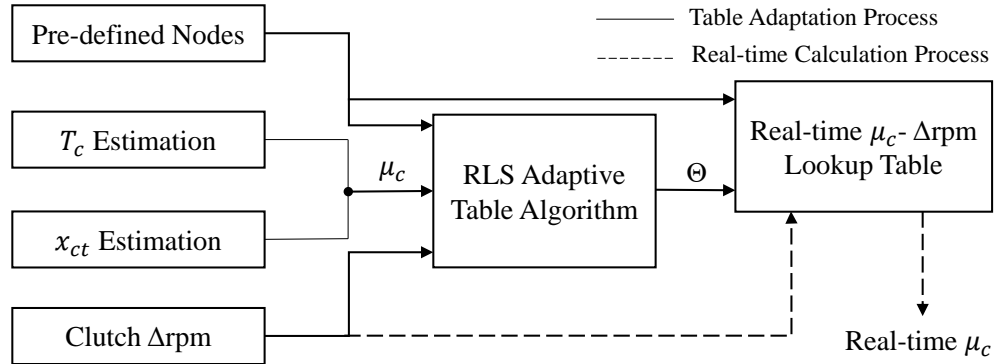


Figure 6.5: Real-time μ_c estimation road map

6.4 Result Evaluation

For this study, T_c estimation is from Chapter 4 and x_{ct} from Chapter 2. The clutch Δ rpm is calculated from the measured tire speed. Figure 6.6 shows the torque estimation result and its associated signals obtained from the torque estimation model in Section 4. Note that the clutch is typically engaged for 4WD mode during vehicle acceleration, which can be confirmed by the vehicle speed signal. The clutch Δ rpm shows that before 80s, it is overtaken (which is not the subject of this study), while between 80-82s, the clutch is slipping with significant speed difference. The last plot shows the torque under this vehicle acceleration.

Based on these estimation results, a clutch surface friction coefficient can be calculated, which is shown in the red line of Figure 6.10. Note that the focus is on clutch slip duration (80-82s). With the clutch touchpoint x_{ct} , clutch torque, and calculated friction coefficient μ_c ready, the algorithm in 6.3.3 can be used to obtain the adaptive lookup table. The table horizontal axis is selected as $\mathbf{x} = [0, 5, 10, 15]^T$ rpm according to the clutch slip speed range. Figure 6.7 shows the adapted

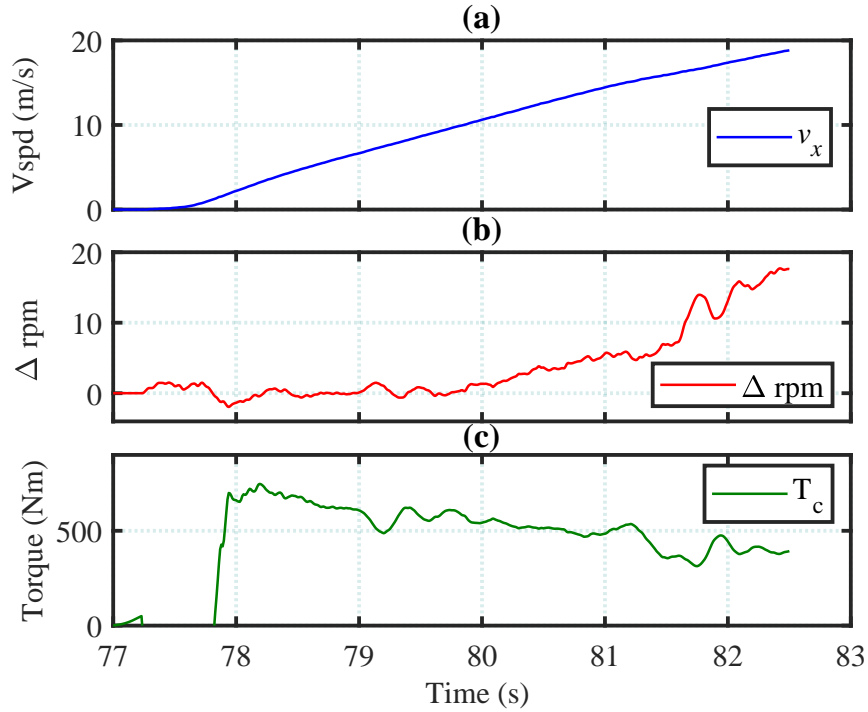


Figure 6.6: Clutch Torque and Associated Signals

table vertical node results. It can be observed that after several clutch engagements, the four-node values are converging. For multiple engagement data as show in Figure 6.7, the average of table nodes can be calculated as the updated node value, which is show in Figure 6.8, it is obvious that in the future, with the help of clutch slip speed obtained from the tire rotational speed, the friction coefficient table can be updated in real-time. Furthermore, the convergence of the table notes can be observed from the 3-D view presented in Figure 6.9.

Therefore, with these converged nodes, a lookup table (vertical-horizontal node, namely, μ_c - Δrpm) can be established so that in the future, real-time friction coefficient μ_c can be obtained with known Δrpm , which depends only on the measured vehicle tire speed. The friction coefficient μ_c obtained from the model calculation in Chapter 4 and adaptive table is compared in Figure 6.10. It can be observed that under clutch slip operation, they are close.

A further clutch torque validation is presented in Fig. 6.11, where red-line represents the same clutch torque from modeling approach as show in Fig. 6.6, and blue-line is obtained from the lookup table estimation. Note that there is no production-ready torque sensor available on the vehicle to

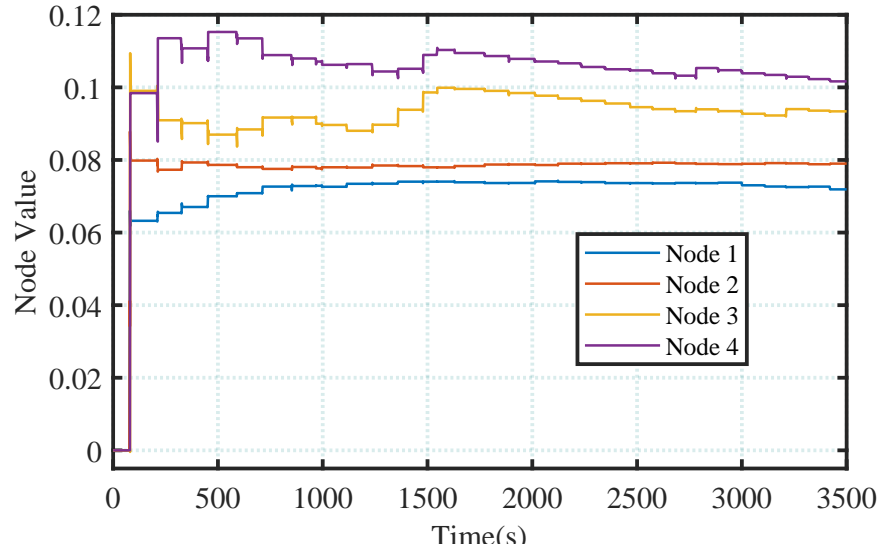


Figure 6.7: Adaptive table nodes convergence vs. time

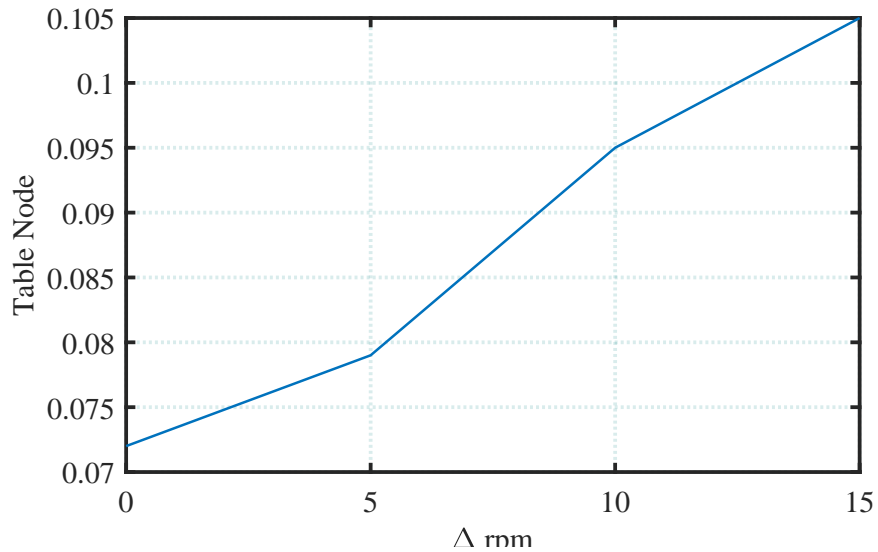


Figure 6.8: Adaptive table nodes convergence vs. Δrpm

measure clutch output torque directly, therefore, another clutch torque estimation result via EKF-UI algorithm using engine torque as input (see [106] for details) is presented in black-line and used as ground truth due to its high estimation accuracy. It can be seen that during clutch slip between 80 and 81s, the table resulted and estimated torques are all pretty close. Furthermore, error analysis reveals that the Absolute Mean Squared Error (AMSE) between T_f modeling and T_f EKF-UI is 35 Nm, and the Relative Mean Squared Error (RMSE) is 5.9% while the AMSE between T_f modeling and T_f is 14.8 Nm, and RMSE is 2.66%. It can be concluded that the clutch torque estimation

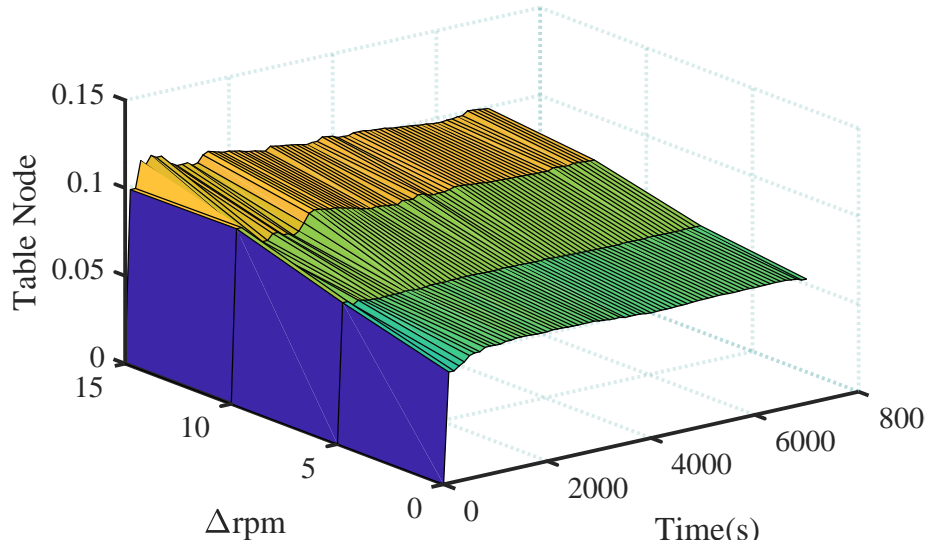


Figure 6.9: 3D convergence view

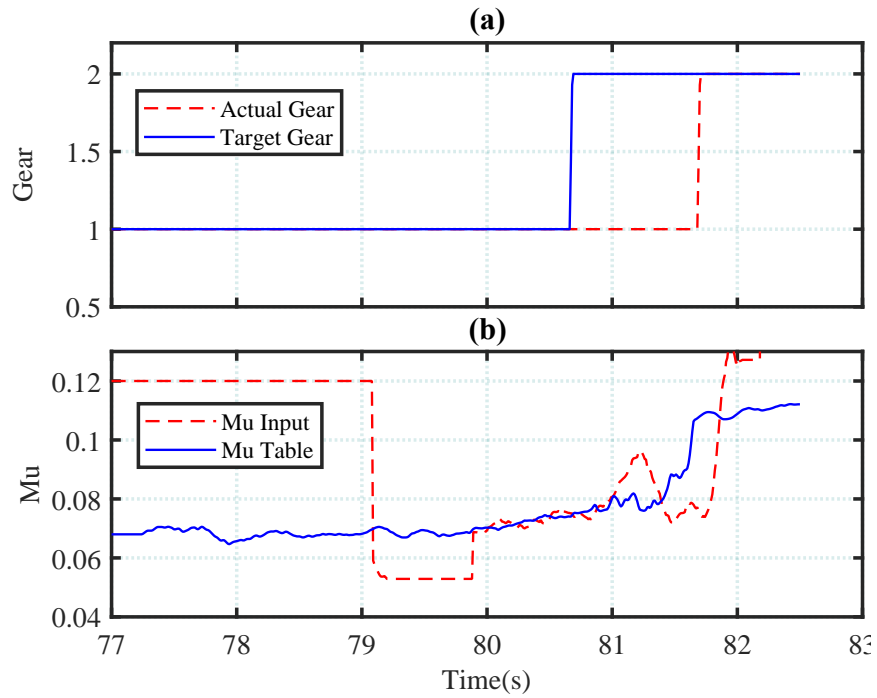


Figure 6.10: μ_c obtained from adaptive lookup table

results based on the real-time adaptive lookup table is effective and accurate. Other clutch torque estimation results are similar and therefore omitted.

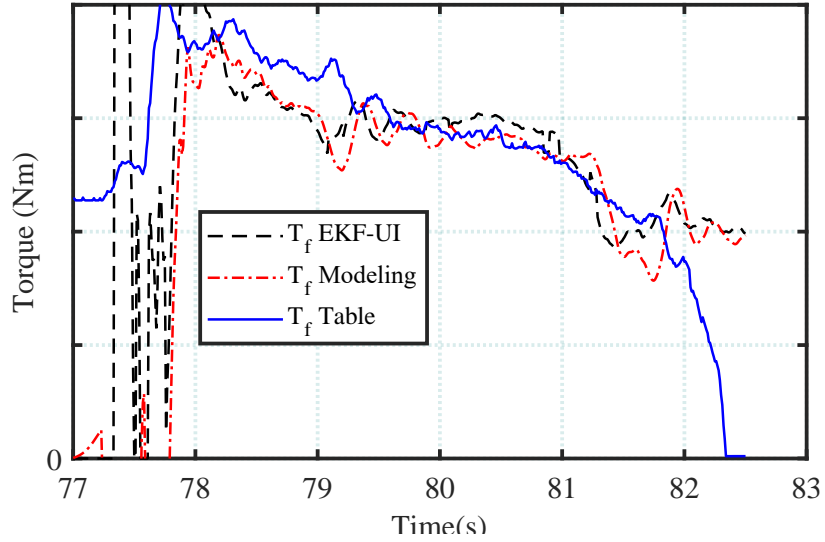


Figure 6.11: Torque estimation obtained from adaptive lookup table

6.5 Conclusion

In conclusion, the following are achieved in this chapter:

1. The clutch-parameter-dependent surface friction coefficient is calculated based on the clutch touchpoint estimation in Chapter 2 and clutch output torque estimation in Chapter 4, both of which are used as inputs to the recursive Least-Squares adaptive lookup table;
2. The recursive Least-Squares adaptive lookup table is established based on the input and output data; the input data are the measured clutch slip speed, while the output data are the estimated clutch surface friction coefficient in the previous step. The recursive solution uses the real-time implementable Thomas Algorithm.
3. With the established adaptive lookup table, several measured inputs are employed to obtain the real-time clutch-parameter-independent friction coefficient to be used to come up with a real-time clutch torque, which is compared to the estimated clutch torque. Comparison shows that under the clutch slip condition, the real-time estimated clutch torque is close to the one from adaptive table.

CHAPTER 7

CONCLUSIONS AND FUTURE WORK

7.1 Conclusions

In summary, to estimate the clutch surface friction coefficient, the clutch touchpoint displacement and the clutch torque are estimated first, they can be concluded in the following two aspects.

Touchpoint Estimation

1. With the current PID control scheme employed, the model-based adaptive estimation algorithm along with modified friction model is proposed to estimate the touchpoint separately and validated using experimental data showing improved accuracy and robustness over the existing method;
2. An integrated estimation scheme, based on the deadbeat adaptive backstepping control technique, is proposed to estimate touchpoint and tracks the reference position simultaneously and shows its potential of performance improvement.

Clutch Torque Estimation

1. The proposed vehicle acceleration compensation to the effective tire radius and vehicle speed estimator based on the four-tire traction force provide accurate vehicle speed and clutch torque estimations under clutch overtaken condition;
2. While when the clutch is slipping, the proposed linear speed compensation to front tire speed also promotes to a more accurate torque estimation.

Clutch Surface Friction Coefficient Estimation

1. The recursive Least-Squares adaptive Lookup table is established for obtaining real-time clutch surface friction coefficient. The adaptive lookup table is updated in two steps. The first

step is to obtain the clutch-parameter-dependent friction coefficient through direct calculation; and the second step is to parameterize the friction coefficient to make it dependent on the clutch slip speed. This is done by updating the nodes of adaptive lookup table, which is realized by the Recursive Least-Squares (RLS) algorithm. The output of the RLS algorithm is the updated table nodes. The adaptive lookup table could be used to obtain the clutch-parameter-independent friction coefficient.

2. The real-time clutch surface friction coefficient further leads to the real-time clutch torque estimation based on the direct clutch geometry relationship. The calculated clutch torque is then compared to the actual measured torque that confirms the effectiveness of the proposed Recursive Least-Squares Adaptive Lookup table.

7.2 Recommendation for Future Work

Future work following the research work presented in this dissertation includes implementation of the developed algorithm into the physical system.

It is recommended to implement the adaptive clutch touchpoint estimation algorithm for transfer case bench tests, including the following:

1. Calibrating the friction model using experimental data to provide a more accurate ball friction torque in the clutch actuation system for improving clutch touchpoint estimation;
2. Implementing the adaptive estimation algorithm vehicle environment and comparing the vehicle tested clutch touchpoint with that from the existing algorithm to demonstrate the advantage of proposed estimation algorithm.

For the deadbeat adaptive backstepping control, the advantage is that it is an integrated estimation and control algorithm. The successful implementation of this algorithm will, on one hand, reduces the tuning effort of the controller for the clutch displacement and touchpoint, and on the other hand, eliminates redundant algorithm to reduce both control module throughput and memory.

The implementation of clutch torque estimation algorithm would be more of practical importance since currently, there is no production ready torque sensor installed on the vehicle. Therefore, the implementation of this algorithm will provide the estimated clutch torque in the absence of torque sensor. This can be greatly beneficial for vehicle torque distribution control for improved traction performance.

The implementation of friction coefficient algorithm will also be beneficial since it can provide clutch-parameter-independent friction coefficient, which can make accurately control the clutch output torque during slip phase easier, and therefore, slowing down the clutch wearing rate.

APPENDIX

APPENDIX

APPENDIX A

A.1 Derivation of System Transformation

This section shows clutch overtaken condition ($\Delta rpm = 0$) system formulation. According to equations listed in Section 5.2, by choosing the system states, inputs and outputs stated in (5.14), the state-space representation of the system becomes

$$\dot{x} = \begin{bmatrix} -\frac{C_f}{J_f} r_{ref} + \frac{C_f}{J_f} \frac{x_3}{x_1} + \frac{i_{fd}}{J_f} u_1 \\ -\frac{C_r}{J_r} r_{ref} + \frac{C_r}{J_r} \frac{x_3}{x_2} - \frac{i_{rd}}{J_r} u_1 + \frac{i_{rd}}{J_r} u_2 \\ \frac{C_f}{m} - \frac{C_f}{m} \frac{x_3}{x_1} + \frac{C_r}{m} - \frac{C_r}{m} \frac{x_3}{x_2} - \frac{F_a + F_{r0}}{m} \end{bmatrix} \quad (\text{A.1})$$

A.2 Derivation of system linearization

Proceeding the discretization with sampling period T_s using forward Euler Approximation formula as below,

$$\dot{x} \approx \frac{x(k+1) - x(k)}{T_s} \quad (\text{A.2})$$

the system governing function in (5.14) becomes

$$\begin{aligned} \dot{x} &= \begin{bmatrix} f_1 & f_2 & f_3 \end{bmatrix}^T \\ f(x_k, u_k) &= \begin{bmatrix} x_{1,k} + T_s f_1 \\ x_{2,k} + T_s f_2 \\ x_{3,k} + T_s f_3 \end{bmatrix} = \begin{bmatrix} F_1 \\ F_2 \\ F_3 \end{bmatrix} \end{aligned} \quad (\text{A.3})$$

Therefore, the linearization can be proceeded according to equations (5.18) and (5.19). The linearization with respect to state vector x_k can be proceeded as follows.

$$\frac{\partial f(x_k, u_k)}{\partial x_k} = \begin{bmatrix} \frac{\partial F_1}{\partial x_k} & \frac{\partial F_2}{\partial x_k} & \frac{\partial F_3}{\partial x_k} \end{bmatrix}^T \quad (\text{A.4})$$

$$\begin{aligned}\frac{\partial F_1}{\partial x_k} &= \begin{bmatrix} \frac{\partial F_1}{\partial x_{1,k}} & \frac{\partial F_1}{\partial x_{2,k}} & \frac{\partial F_1}{\partial x_{3,k}} \end{bmatrix} \\ &= \begin{bmatrix} 1 - T_s \frac{C_f x_{3,k}}{J_f x_{1,k}^2} & 0 & T_s \frac{C_f}{J_f} \frac{1}{x_{1,k}} \end{bmatrix}\end{aligned}\quad (\text{A.5})$$

$$\begin{aligned}\frac{\partial F_2}{\partial x_k} &= \begin{bmatrix} \frac{\partial F_2}{\partial x_{1,k}} & \frac{\partial F_2}{\partial x_{2,k}} & \frac{\partial F_2}{\partial x_{3,k}} \end{bmatrix} \\ &= \begin{bmatrix} 0 & 1 - T_s \frac{C_r x_{3,k}}{J_r x_{2,k}^2} & T_s \frac{C_r}{J_r} \frac{1}{x_{2,k}} \end{bmatrix}\end{aligned}\quad (\text{A.6})$$

$$\begin{aligned}\frac{\partial F_3}{\partial x_k} &= \begin{bmatrix} \frac{\partial F_3}{\partial x_{1,k}} & \frac{\partial F_3}{\partial x_{2,k}} & \frac{\partial F_3}{\partial x_{3,k}} \end{bmatrix} \\ &= \begin{bmatrix} \frac{T_s C_f x_{3,k}}{m r_{fef} x_{1,k}^2} & \frac{T_s C_r x_{3,k}}{m r_{ref} x_{2,k}^2} & F_{3,p} \end{bmatrix}\end{aligned}\quad (\text{A.7})$$

$$F_{3,p} = 1 - T_s \left[\frac{C_f}{m r_{fef} x_{1,k}} + \frac{C_r}{m r_{ref} x_{2,k}} + \left(\frac{C_a \rho_a A_a}{m} + 2b_{rog} \right) x_{3,k} \right]$$

By stacking up equations (A.5) to (A.7) as shown in equation (A.4) and evaluating each element at the estimated states (\hat{x}_k) and unknown input ($\hat{u}_{1,k}$), namely, $x_k = \hat{x}_k$ and $u_{1,k} = \hat{u}_{1,k}$, the system matrix A_k in equation (5.18) can be obtained.

Similarly, the linearization with respect to the unknown input $u_{1,k}$ can be proceed as

$$\frac{\partial f(x_k, u_k)}{\partial u_{1,k}} = \begin{bmatrix} \frac{i_{fd}}{J_f} T_s, & -\frac{i_{rd}}{J_r} T_s, & 0 \end{bmatrix}^T \quad (\text{A.8})$$

and evaluating each element at the estimated states (\hat{x}_k) and unknown input ($\hat{u}_{1,k}$), namely, $x_k = \hat{x}_k$ and $u_{1,k} = \hat{u}_{1,k}$ using equation (A.8), the input matrix B_k in equation (5.19) can be obtained. Note that B_k in the target system is a constant matrix once the sampling period is selected.

BIBLIOGRAPHY

BIBLIOGRAPHY

- [1] D. Kim, S. Hwang, and H. Kim, "Vehicle stability enhancement of four-wheel-drive hybrid electric vehicle using rear motor control," *IEEE Transactions on Vehicular Technology*, vol. 57, no. 2, pp. 727–735, 2008.
- [2] J. Kang, J. Yoo, and K. Yi, "Driving control algorithm for maneuverability, lateral stability, and rollover prevention of 4wd electric vehicles with independently driven front and rear wheels," *IEEE Transactions on vehicular technology*, vol. 60, no. 7, pp. 2987–3001, 2011.
- [3] S. Mohan, "All-wheel drive/four-wheel drive systems and strategies," in *FISITA World Automotive Congress*, 2000, pp. 12–15.
- [4] C. Miao, H. Liu, G. G. Zhu, and H. Chen, "Connectivity-based optimization of vehicle route and speed for improved fuel economy," *Transportation Research Part C: Emerging Technologies*, vol. 91, pp. 353–368, 2018.
- [5] G. G. Zhu and C. Miao, "Real-time co-optimization of vehicle route and speed using generic algorithm for improved fuel economy," *Mechanical Engineering*, vol. 141, no. 03, pp. S08–S15, 2019.
- [6] Z. Fu, B. Li, and X.-B. Ning, "High-performance torque controller design for ac driving 4wd electric vehicle in two time scales." *IJMIC*, vol. 30, no. 1, pp. 9–18, 2018.
- [7] S. F. da Silva, E. de Moura Fernandes, and W. F. de Amorim Junior, "Modeling and simulation of the performance and efficiency of a sport utility vehicle powertrain with automatic transmission through model-based design," in *2018 13th IEEE International Conference on Industry Applications (INDUSCON)*. IEEE, 2018, pp. 1128–1132.
- [8] G. Panzani, M. Corno, M. Tanelli, A. Zappavigna, S. M. Savaresi, A. Fortina, and S. Campo, "Designing on-demand four-wheel-drive vehicles via active control of the central transfer case," *IEEE Transactions on Intelligent Transportation Systems*, vol. 11, no. 4, pp. 931–941, 2010.
- [9] H. Ham and H. Lee, "Sliding mode control strategy for the four wheel drive vehicles," in *IECON 2011-37th Annual Conference of the IEEE Industrial Electronics Society*. IEEE, 2011, pp. 746–750.
- [10] D. Crolla, "Automotive engineering: powertrain, chassis system and vehicle body," 2009.
- [11] G. Lechner and H. Naunheimer, *Automotive transmissions: fundamentals, selection, design and application*. Springer Science & Business Media, 1999.
- [12] S. Pace and G. G. Zhu, "Transient air-to-fuel ratio control of an spark ignited engine using linear quadratic tracking," *Journal of Dynamic Systems, Measurement, and Control*, vol. 136, no. 2, 2014.

- [13] X. Chen, Y. Wang, I. Haskara, and G. Zhu, "Optimal air-to-fuel ratio tracking control with adaptive biofuel content estimation for Int regeneration," *IEEE Transactions on Control Systems Technology*, vol. 22, no. 2, pp. 428–439, 2013.
- [14] L. Mingxue, Y. Guolai, L. Xiaoqing, and B. Guixiang, "Variable universe fuzzy control of adjustable hydraulic torque converter based on multi-population genetic algorithm," *IEEE Access*, vol. 7, pp. 29 236–29 244, 2019.
- [15] L. Glielmo, L. Iannelli, V. Vacca, and F. Vasca, "Gearshift control for automated manual transmissions," *IEEE/ASME transactions on mechatronics*, vol. 11, no. 1, pp. 17–26, 2006.
- [16] J. Yang and G. G. Zhu, "Adaptive recursive prediction of the desired torque of a hybrid powertrain," *IEEE transactions on vehicular technology*, vol. 64, no. 8, pp. 3402–3413, 2014.
- [17] X. Song, Z. Sun, X. Yang, and G. Zhu, "Modelling, control, and hardware-in-the-loop simulation of an automated manual transmission," *Proceedings of the Institution of Mechanical Engineers, Part D: Journal of Automobile Engineering*, vol. 224, no. 2, pp. 143–160, 2010.
- [18] M. Pisaturo and A. Senatore, "Simulation of engagement control in automotive dry-clutch and temperature field analysis through finite element model," *Applied Thermal Engineering*, vol. 93, pp. 958–966, 2016.
- [19] A. Senatore, C. DAuria, and M. Pisaturo, "Frictional behaviour and engagement control in dry clutch based automotive transmissions," *Vehicle Engineering*, vol. 4, pp. 1–12, 2017.
- [20] Z. Zhigang, S. Xiaohui, and G. Dong, "Dynamic temperature rise mechanism and some controlling factors of wet clutch engagement," *Mathematical Problems in Engineering*, vol. 2016, 2016.
- [21] A. Myklebust and L. Eriksson, "Modeling, observability, and estimation of thermal effects and aging on transmitted torque in a heavy duty truck with a dry clutch," *IEEE/ASME transactions on mechatronics*, vol. 20, no. 1, pp. 61–72, 2014.
- [22] L. Li, X. Wang, X. Qi, X. Li, D. Cao, and Z. Zhu, "Automatic clutch control based on estimation of resistance torque for amt," *IEEE/ASME Transactions on Mechatronics*, vol. 21, no. 6, pp. 2682–2693, 2016.
- [23] H. Pacejka, *Tire and vehicle dynamics*. Elsevier, 2005.
- [24] C. R. Carlson and J. C. Gerdes, "Consistent nonlinear estimation of longitudinal tire stiffness and effective radius," *IEEE Transactions on Control Systems Technology*, vol. 13, no. 6, pp. 1010–1020, 2005.
- [25] H. K. Khalil, "Nonlinear systems," *Upper Saddle River*, 2002.
- [26] W. Wei, H. Dourra, and G. Zhu, "Adaptive transfer case clutch touchpoint estimation with a modified friction model," *IEEE/ASME Transaction on Mechatronics*, vol. 25, no. 4, pp. 2000–2008, 2020.

- [27] W.-F. Xie, “Sliding-mode-observer-based adaptive control for servo actuator with friction,” *IEEE Transactions on Industrial Electronics*, vol. 54, no. 3, pp. 1517–1527, 2007.
- [28] F. Al-Bender and J. Swevers, “Characterization of friction force dynamics,” *IEEE Control Systems Magazine*, vol. 28, no. 6, pp. 64–81, 2008.
- [29] W. Townsend and J. Salisbury, “The effect of coulomb friction and stiction on force control,” in *Proceedings. 1987 IEEE International Conference on Robotics and Automation*, vol. 4. IEEE, 1987, pp. 883–889.
- [30] O. Reynolds, “Iv. on the theory of lubrication and its application to mr. beauchamp towers experiments, including an experimental determination of the viscosity of olive oil,” *Philosophical transactions of the Royal Society of London*, no. 177, pp. 157–234, 1886.
- [31] F. Dai, X. Gao, S. Jiang, W. Guo, and Y. Liu, “A two-wheeled inverted pendulum robot with friction compensation,” *Mechatronics*, vol. 30, pp. 116–125, 2015.
- [32] R. Kelly, J. Llamas, and R. Campa, “A measurement procedure for viscous and coulomb friction,” *IEEE Transactions on instrumentation and measurement*, vol. 49, no. 4, pp. 857–861, 2000.
- [33] A. J. Morin, “New friction experiments carried out at metz in 1831–1833,” *Proceedings of the French Royal Academy of Sciences*, vol. 4, no. 1, p. 128, 1833.
- [34] B. Jacobson, “The stribeck memorial lecture,” *Tribology International*, vol. 36, no. 11, pp. 781–789, 2003.
- [35] L. Freidovich, A. Robertsson, A. Shiriaev, and R. Johansson, “Lugre-model-based friction compensation,” *IEEE Transactions on Control Systems Technology*, vol. 18, no. 1, pp. 194–200, 2009.
- [36] L. Márton, S. Fodor, and N. Sepehri, “A practical method for friction identification in hydraulic actuators,” *Mechatronics*, vol. 21, no. 1, pp. 350–356, 2011.
- [37] F. L. Lewis, D. Vrabie, and V. L. Syrmos, *Optimal control*. John Wiley & Sons, 2012.
- [38] G. Tao, *Adaptive control design and analysis*. John Wiley & Sons, 2003, vol. 37.
- [39] A. Bisoffi, M. Da Lio, A. R. Teel, and L. Zaccarian, “Global asymptotic stability of a pid control system with coulomb friction,” *IEEE Transactions on Automatic Control*, vol. 63, no. 8, pp. 2654–2661, 2017.
- [40] H. Olsson, K. J. Åström, C. C. De Wit, M. Gäfvert, and P. Lischinsky, “Friction models and friction compensation,” *Eur. J. Control*, vol. 4, no. 3, pp. 176–195, 1998.
- [41] Q. Shen, H. Tianyi, and G. Z. Guoming, “Switched LPV Modeling and Control of an Engine EGR Valve with Dry Friction,” in *2019 IEEE Conference on Control Technology and Applications (CCTA)*. IEEE, 2019.

- [42] S. Qu, T. He, and G. G. Zhu, “Engine egr valve modeling and switched l_pv control considering nonlinear dry friction,” *IEEE/ASME Transactions on Mechatronics*, vol. 25, no. 3, pp. 1668–1678, 2020.
- [43] R. Beerens, H. Nijmeijer, M. Heemels, and N. van de Wouw, “Set-point control of motion systems with uncertain set-valued stribeck friction,” *IFAC-PapersOnLine*, vol. 50, no. 1, pp. 2965–2970, 2017.
- [44] W. Wei, H. Dourra, and G. Zhu, “Integrated clutch torque control and touchpoint estimation using deadbeat adaptive backstepping,” *IEEE Transactions on Control Systems Technology*, pp. 1–8, 2021, DOI: 10.1109/TCST.2021.3058330.
- [45] W. Wei, H. Dourra, and G. G. Zhu, “Deadbeat adaptive backstepping design for tracking transfer case torque and estimating its clutch touchpoint,” in *2020 IEEE Conference on Control Technology and Applications (CCTA)*, 2020, pp. 188–193.
- [46] J. Kabziński, M. Jastrzębski, and P. Mosiołek, “Comparison of various barrier lyapunov functions for adaptive control of nonlinear systems,” in *2016 21st International Conference on Methods and Models in Automation and Robotics (MMAR)*. IEEE, 2016, pp. 1027–1032.
- [47] P. Kokotovic, M. Krstic, and I. Kanellakopoulos, “Backstepping to passivity: recursive design of adaptive systems,” in *[1992] Proceedings of the 31st IEEE Conference on Decision and Control*. IEEE, 1992, pp. 3276–3280.
- [48] P. V. Kokotovic, “The joy of feedback: nonlinear and adaptive,” *IEEE Control Systems Magazine*, vol. 12, no. 3, pp. 7–17, 1992.
- [49] R. Freeman and P. Kokotović, “Backstepping design of robust controllers for a class of nonlinear systems,” in *Nonlinear Control Systems Design 1992*. Elsevier, 1993, pp. 431–436.
- [50] I. Kanellakopoulos, P. V. Kokotovic, and A. S. Morse, “Systematic design of adaptive controllers for feedback linearizable systems,” in *1991 American Control Conference*. IEEE, 1991, pp. 649–654.
- [51] R. Kanellakopoulos, “A discrete-time adaptive nonlinear system,” in *Proceedings of 1994 American Control Conference-ACC’94*, vol. 1. IEEE, 1994, pp. 867–869.
- [52] K. K. Ahn, D. N. C. Nam, and M. Jin, “Adaptive backstepping control of an electrohydraulic actuator,” *IEEE/ASME transactions on mechatronics*, vol. 19, no. 3, pp. 987–995, 2013.
- [53] C. Yang, Z. Li, R. Cui, and B. Xu, “Neural network-based motion control of an underactuated wheeled inverted pendulum model,” *IEEE Transactions on Neural Networks and Learning Systems*, vol. 25, no. 11, pp. 2004–2016, 2014.
- [54] P. J. Antsaklis and A. N. Michel, *A Linear Systems Primer*, 1st ed. Birkhäuser Basel, 2007.

- [55] W. Chakchouk, J. Chroua, C. B. Regaya, A. Zaafouri, and A. Sellami, “Discrete-time adaptive backstepping control: Application to pumping station,” *Proceedings of the Institution of Mechanical Engineers, Part I: Journal of Systems and Control Engineering*, vol. 232, no. 6, pp. 683–694, 2018.
- [56] J. Lu, R. Wei, X. Wang, and Z. Wang, “Backstepping control of discrete-time chaotic systems with application to the henon system,” *IEEE Transactions on Circuits and Systems I: Fundamental Theory and Applications*, vol. 48, no. 11, pp. 1359–1363, 2001.
- [57] Y. Zhang, C. Wen, and Y. C. Soh, “Discrete-time robust backstepping adaptive control for nonlinear time-varying systems,” *IEEE Transactions on Automatic Control*, vol. 45, no. 9, pp. 1749–1755, 2000.
- [58] B. Yao and M. Tomizuka, “Adaptive robust control of siso nonlinear systems in a semi-strict feedback form,” *Automatica*, vol. 33, no. 5, pp. 893–900, 1997.
- [59] G. C. Goodwin and K. S. Sin, *Adaptive filtering prediction and control*. Courier Corporation, 2014.
- [60] S. Yang, Y. Lu, and S. Li, “An overview on vehicle dynamics,” *International Journal of Dynamics and Control*, vol. 1, no. 4, pp. 385–395, 2013.
- [61] J. Oh, S. B. Choi, Y. Chang, and J. Eo, “Engine clutch torque estimation for parallel-type hybrid electric vehicles,” *International Journal of Automotive Technology*, vol. 18, no. 1, pp. 125–135, 2017.
- [62] Z. Zhao, L. He, Y. Yang, C. Wu, X. Li, and J. K. Hedrick, “Estimation of torque transmitted by clutch during shifting process for dry dual clutch transmission,” *Mechanical Systems and Signal Processing*, vol. 75, pp. 413–433, 2016.
- [63] J. J. Oh, S. B. Choi, and J. Kim, “Driveline modeling and estimation of individual clutch torque during gear shifts for dual clutch transmission,” *Mechatronics*, vol. 24, no. 5, pp. 449–463, 2014.
- [64] S. Iqbal, F. Al-Bender, A. P. Ompusunggu, B. Pluymers, and W. Desmet, “Modeling and analysis of wet friction clutch engagement dynamics,” *Mechanical Systems and Signal Processing*, vol. 60, pp. 420–436, 2015.
- [65] C. El Tannoury, F. Plestan, S. Moussaoui, and N. Romani, “Tyre effective radius and vehicle velocity estimation: A variable structure observer solution,” in *Eighth International Multi-Conference on Systems, Signals & Devices*. IEEE, 2011, pp. 1–6.
- [66] R. Rajamani, G. Phanomchoeng, D. Piyabongkarn, and J. Y. Lew, “Algorithms for real-time estimation of individual wheel tire-road friction coefficients,” *IEEE/ASME Transactions on Mechatronics*, vol. 17, no. 6, pp. 1183–1195, 2011.
- [67] K. Jo, K. Chu, J. Kim, and M. Sunwoo, “Distributed vehicle state estimation system using information fusion of gps and in-vehicle sensors for vehicle localization,” in *2011 14th International IEEE Conference on Intelligent Transportation Systems (ITSC)*. IEEE, 2011, pp. 2009–2014.

- [68] T. A. Wenzel, K. J. Burnham, M. V. Blundell, and R. A. Williams, “Dual extended kalman filter for vehicle state and parameter estimation,” *Vehicle System Dynamics*, vol. 44, no. 2, pp. 153–171, 2006.
- [69] K. Berntorp and S. Di Cairano, “Tire-stiffness and vehicle-state estimation based on noise-adaptive particle filtering,” *IEEE Transactions on Control Systems Technology*, vol. 27, no. 3, pp. 1100–1114, 2018.
- [70] M. Blundell and D. Harty, *Multibody systems approach to vehicle dynamics*. Elsevier, 2004.
- [71] C. E. Tannoury, S. Moussaoui, F. Plestan, N. Romani, and G. Pita-Gil, “Synthesis and application of nonlinear observers for the estimation of tire effective radius and rolling resistance of an automotive vehicle,” *IEEE Transactions on Control Systems Technology*, vol. 21, no. 6, pp. 2408–2416, 2013.
- [72] C. Lundquist, R. Karlsson, E. Ozkan, and F. Gustafsson, “Tire radii estimation using a marginalized particle filter,” *IEEE Transactions on Intelligent Transportation Systems*, vol. 15, no. 2, pp. 663–672, 2014.
- [73] R. N. Jazar, *Vehicle dynamics: theory and application*. Springer, 2017.
- [74] A. N. Gent and J. D. Walter, “Pneumatic tire,” 2006.
- [75] A. Tanikawa and Y. Sawada, “Minimum variance state estimators with disturbance decoupling property for optimal filtering problems with unknown inputs,” in *Proceedings of the ISCIE and its Applications*, vol. 2004, 2004, pp. 96–99.
- [76] J. Chen and R. J. Patton, “Optimal filtering and robust fault diagnosis of stochastic systems with unknown disturbances,” *IEE Proceedings-Control Theory and Applications*, vol. 143, no. 1, pp. 31–36, 1996.
- [77] Y. Sawada and A. Tanikawa, “Optimal filtering and robust fault diagnosis of stochastic systems with unknown inputs and colored observation noises,” in *Proc. 5th IASTED Conf. Decision and Control*, 2002, pp. 149–154.
- [78] C.-S. Hsieh, “Robust two-stage kalman filters for systems with unknown inputs,” *IEEE Transactions on Automatic Control*, vol. 45, no. 12, pp. 2374–2378, 2000.
- [79] D. Wang and K.-Y. Lum, “Adaptive unknown input observer approach for aircraft actuator fault detection and isolation,” *International Journal of Adaptive Control and Signal Processing*, vol. 21, no. 1, pp. 31–48, 2007.
- [80] B. Moaveni, M. Khosravi Roqaye Abad, and S. Nasiri, “Vehicle longitudinal velocity estimation during the braking process using unknown input kalman filter,” *Vehicle System Dynamics*, vol. 53, no. 10, pp. 1373–1392, 2015.
- [81] M. Darouach, M. Zasadzinski, and M. Boutayeb, “Extension of minimum variance estimation for systems with unknown inputs,” *Automatica*, vol. 39, no. 5, pp. 867–876, 2003.

- [82] S. Gillijns and B. De Moor, “Unbiased minimum-variance input and state estimation for linear discrete-time systems,” *Automatica*, vol. 43, no. 1, pp. 111–116, 2007.
- [83] W. Wei, H. Dourra, and G. Zhu, “Vehicle Tire Traction Torque Estimation using a Dual Extended Kalman Filter,” *Journal of Dynamic Systems, Measurement and Control*, (submitted).
- [84] S. Pan, H. Su, J. Chu, and H. Wang, “Applying a novel extended kalman filter to missile–target interception with apn guidance law: A benchmark case study,” *Control Engineering Practice*, vol. 18, no. 2, pp. 159–167, 2010.
- [85] S. Pan, D. Xiao, S. Xing, S. Law, P. Du, and Y. Li, “A general extended kalman filter for simultaneous estimation of system and unknown inputs,” *Engineering Structures*, vol. 109, pp. 85–98, 2016.
- [86] E. Ghahremani and I. Kamwa, “Dynamic state estimation in power system by applying the extended kalman filter with unknown inputs to phasor measurements,” *IEEE Transactions on Power Systems*, vol. 26, no. 4, pp. 2556–2566, 2011.
- [87] G. E. K. I, “Simultaneous state and input estimation of a synchronous machine using the extended kalman filter with unknown inputs,” in *2011 IEEE International Electric Machines & Drives Conference (IEMDC)*. IEEE, 2011, pp. 1468–1473.
- [88] H. M. Herab, H. Alikhani, and H. Khaloozadeh, “Unknown input estimation by applying extended kalman filter based on unknown but bounded uncertainties,” in *Iranian Conference on Electrical Engineering (ICEE)*. IEEE, 2016, pp. 1967–1973.
- [89] J. Na, A. S. Chen, G. Herrmann, R. Burke, and C. Brace, “Vehicle engine torque estimation via unknown input observer and adaptive parameter estimation,” *IEEE Transactions on Vehicular Technology*, vol. 67, no. 1, pp. 409–422, 2017.
- [90] I. Salgado and I. Chairez, “Adaptive unknown input estimation by sliding modes and differential neural network observer,” *IEEE transactions on neural networks and learning systems*, vol. 29, no. 8, pp. 3499–3509, 2017.
- [91] W. Wei, H. Dourra, and G. G. Zhu, “Transfer case clutch torque modeling and validation under slip and overtaken conditions,” *Journal of Dynamic Systems, Measurement, and Control*, vol. 143, no. 7, 02 2021.
- [92] L. Li, J. Song, H. Li, D. Shan, L. Kong, and C. Yang, “Comprehensive prediction method of road friction for vehicle dynamics control,” *Proceedings of the Institution of Mechanical Engineers, Part D: Journal of Automobile Engineering*, vol. 223, no. 8, pp. 987–1002, 2009.
- [93] D. Hu and L. Xu, “Characterizing the torque lookup table of an ipm machine for automotive application,” in *2014 IEEE Conference and Expo Transportation Electrification Asia-Pacific (ITEC Asia-Pacific)*. IEEE, 2014, pp. 1–6.
- [94] T. He, A. K. Al-Jiboory, G. G. Zhu, S. S.-M. Swei, and W. Su, “Application of ICC LPV control to a blended-wing-body airplane with guaranteed h_∞ performance,” *Aerospace Science and Technology*, vol. 81, pp. 88–98, 2018.

- [95] T. He, A. Al-jiboory, G. G. Zhu, S. S.-M. Swei, and W. Su, "Guaranteed h_∞ performance LPV ICC control with application to blended-wing-body model," in *2018 AIAA/ASCE/AHS/ASC Structures, Structural Dynamics, and Materials Conference*, 2018, p. 2211.
- [96] T. He, G. G. Zhu, S. S.-M. Swei, and W. Su, "Smooth-switching lpv control for vibration suppression of a flexible airplane wing," *Aerospace Science and Technology*, vol. 84, pp. 895–903, 2019.
- [97] F. Zurbriggen, T. Ott, and C. H. Onder, "Fast and robust adaptation of lookup tables in internal combustion engines: feedback and feedforward controllers designed independently," *Proceedings of the Institution of Mechanical Engineers, Part D: Journal of Automobile Engineering*, vol. 230, no. 6, pp. 723–735, 2016.
- [98] B. Fridholm, T. Wik, and M. Nilsson, "Kalman filter for adaptive learning of look-up tables with application to automotive battery resistance estimation," *Control Engineering Practice*, vol. 48, pp. 78–86, 2016.
- [99] M. Brown and C. J. Harris, "Neurofuzzy adaptive modelling and control," 1994.
- [100] M. Vogt, N. Müller, and R. Isermann, "On-line adaptation of grid-based look-up tables using a fast linear regression technique," *J. Dyn. Sys., Meas., Control*, vol. 126, no. 4, pp. 732–739, 2004.
- [101] J. C. P. Jones and K. R. Muske, "Identification and adaptation of linear look-up table parameters using an efficient recursive least-squares technique," *ISA transactions*, vol. 48, no. 4, pp. 476–483, 2009.
- [102] C. Guardiola, B. Pla, D. Blanco-Rodriguez, and P. Cabrera, "A learning algorithm concept for updating look-up tables for automotive applications," *Mathematical and Computer Modelling*, vol. 57, no. 7-8, pp. 1979–1989, 2013.
- [103] E. Hockerdal, E. Frisk, and L. Eriksson, "EKF-based adaptation of look-up tables with an air mass-flow sensor application," *Control Engineering Practice*, vol. 19, no. 5, pp. 442–453, 2011.
- [104] W. Wei, H. Dourra, and G. Zhu, "Slip-Clutch Torque Estimation via Real-Time Adapted Lookup Table," *ASME Letters in Dynamic Systems and Control*, (submitted).
- [105] W. H. Press, B. P. Flannery, S. A. Teukolsky, W. T. Vetterling *et al.*, "Numerical recipes," 1989.
- [106] W. Wei, H. Dourra, and G. Zhu, "Transfer Case Clutch Torque Estimation using an Extended Kalman Filter with Unknown Input," *IEEE/ASME Transactions on Mechatronics*, (submitted).